A Thesis for the Degree of Doctor of Philosophy

Enhancement of the Predictability in One-way Nesting of a Regional Ocean Model

지역해양 모델의 일방향 둥지화 예측력 개선

August 2018

Graduate School of Seoul National University

Department of Civil and Environmental Engineering

Pham Van Sy

Enhancement of the Predictability in One-way Nesting of a Regional Ocean Model

지역해양 모델의 일방향 둥지화 예측력 개선

지도교수 황 진 환

이 논문을 공학박사 학위논문으로 제출함

2018 년 04 월

서울대학교 대학원
건설환경공학부
Pham Van Sy

Pham Van Sy의 공학박사 학위논문을 인준함

2018 년 06 월

위 원 장 서 일 원 (인)

부 위 원 장 황 진 환 (인)

위 원 김 영 오 (인)

위 원 박 영 규 (인)

위 원 손 상 영 (인)

ABSTRACT OF DISSERTATION

Enhancement of the Predictability in One-way Nesting of a Regional Ocean Model

By Pham Van Sy

Department of Civil and Environmental Engineering

College of Engineering

Graduation School of Seoul National University

Advisor: Professor Jin Hwan Hwang

Dynamical downscaling with nested regional oceanographic models has been demonstrated to be an effective approach for both operationally forecasted sea weather on regional scales and projections of future climate change and its impact on the ocean. However, when nesting procedures are carried out in dynamic downscaling from a larger-scale model or set of observations to smaller scales, there are two big issues which affect to quality of nested solution. The first issue is

unavoidable errors due to the differences in grid sizes and updating intervals. The present work assesses the impact of such errors produced by nesting procedures on the downscaled results from Ocean Regional Circulation Models. Errors are identified and evaluated based on their sources and characteristics by employing the Big-Brother Experiment (BBE). The BBE uses the same model to produce both nesting and nested simulation; so it addresses those error sources separately (i.e., with out combining the contributions of errors from different sources). Here, we focus on discussing errors resulting from the spatial grids' differences, the updating times and the domain sizes. After the BBE was separately run for diverse cases, a Taylor diagram was used to analyze the results and recommend an optimal combination of grid size, updating period and domain sizes. Then, suggested setup for the dowscaling were evaluate by examining the spatial correlations of variables and the relative magnitude of variances between the nested model and the original data.

The second issue is underestimation of small scale generation in dynamical downscaling using nested regional oceanographic models. Numerous studies have shown the successfully generating fine-scales feature in one-way nested regional circulation model when driven by the large scale information that supplied from global output at the lateral boundary and incorporate with local forcing. However, others also observed un-reasonable reproducibility of small scales with under-estimation, even they recognized the lost of energy at large-scales, then leading to degradation of nested simulations. The present work focused on the second aspect

with identified original reasons behind such issue relating to “stimulated sources” which can support for the development of small scales (i.e., advection producing shearing, island). Base on that, we proposed an efficient technique, named "small scales-adding boundary technique" to improve the results and to help one-way nested model can run with higher spatial resolution different between the driver and the nested model.

Keywords: Downscaling ability, Error, Ocean regional circulation model, Big-Brother Experiment, Small scales generation, Added small scales.

Student Number: 2014-30863

TABLE OF CONTENTS

LIST OF FIGURES

LIST OF TABLES

LIST OF SYMBOLS

Latin uppercase

B	Buoyancy
B_f	Buoyancy flux
B_r	Buoyancy at a near surface reference depth
C	Scalar quantity (temperature (T), Salinity(S))
C_v	Ratio of interior N to N at the entrainment depth
COR	Correlation coefficient
CRMSD	Center Root-Mean-Squared Difference
E	Mean squared root of different
$G_{(\sigma)}$	Non-dimensional shape function
J	Ration of resolution jump
K_M	Vertical eddy viscosity
K_C	Vertical eddy diffusivity
K_x	Turbulent viscosity and diffusivity
K_x^s	Shear mixing
K_x^d	Double diffusive mixing
K_x^w	Internal wave generated mixing

KE	Kinetic energy
L	Monin-Obukhov depth
N	Total number of grid
R_{KE}	Ratio of kinetic energy
Ri_b	Bulk Richardson number
Ri_c	Critical bulk Richardson number
SDS	Standard Deviation
SCOR	Spatial correlation coefficient
T	Total number of time steps
$\vec{V}$	Vector velocity
$\vec{V}_a$	Mean horizontal velocity
$\vec{V}_t$	Turbulent velocity contribution to velocity shear
$\vec{V}_r$	Velocity at the near surface reference depth

Latin lowercase

c	Wave velocity
f	Coriolis parameter
g	Gravitational Acceleration

h	Local water depth
h_e	Ekman depth
h_{sbl}	Surface boundary layer depth
p	Pressure
u	Velocity in x direction
u_*	Friction velocity
v	Velocity in y direction
v_n	Light intensity adjustment function
w	Velocity in z direction
w_x	Non-dimensional shape function
w_s	Turbulent velocity scale for scalars

Greek Symbols

β_T	Ratio of entrainment flux to surface buoyancy flux
κ	Karman's constant
ℓ	Wave Length
η	Surface elevation
ϕ	Prognostic model variables

ϕ_x	Non dimensional flux profile
ϕ_m	Non dimensional flux profile for momentum
ϕ_s	Non dimensional flux profile for scalar
σ	Vertical coordinate system
τ	Time scale for nudging
τ_x	Bed shear stress in x direction
τ_y	Bed shear stress in y direction
ν	Molecular viscosity
ν_θ	Molecular diffusivity
ζ	Surface layer stability parameter
Γ	Variance ratios

Acronyms

BB	Big-Brother
BBE	Big-Brother Experiment
GCM	Global Circulation Models
ICs	Initial Conditions

KPP	K-Profile Parameterrization
LB	Little-Brother
LBCs	Lateral Boundary Conditions
OBCs	Open Boundary Conditions
OGCMs	Ocean Global Circulation Models
ORCMs	Ocean Regional Circulation Models
RCM	Regional Circulation Models
ROMS	Regional Ocean Modeling Systems

Subscript or Superscript

B	Referring Big-Brother
BB	Referring Big-Brother
ext	Referring external information
in	Inward propagation
L	Referring Little-Brother
LB	Referring Little-Brother
ls	Referring Large spatial
n	Referring barotropic

out	Outward propagation
ss	Small spatial
stat	Stationary
tran	Transient

CHAPTER ONE

1. INTRODUCTION

1.1 Dynamical downscaling and one-way nesting

The Global Circulation Models (GCM) simulates various physical processes of Earth's system through numerous mathematical equations that present atmospheric, oceanic, interactions, and feedbacks. GCMs are the very useful tools that construct reasonably accurate global, continental-scale climate information, and are used to study present climate and predict future climate under scenarios. The domain of GCM covers the Earth with composed of many grid cells presenting horizontal and vertical areas on the Earth system (Fig. 1.1). In each of the grid cell, GCM compute various combined processed such as radiation, precipitation, storage of heat in oceans, large-scale transport of heat and water by ocean and atmosphere (Trzaska and Schnarr. 2014).

However, the spatial resolution of GCMs is quite coarse due to limitations on computing resources and input data. A grid cell is often in the order of 200 km in the atmospheric GCM and usually is 30 km in the ocean GCM. The minimum resolution could be 9 km which can be produced by the earth simulator from Japan. Each simulated grid cell is homogenous with only one value for a given variable. The GCMs only resolves for large scale dynamics and it uses an appropriate

parameterization with sub grid-scale for small scale processes. In addition, the results of GCM are often considered for climatic conditions averaged at temporal scales of monthly, seasonal, annual, and longer times scale. Thus, it is difficult to use GCM output directly in studying regional and local scale environmental problems (Oddo and Pinardi, 2008; Li et al., 2012; Trzaska and Schnarr. 2014; Herbert et al., 2014). Therefore, in order to have finer resolution at a regional scale, there is a necessary to downscale the GCM output in order to generate small scale features.

Downscaling is a general name for a procedure to use large-scales information from GCM to make predictions at local scales. There are two main approaches of downscaling including statistical downscaling and dynamical downscaling. Statistic downscaling refers to use of statistical relationship which is in two step processes consisting of (1) the development of statistical relationships between large-scale predictors and local climate variables such as surface air temperature and precipitation, and (2) the application of these relationships to the output of GCM experiments in order to simulate local features in the future.

Whereas, dynamical downscaling refers to the use of numerical models running at high resolution over a regional sub-domain, taking observation data or coarse resolution of GCMs output as a boundary condition in order to achieve detailed regional and local data (Giorgi and mearns. 1999; Castro et al. 2005; Trzaska and Schnarr. 2014). The term “nesting” which is often used in downscaling approach, specifies the dynamical downscaling. Each method has its own

advantage and disadvantage. One can refer in more detail in the report of Intergovernmental Panel on Climate Change (Giorgi and mearns. 1999; Castro et al. 2005; Trzaska and Schnarr. 2014). The present work only focused on dynamical downscaling with an ocean regional circulation model (Giorgi and mearns. 1999; Castro et al. 2005; Trzaska and Schnarr. 2014).

Figure 1.1 Example of grid domain of global circulation model with resolution of 200 km. Extracted from http://www.pnnl.gov/

There are two kinds of nesting method including one-way and two-way. The important distinction between the two is exchange of information. In the two-way nesting, there is a dual exchange of information between two models: external model to nested model and nested model to external model. This technique must be performed online, requiring additional software tools based on the model code

itself to allow the transmission and transformation of various distributed information between two models. It, therefore, requires high storage volume and expensive computational cost. Whereas, the one-way nesting method can be performing off-line in which the large-scale information only transfer from global model to the regional model along the open boundary. Therefore, there is no feedback from the RCM to GCM. Both methods can yield realistic high resolution solutions that can permit study of local problems and have been generally in the scientist community. However, one-way nesting can limit the storage volume and reduce the computational requirement. (Spall and Holland. 1991; Cailleau et al. 2008).

Dickingson et al. (1989) and Groirgi (1990) first proposed an idea using regional model to downscale GCM's output. This idea relies on the concept of one-way nesting that large scale features from GCM output supplies initial and time dependent fields at lateral boundary conditions for high resolution Regional Circulation Model (RCM) simulation. RCM is similar to the GCM in its principle but it run at higher resolution. RCM gets large scales information provided from GCM and corporate with local conditions to generate a realistic regional feature at scales in a higher resolution (Giorgi and Mearns. 1999; Trzaska and Schnarr. 2014) (Fig. 1.2). Smaller scales which are unresolved by coarse grid cell simulations results from an interaction from larger scales of GCM's output and local physiographic detail. For instance, coastal current is under a dynamical phenomenon interaction of multiple scales. In which, the large-scale circulation

generates meso-scale current, named offshore currents. The offshore currents corporate to coastal waveguide, local wind forcing, tides to develop smaller-scale coastal currents with local jets in large topographically modulated variability (Marchesiello et al. 2001).

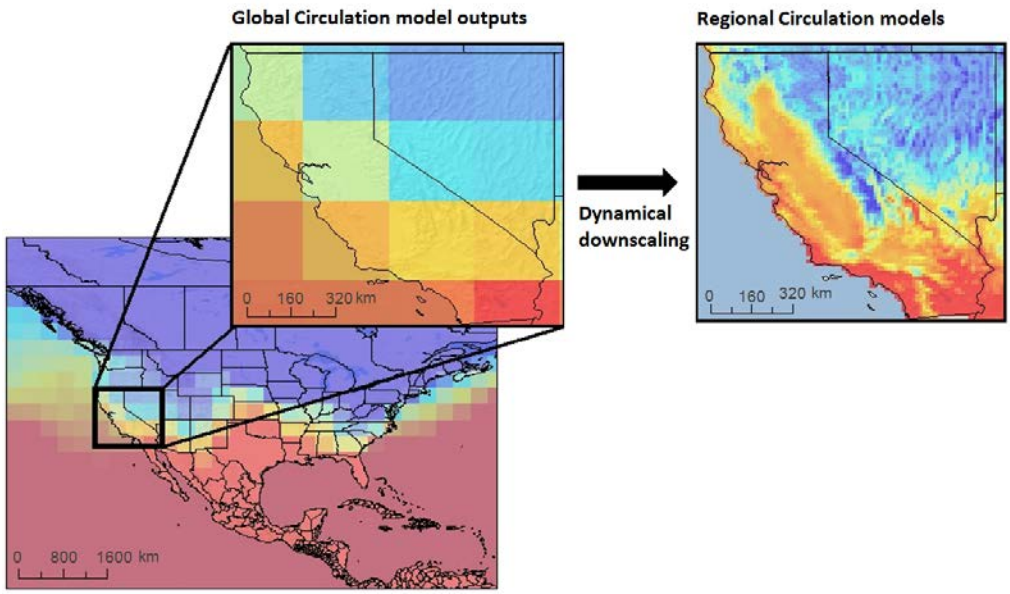

Figure 1.2 Example of generating small scales features after dynamical downscaling from low-resolution global model output (large scales information) by regional model for temperature in United State. The figure shows the output of global model at resolution of 150 km, and the right figure describes nested simulation using regional model. Extracted from http://www.cal-adapt.org/

1.2 Error sources generating during the nesting procedure

The high-resolution grid of atmospheric and Regional Circulation Models (RCMs) allows for the resolution of fine-scale interactions and forcings that are

unresolved by coarse-mesh simulations (e.g., Denis et al., 2003). Along with simulating small-scale dynamics by RCMs, one-way nesting schemes help with the representation of large-scale features in RCMs by imposing initial and lateral boundary conditions, which are constructed by downscaling information from global models (Ådlandsvik and Bentsen, 2007; Li et al., 2012; Herbert et al., 2014).

However, the procedures employed for such downscaling of large-scale information supplied at the boundary conditions into small-scale models generate unwanted errors (Warner et al., 1997; Denis et al., 2002). Such errors limit the application of RCMs to short-term forecasts and long-term projections of local weather. Therefore, those errors need to be identified and qualitatively evaluated, to find the optimal temporal and spatial resolutions of the RCMs and to determine whether the RCMs may reasonably forecast the future (e.g., Denis et al. 2002 and 2003; Leduc and Laprise, 2008).

ORCMs have modeled coastal seas over several decades in a variety of domains (e.g., Kourafalou and Tsiaras, 2007; Costa et al. 2012) and have operationally forecasted sea weather on regional scales (e.g., Lim et al. 2013; Rowley and Mask, 2014). However, compared with the many “atmospheric climate” studies of downscaling capabilities, the errors produced by the nesting with Ocean Regional Circulation Models (RCMs) (Spall and Holland. 1991), have not yet been studied well. Many previous studies with RCMs have focused on optimizing RCMs to reduce errors from the nesting; but no standard method to identify, assess and reduce those errors has so far been published. As a first step for assessing the

oceanic dynamical downscaling feasibility in an RCM, we investigated the errors produced by one-way nesting on the basis of error evaluation schemes used for assessing downscaling capability in atmospheric climate studies.

According to Warner et al. (1997), Giorgi and Mearns (1999) and Denis et al. (2002a), there are several sources of error in atmospheric climate dynamic downscaling. Denis et al. (2002a) discussed these error sources for atmospheric models and we modified this approach slightly to suit oceanic circulation studies, as follows:

(1) Boundary condition types: To reduce the above errors, artificial boundaries are constructed with each field from the GCMs and supplied to each point at the LBCs (McDonald, 1999). However, it is difficult to define a set of formulations to construct boundary conditions that guarantee the existence of a stable and unique solution. Therefore, such over-specified values at the boundaries may differ from the neighboring interior solution and still cause a discontinuity at the boundaries. Such discontinuities, in turn, may result in unstable integration and cause transference of numerical instability to the domain from the lateral boundary, generating unnecessary errors (McDonald, 1999; Marchesiello et al., 2001; Oddo and Pinardi, 2008).

(2) Spin-up for regenerating smaller scale signals: Coarse data from Ocean Global Circulation Models (GCMs) or observations are interpolated to construct finer Initial Conditions (ICs) which are fed into RCMs. The small-scale perturbations lacking at ICs, takes a certain amount of time to regenerate such

small-scale features (Fig. 1.3 & 1.4), even with the finer grids of RCMs (Warner et al., 1997).

(3) Spatial and temporal inconsistencies between Lateral Boundary Conditions (LBCs) of the nesting and nested models: As with the ICs, the GCMs'data should be spatially and temporally interpolated (Fig. 1.3) and then supplied as LBCs to the RCMs (Warner et al., 1997; Denis et al., 2002). Such even smooth interpolation step cannot generate small scale perturbation (Fig. 1.3). In the vicinity of the boundaries, however, significant discontinuities occur when data are updated with new LBC information interpolated from GCMs. For example, velocities at the boundaries before and after updating have neither the same direction nor the same magnitude; in particular, newly interpolated LBCs do not have enough small-scale features. Such inconsistencies occur at every updating with new LBCs.

(4) Sizes of nested domains: Once the aforementioned perturbations develop at the boundaries, they propagate toward the center of the domain along with the cross-boundary flow (Warner et al., 1997). If the domain of interest is located far enough away from the lateral boundaries, then errors can be prevented from quickly propagating into the domain of interest. This buffering distance may help reduce the effects of errors at the boundary on the central domain of interest.

(5) Sub-grid scale parameterization: RCMs usually consider more complicated sub-grid parameterization schemes or different coefficients from those of GCMs (Samelson et al., 2008). In particular, the performance of sub-grid-scale

turbulence closure models could differ depending on their grid sizes. Thus, inconsistent physical parameterizations between driving and driven models could cause non-physical forcing gradients, which can generate unavoidable errors, near boundaries in particular (Warner et al., 1997; Denis et al., 2002).

(6) Addition of local forcing: Atmospheric weather data, such as pressure, wind stress, precipitation and surface flux, are interpolated from the Global Climate Model or from the NCEP analyses. However, the atmospheric forcing obtained from the global models has poor spatial and temporal resolutions as do the oceanic variables from the GCMs. Therefore, errors from interpolation of the local atmospheric forcing could also cause large gradients and accelerations, in particular near boundaries (Warner et al., 1997).

Among all these error sources, the present work focuses on error sources 1, 2, 3 and 4, namely, boundary condition types, spatial resolution of initial conditions, spatial resolution and temporal updating of LBCs, and domain sizes. Error source number 5 should be related to sources 2 and 3, but too much depends on the numerical scheme of a certain model, so it is beyond the scope of this discussion. To focus attention on the RCM itself, the effects and variations due to source 6 are also neglected here.

1.2 Generation of small scales motion in one-way nesting procedure

The resolution of GCM is quite coarse, it therefore only resolves the large scales which are larger than grid size, and uses sub-grid mode closure for smaller

scales process. The RCM running with high resolution can resolve scales much smaller than that of GCM. The RCM must need information of large scales provided from GCM or observations at boundary and in the initial stage in dynamical downscaling process. In the one-way nesting procedure, the RCM domain must embed in the GCM. The initial conditions (ICs) and boundary conditions (BCS) of RCM are constructed by interpolation from GCM (Fig.1.3 (a)).

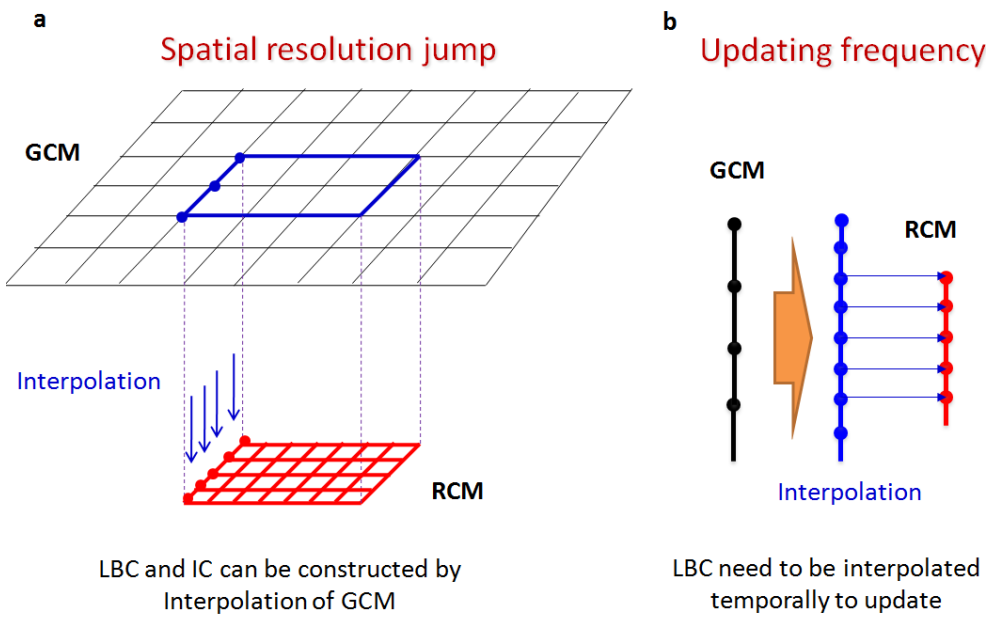

Figure 1.3 Construction of the LBC and IC by spatial and temporal interpolation of GCM for RCM. (a) spatial interpolation, and (b) temporal interpolation

Besides, the updating frequency of lateral boundary condition (LBC) also needs to be interpolated at every time step of RCM (Fig. 1.3 (b)). For example, output of GCM is every 12 hours, the time step of RCM is 10 minutes. The LBC of

RCM needs to be interpolated at every 10 minutes from 12 hours of GCM. However, such smooth interpolations cannot generate small scales perturbations to the ICs and BCs in RCM.

Such small scales only are generated during a dynamical downscaling process which is used a RCM running at high resolution directly downscales low resolution GCM output. In other word, RCM generates small scales features when it directly downscales the large scale information from GCM.

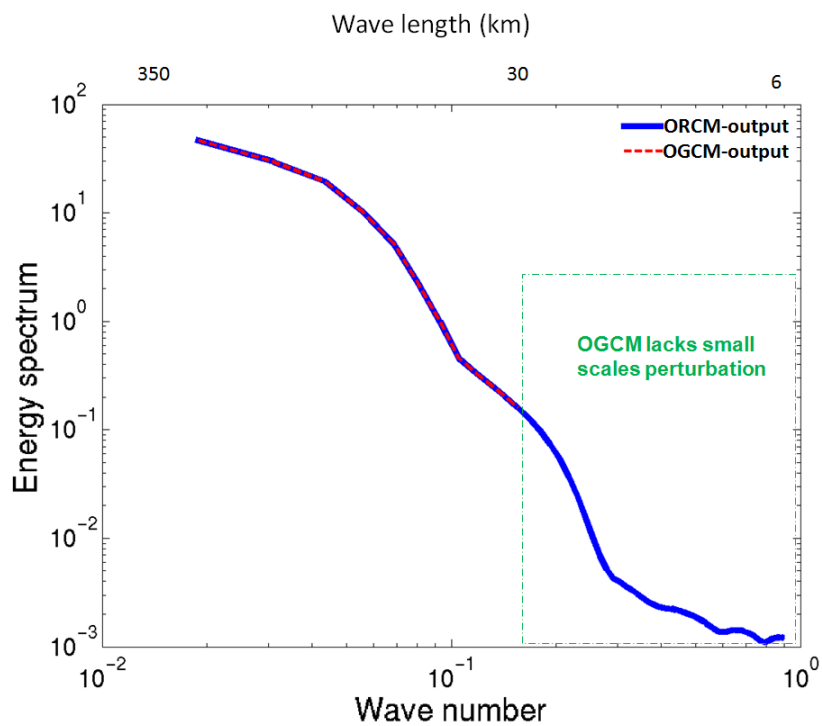

Figure 1.4 Energy spectrum of OGCM-output (red line) with resolution of 15 km × 15 km and ORCM-output (blue line) having resolution of 3× 3 km. Small scales in smaller than 30 km are absent from GCM-output.

As shown in the Fig. 1.4, The Ocean Global Circulation Model (OGCM) with resolution of 15 km × 15 km (the red line) only has energy spectrum at scales larger than 30 km. While Ocean Regional Circulation Model (ORCM) with resolution of 3 km × 3 km can recovery small scales smaller than 30 km, which are absent in OGCM when directly dynamical downscales from the OGCM output.

In studying generation of small scale features using regional climate model, Denis et al. (2002a) proposed three types of sources which develop small scale feature in a high resolution of regional climate model. We names “stimulated sources”. They are the surface forcings, the nonlinearities interaction present in the dynamical equations, and hydrodynamic instabilities. The first type, for example island appearance and complex topography, can be thought that regional model exploits the most. The intensity of such forcing plays an important role in determining surface regional model. The second one, nonlinear dynamics, also has a great role. The interactions of internal dynamics processes exhibit a nonlinear downscale cascade (from large to small scales) by stretching and stirring the flow. This phenomenon can happen even in the absence of surface forcing. The last type is through from shear and buoyancy in the flow through hydrodynamic instabilities. This type can produce small scale features without the support from surface forcing.

The small scales motions absenting from coarse resolution field are not generated instantaneously in time and space in an RCM simulation. For instant, in the inner domain, the small scales absented from initial condition were reconstructed under the separate or combination of above sources. In a region near

the lateral boundary, the large scales motions of the coarse grid model generated small scales motions when it goes inward the inner domain. It takes place, or distance, to develop the enough fine scale motions before they reach their equilibrium amplitudes. This process occurs after every temporal updating the LBCs (Laprise et al. 2008). Therefore, generating small scales motions is necessary to carefully assessed in designing RCM implementation. In this section, we constructed the experimental framework to focus on two sources in developing the small scale motion, namely surface forcing and the hydrodynamic instabilities.

A high ability of regional model is that, it can takes large scales information provided from global model and corporate with local conditions to generate a realistic regional feature at scales in a higher resolution. Although regional model has been achieved many great advancement and improved downscaling capabilities over several decades via operationally forecasted sea weather on regional scale in variety of domain (Lim et al. 2013; Rowley and Mask, 2014, Pham et al. 2016), the reliability of nesting strategy in using RCM still has been skepticized in modeling community. The numerical experts of the World Climate Research Program (WCRP) have suggested regional modeling community to make diversified experiments to prove and improve the ability of one-way nested regional circulation model, since RCM bears a variety of error sources associated to one-way nesting procedure (Warner et al. 1997; Denis et al. 2002a; Antic et al. 2006; Pham et al. 2016).

The effect of such error sources might vary, regarding to the different geographical domain, the nesting spatial resolution jump, update frequency of driving data at lateral boundary condition, the season (Denis et al. 2002a; Pham et al. 2016) and even also depend on the type of regional numerical model (Chen et al. 2007; Huang et al. 2008). Such error sources are generally unavoidable and affect the quality of RCM results. Therefore, the performances of nested regional model also are in difference.

Some studies have shown the successfully generating fine-scales feature in one–way nested regional circulation model when driven by the large scale information that supplied from global output at the lateral boundary and incorporates with local forcing (Warner et al. 1997; Denis et al. 2002a). Whereas, others observed un-reasonable reproducibility of small-scales with under-estimation, even recognized the loss of energy at large-scales (Castro et al. 2005; Feser et al. 2011), later leading to degrade the nested simulation. Moreover, Winterfeldt et al. (2010) and Feser et al. (2011) mentioned that dynamical downscaling does not generate small scales in a region which was not present of stimulated sources. Denis et al. 2002a also experienced this matter when finding underestimation of nested small scale relative vorticity at 500 hPa where small scale dynamics are in free atmosphere. In this perspective, we suspected reasons behind such issue highly relate to stimulated sources to support the development of small scales which have not been identified yet. The Big-Brother Experiment is also employed to address separately role of “stimulated sources” contributing to the

generation and development of small-scales during nesting procedure. Base on that, we proposed a “small scale-adding boundary technique” to simulate the generation and development of small scales. It helps to improve the results and increase the horizontal resolution difference between driving data and nested model.

1.3 Objectives

The objectives of this study can be summarized as follows:

1. To accurately assess the errors sources associated with the downscaling technique affecting the results of the ORCM;
2. To suggest an optimizing setup for dynamic downscaling in one-way nesting;
3. To evaluate the downscaling ability of one-way nested using ORCMs;
4. To investigate stimulated sources contributing to small scale generation;
5. To identify small scale effect on the large scales and nested solution in case of without stimulated sources.
6. To propose a small scale-adding boundary technique in improving quality of ORCMs results and enhance the predictability of one-way nested procedure ;

In order to achieve the above objectives, we employed the Big-Brother Experiment (BBE), which enables us to separate each source from the others and to quantitatively assess the individual effects on the results of the ORCMs. The

domains of research were setup in both ideal and real coastal region, running in 3 dimensions to diversity the circumstance and enhance the conclusions.

1.4 Outline of the Thesis

The Big-Brother Experiment is presented in chapter two. In which, the Big-Brother experiment concept as well as analysis are introduced in detail. Thesis is following with a description of applied regional ocean model system. In chapter three, the results of error sources associated with downscaling technical affect to the results of ORCMs were presented and optimal setup for ORCM based on these outcomes is suggested. Then the downscaling ability in one-way nested using ORCMs is reported. Chapter four focused on the characteristic of generating small scale motions which are absent at ICs and BCs. Following that, the role of stimulated sources in generating small scale motions is investigated. Chapter five describes effect of small scales on large scales, and then degrading the ORCM's results. Besides, an efficient technique to improving results and increase the spatial resolution jump is presented. The thesis ends with summary and future work in chapter six. The content of the thesis can be summarized in the thesis overview as shown in Fig. 1.5.

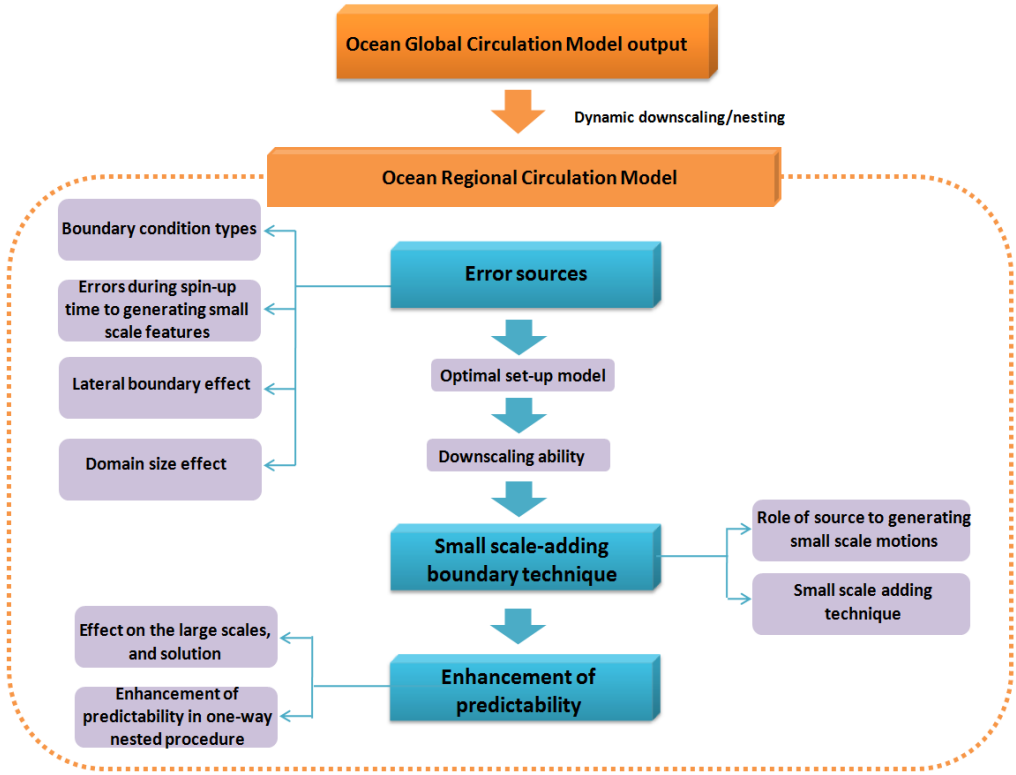

Figure 1.5. Thesis overview

CHAPTER TWO

2. BIG-BROTHER EXPERIMENT

2.1 The Big-Brother Experiment concept

The principle behind the nested modeling is that, it can generate realistic regional structures when the ORCM takes the large-scale information supplied by global model output at lateral boundaries and incorporate with local forcing and detailed descriptions of physical processes. In other word, the reliability of nested models is generating meaningful fine-scale feature which are absent in the IC and LBCs. Therefore, validation of the ORCM's small scales is also important and necessary. However, validation of small-scale generation from ORCMs simulation when using coarse resolution global model output as driving data is impossible because small-scales which generated by the ORCM are absent from the global model. Data of other sources can be used for validation, but such kind of data is restricted to region with high density observation network at whole depth and limited number of oceanic variables such as velocity, temperature and salinity Denis et al. (2002a).

In order to circumvent these issues, Big-Brother Experiment which is thought as "perfect prognosis" approach, was adopted. It is similar to the work conducted by Denis et al. (2002a) in the field of atmospheric research. Fig. 2.1 & 2 shows a schematic diagram of the present BBE scheme.

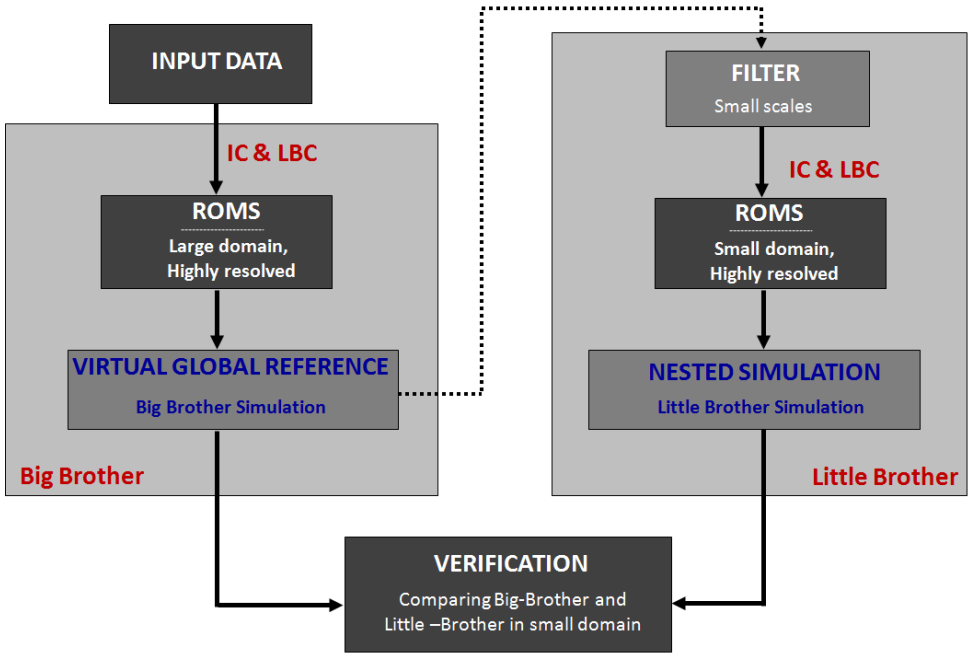

Figure 2.1. Flowchart of the BBE. IC: initial condition; BC: boundary condition; BC and IC of Big-Brother are generated from the hind-cast HYCOM (Hybrid Coordinate Ocean Model). Atmospheric variables were generated with the WRF (Weather Research & Forecasting) model.

First the BBE was used to simulate a large area with high resolution using ORCMs and these results were named Big-Brother. Such highly resolved data were taken as real values, to be used as reference data in later steps. Big-Brother data were then intentionally degraded by removing high-wave number signals with a low-pass filter. By filtering out high wave number-signals, the data can be taken as if produced by a coarser-grid global model. Since the ICs and BCs had lost small-scale signals and were underspecified, the filtered data needed to be interpolated

again to fill the IC and BC grids in the nested model which is the same ORCMs with BB. With these interpolated ICs and BCs, our simulations produced data for the Little-Brother, which has a finer resolution and shorter updating intervals.

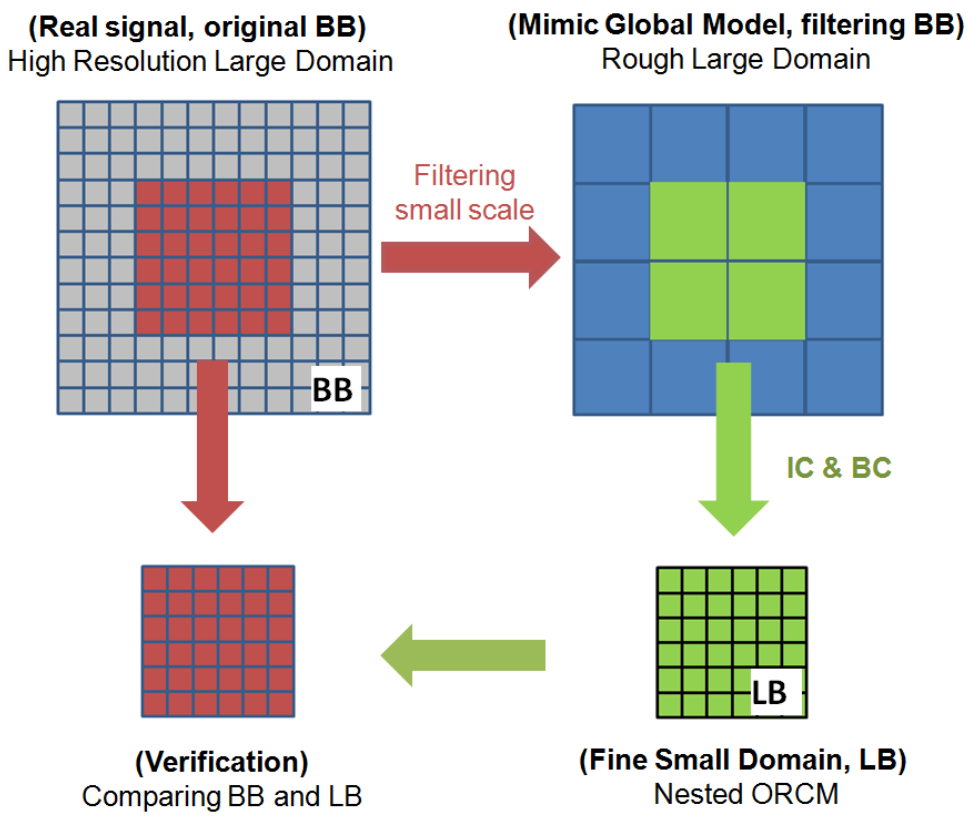

Figure 2.2 Conceptual schematics of the BBE. Original Big-Brother is high resolution large domain. Filtered Big-Brother is low resolution large domain. Little-Brother is high resolution small domain which embedded in Big-Brother domain.

Now, the Little-Brother results have the same resolution as the original Big-Brother results before filtering. Note that the Little-Brother uses the filtered Big-Brother results to construct ICs and BCs that mimic the coarser OGCM results. Therefore, Big-Brother results before filtering can be thought as a true reference that Little-Brother results can be compared directly to. Such a comparison can evaluate the difference between the nested modeling results.

This experimental method has the advantage of separating the numerical error from other error sources in the nesting and downscaling. Furthermore, this method is free of limitations associated with observational methods, such as coarse resolution at the deep layers and the possible lack of observational variables. Moreover, the simulated variables of the Little-Brother can be easily compared with the Big-Brother results, as they have exactly the same resolution. The differences between the results of Big-Brother and Little-Brother can be regarded as errors resulting from the nesting and downscaling, and are not attributable to model errors or observational errors.

In addition, Big-Brother reference can be constructed from ocean global circulation model running at high resolution as shown in the Figure 2.3, we call it “expensive Big-Brother Experiment”. However, this approach takes so high computational cost and may induce errors due to using different computational model having different parameters and numerical schemes.

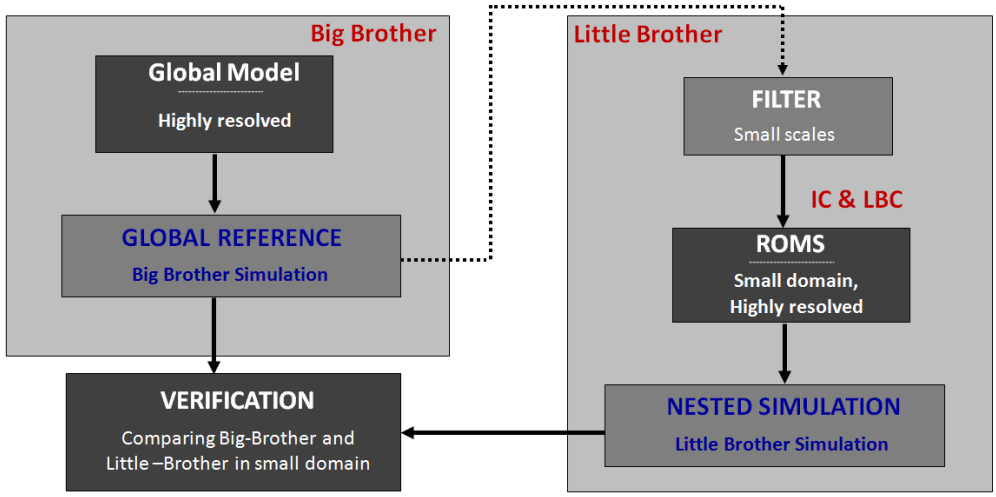

Figure 2.3 The expensive Big-Brother Experiment. IC: initial condition; BC: boundary condition.

2.2.1 Filtering method

In order to filtering small scales, discrete cosine transform (DCT) is employed. DCT is a special spectral analysis technique, first in introduced by Ahmed et al. (1974). It can be thought as a special Fourier transform and work well with aperiodic fields in a given domain. DCT makes the aperiodic signal becomes analyzed periodic by a summarization process. Such process consists simply extending a mirror image of the original function prior to the Fourier transform (Fig. 2.4) (Denis. et al 2002b).

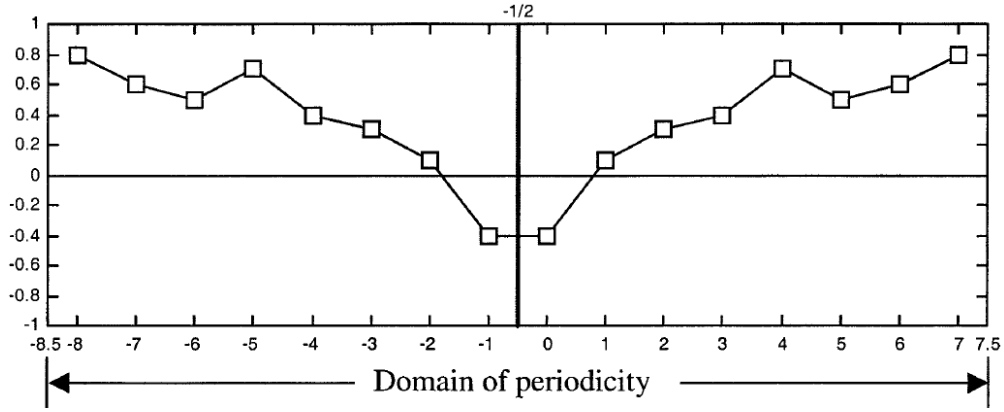

Figure 2.4 Example of taking a mirror signal from the original signal in 1D-DCT. Panel on the right-hand side is original signal, and Panel on the left-hand side is extending signal. Extracted from Denis. et al 2002b.

The direct and inverse DCT in a two-dimensional field *f(m,n)* of N_m by N_n grid points are respectively defined as:

$$F(i,j)=\beta(i)\beta(j)\sum_{m=0}^{N_m-1}\sum_{n=0}^{N_n-1} f(m,n)\times\cos\left[\pi i\frac{(m+1/2)}{N_m}\right]\cos\left[\pi i\frac{(n+1/2)}{N_n}\right] \quad (1)$$

and

$$f(m,n)=\sum_{i=0}^{N_i-1}\sum_{j=0}^{N_j-1}\beta(i)\beta(j)f(i,j)\times\cos\left[\pi i\frac{(m+1/2)}{N_m}\right]\cos\left[\pi i\frac{(n+1/2)}{N_n}\right] \quad (2)$$

With

$$\beta(i)=\begin{cases}\sqrt{\dfrac{1}{N_m}}, i=0\\ \sqrt{\dfrac{1}{N_m}}, i=1,2,...,N_m-1\end{cases} \quad (3)$$

and

$$\beta(j)=\begin{cases}\sqrt{\frac{1}{N_n}}, j=0\\ \sqrt{\frac{1}{N_n}}, j=1,2,...,N_n-1\end{cases} \quad (4)$$

Here, *f(m,n)* is the field value at grid point integer numbers *(m,n)*, and *F(i,j)* is the spectral coefficient corresponding to the *(i,j)* a dimensional wavenumbers. A 2D-DCT employed to a physical field *f(m,n)* of N_m by N_n value produces a N_m by N_n array of *F(i,j)* real spectral coefficients.

The wavelength λ bases on two-dimensional wavenumber pair *(i,j)* with a square domain, $N_m = N_n = N$ is calculated as

$$\lambda=\frac{2N\Delta}{k_s} \quad (5)$$

Where Δ is the space of gridpoint, and k_s is the 2D wave-number define as

$$k_S=\sqrt{i^2+j^2} \quad (6)$$

In case of rectangular domains wavelength λ is defined as below:

$$\lambda=\frac{2N\Delta}{k_r}, \qquad k_r=\sqrt{\frac{i^2}{N_m^2}+\frac{j^2}{N_n^2}} \quad (7)$$

Another advantage of the Discrete Cosine Transform is that it can control the wavelengths. Therefore, its low-pass filter can easily remove scales with the

chosen wavelengths (Denis. et al 2002b). For instance, for simplicity we used 1D – Discrete Cosine Transform to apply on grid of order of 100 grid points with grid space of 1 km. Assuming that small scales which have wavelength smaller than 20 km will be filtered. As shown in the Figure 2.5, the low-pass filter of 1D – DCT only enables large scale (low frequency) of waves with wavelength greater than 20 km pass. Whereas, all small waves (high frequency) having wavelength smaller than 20 km were removed and their value equate to zero.

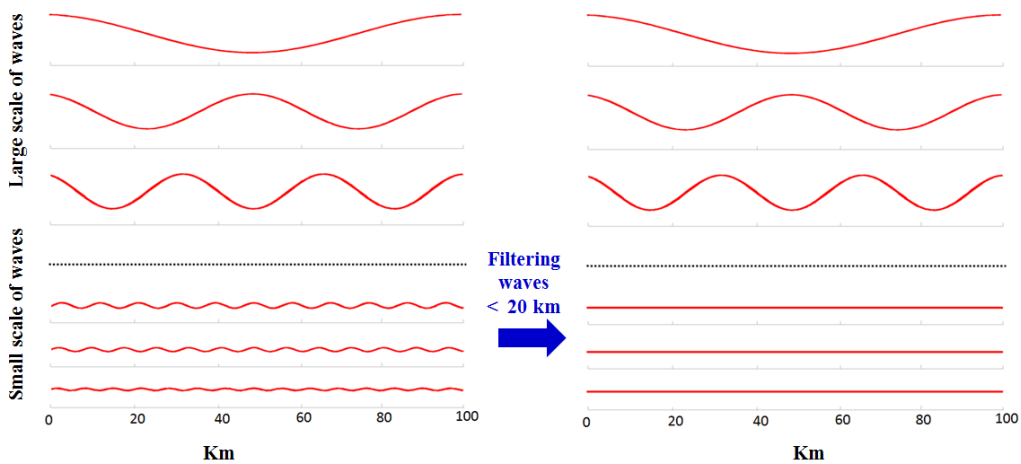

Figure 2.5 Example of filtering small scales by using low-pass filter of 1D - Discrete Cosine Transform applied on grids of the order of 100 grid points, with grid space of 1 km. Assuming that small scales have wavelength smaller than 20km.

2.2 Analytic method

The appropriateness of the downscaling procedures were evaluated in two steps. First, a Taylor diagram was used to find an optimized combination of each setup condition to simulate with the dynamic downscaling. A 2-D Taylor diagram can provide a convenient way to graphically summarize how closely marching between two sets of data (Taylor. 2001). On this diagram, the correlation coefficient (COR) and the Center Root-Mean-Squared Difference (CRMSD), along with the ration of the Standard Deviations (SDS) of the two data sets are all presented by a single point of the 2D plot. Therefore, this diagram was used to assess the overall error during downscaling. Similarity among results was quantified in terms of three statistics: SDS, COR and CRMSD. The combination of such statistics can give useful information to help assess the level of agreement, similarity in standard deviation, and magnitude of difference in error between the two sets of results (Little- and Big-Brother).

Where *i*, *j*, and *k* are the indices of grid points and *t* denotes time steps, a time series of three-dimensional spatial variables such as temperature, salinity or vorticity, $\phi = \phi(i, j, k, t)$ was decomposed into time-average and fluctuation terms, as follows:

$$\phi = \overline{\phi} + \phi' , \qquad (8)$$

where the over-barred variables are time-averages and the primed variables denote fluctuations. Also, the spatially-averaged value is calculated as follow:

$$\left\langle \phi \right\rangle = \frac{\sum_{i,j,k} \phi_{i,j,k}}{N}, \qquad (9)$$

Where N is a total number of grid points in the Little-Brother domains. The SDSs in each domain may be calculated thus:

$$\mathrm{SDS}_L = \sqrt{\frac{1}{T}\sum_{t=1}^{T}\left(\left\langle \phi_{t,L} \right\rangle - \overline{\left\langle \phi_{t,L} \right\rangle}\right)^2}, \qquad (10)$$

$$\mathrm{SDS}_B = \sqrt{\frac{1}{T}\sum_{t=1}^{T}\left(\left\langle \phi_{t,B} \right\rangle - \overline{\left\langle \phi_{t,B} \right\rangle}\right)^2}, \qquad (11)$$

Where T is the total number of time steps for the period of interest and the sub-scripts of L and B indicate Little- and Big-Brothers, respectively. The COR is:

$$\mathrm{COR} = \frac{1}{T}\sum_{t=1}^{T}\frac{\left(\left\langle \phi_{t,B} \right\rangle - \overline{\left\langle \phi_{t,B} \right\rangle}\right)\left(\left\langle \phi_{t,L} \right\rangle - \overline{\left\langle \phi_{t,L} \right\rangle}\right)}{\mathrm{SDS}_B \mathrm{SDS}_L}, \qquad (12)$$

The CRMSD can be defined as:

$$\mathrm{CRMSD} = \sqrt{E^2 - \overline{E^2}}, \qquad (13)$$

When the mean squared root of difference between two experiments, E, is

$$E = \sqrt{\frac{1}{T}\sum_{t=1}^{T}\left(\left\langle \phi_{t,B} \right\rangle - \left\langle \phi_{t,L} \right\rangle\right)^2}\,. \qquad (14)$$

The relationships among the above variables can be found as follows (Fig. 2.6) (according to Taylor, 2001):

$$\mathrm{CRMSD}^2 = \mathrm{SDS}_B^2 + \mathrm{SDS}_L^2 - 2\mathrm{SDS}_B \times \mathrm{SDS}_L \times \mathrm{COR}\,. \qquad (15)$$

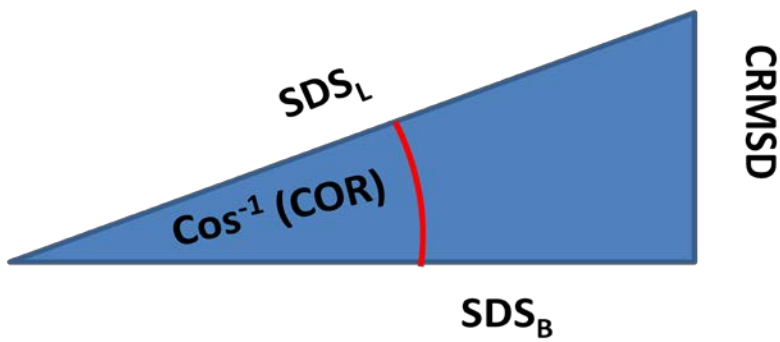

Figure 2.6 The relationship between COR, SDS and CRMSD as the law of cosines

Such statistic terms can conveniently present as a single point on the plot in two dimensions (Fig. 2.7). For example, the Little-Brother, a green rectangular on the plot compares to the Big-Brother which is a red star point. The Big-Brother is considered as a reference that Little-Brother want to get closer. For instant, the better Little-Brother must have higher COR, smaller CRMSD and closer to SDS of Big-Brother.

Finally, following Denis et al. (2003), the SDS of the Little-Brother and CRMSD are percentile relative with Big-Brother's SDS. After the Taylor analysis was conducted with those ratios and COR, the optimal resolutions were reconfirmed by assessing the downscale ability, as described by Denis et al. (2002a).

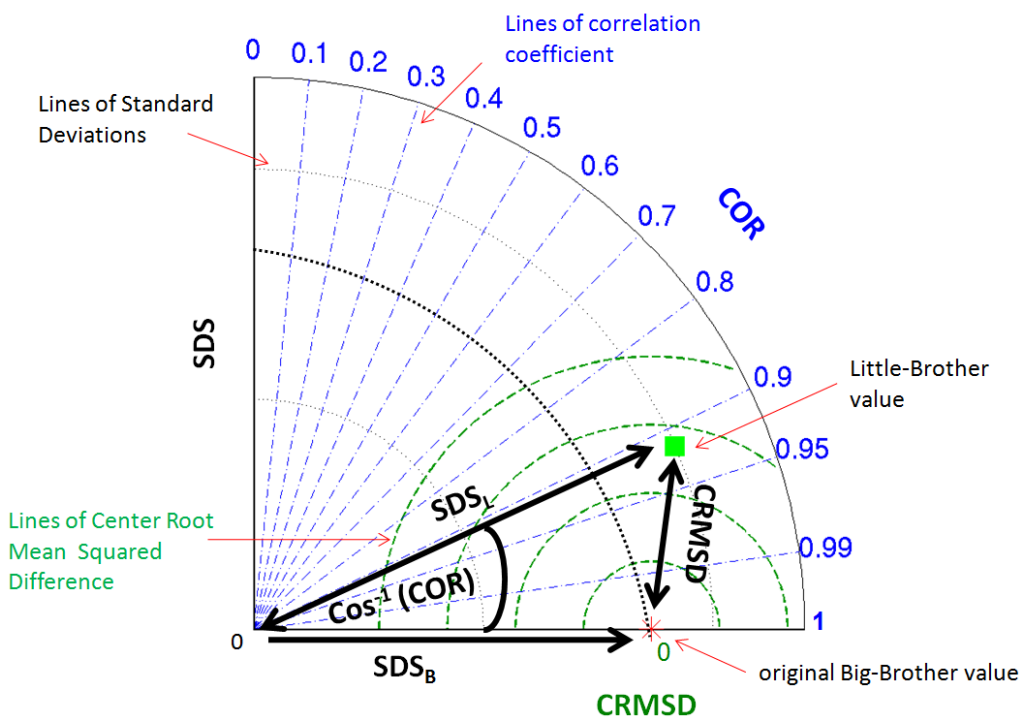

Figure 2.7 Example of Taylor diagram displaying a statistical comparison of Little-Brother with Big-Brother

2.3 Nested regional model description

Ocean regional circulation models have been developed by numerous institutions over several decades. Although such models differ in their numerical, physical and technical aspects, the can be adapted to any given region of the globe by incorporating appropriate local information. There are some common ocean regional circulation models including ROMS (Regional Ocean Modeling System), POM (Princeton Ocean Model), Delft3D-FLOW, and FVCOM (Finite Volume Community Ocean Model) which have been using widely in self research studies and operationally forecasting sea weather on regional scales in over the world.

However, it is important to note that a single ocean regional circulation model can most likely not give accurate results, and nested results can differ depending on the which ocean regional circulation model is used. Among aforementioned common regional circulation model, ROMS is one deserving highly reliable with a lot of high quality publication relate to ROMS. Moreover, there a vast of modelers are using ROMS with highly interacting via internet and annual meeting. Its model code, solutions to problem and reports of bugs are often repaired and developed (Marchesiello et al. 2001; Hedström, 2009; Penven et al. 2010; Pham et al 2016).

2.3.1 Governing equation

We employed Regional Ocean Modeling System (ROMS) for a simulation tool (Cambon et al. 2014). ROMS was originally based on a split-explicit, free-surface, terrain-following numerical model that solves the Reynolds-averaged Navier-Stokes equations subject to the Boussinesq approximation and hydrostatic vertical momentum balances (e.g., Hedström, 2009; Penven et al. 2010; Marchesiello et al. 2001).

The governing equations are:

$$\frac{\partial u}{\partial t}+\vec{V}\nabla u-fv=-\frac{1}{\rho}\frac{\partial p}{\partial x}-\frac{\partial}{\partial z}\left(\overline{u'w'}-\nu\frac{\partial u}{\partial z}\right) \quad (16)$$

$$\frac{\partial v}{\partial t}+\vec{V}\nabla v+fu=-\frac{1}{\rho}\frac{\partial p}{\partial y}-\frac{\partial}{\partial z}\left(\overline{v'w'}-\nu\frac{\partial v}{\partial z}\right) \quad (17)$$

$$\frac{\partial p}{\partial z}=-\rho g \quad (18)$$

The continuity equation is given by:

$$\frac{\partial u}{\partial x}+\frac{\partial v}{\partial y}+\frac{\partial w}{\partial x}=0 \quad (19)$$

The scalar transport is written as:

$$\frac{\partial C}{\partial t}+\vec{V}\nabla C=-\frac{\partial}{\partial z}\left(\overline{C'w'}-\nu_\theta\frac{\partial C}{\partial z}\right) \quad (20)$$

Where u,v,w represent components of vector velocity $\vec{V}$ in x, y and z direction; f is Coriolis parameter; ν,ν_θ show molecular viscosity and diffusivity; p is pressure; g is acceleration of gravity; C is scalar quantity, i.e. temperature (T), salinity (S). $\rho=\rho(T,S,p)$ is water density. An over bar terms in above equation are Reynolds stresses describing a time average and a prime represents a fluctuation around the mean. Such equations are closed by turbulent closure model.

$$\overline{u'w'}=-K_M\frac{\partial u}{\partial z},\quad \overline{v'w'}=-K_M\frac{\partial v}{\partial z},\quad \overline{C'w'}=-K_C\frac{\partial C}{\partial z} \quad (21)$$

with K_M, K_C are vertical eddy viscosity and diffusivity.

2.3.2 Turbulent closure model

The turbulent closure model in horizontal is Smagorinsky model. The vertical turbulent closure model implied in the research is K-Profile Parameterization (KPP) model which is described in detail in Large et al. (1994). The K-profile parameterization (KPP) has been expressed to perform well in open ocean settings. The main content of KPP is described as bellow (Hedström, 2009):

Surface boundary layer: The KPP matches separate parameterizations for vertical mixing between surface boundary layer with the ocean interior. A

formulation applied in the water column above a calculated boundary layer depth h_{sbl}, is relied on the boundary layer similarity theory. Then this parameterization matched at the interior with schemes that can account for local shear, double diffusive mixing effects and internal wave.

Viscosity and diffusivities above a calculated surface boundary layer depth (h_{sbl}) are the production of three terms including the length scale h_{sbl}, a turbulent velocity scale w_x and a non-dimensional shape function.

$$K_x = h_{sbl} w_x(\sigma) G_x(\sigma) \qquad (22)$$

Where σ is vertical coordinate system indicating depth within the surface boundary layer. The x subscription describe for one of momentum, temperature and salinity.

Surface boundary layer depth: The boundary layer depth h_{sbl} is calculated as the minimum of the Ekman depth $h_e = 0.7u_* / f$, the Monin-Obukhov depth $L = u_*^3 / (\kappa B_f)$, and the shallowest depth at which a critical bulk Richardson number is reached. The critical bulk Richardson number (Ri_c) is typically in the range 0.2-0.5. The bulk Richardson number (Ri_b) is calculated as:

$$Ri_b(z) = \frac{(B_r - B(d))d}{\left|\vec{V}_r - \vec{V}_a(d)\right|^2 + V_t^2(d)}, \qquad (23)$$

$$V_t^2(d) = \frac{C_v(-\beta_T)^{1/2}}{Ri_c\kappa}(c_s\varepsilon)^{-1/2} dNw_s, \quad (24)$$

where u_* is the friction velocity $u_* = \sqrt{\tau_x^2 + \tau_y^2}/\rho$, κ is von Karman's constant and B_f is the buoyancy flux, d is distance down from the surface, B is the buoyancy, B_r is the buoyancy at a near surface reference depth, $\vec{V}_a$ is the mean horizontal velocity, $\vec{V}_r$ the velocity at the near surface reference depth and V_t is an estimate of the turbulent velocity contribution to velocity shear, C_v is the ratio of interior N to N at the entrainment depth, β_T is ratio of entrainment flux to surface buoyancy flux, c_s and ε are constants, and w_s is the turbulent velocity scale for scalars

Turbulent velocity scale: Estimation of w_x (where x is m - momentum or s – any scalar) through the boundary layer is utilized surface layer similarity theory. The velocity scale is calculated as:

$$w_x = \frac{\kappa u_*}{\phi_x(\zeta)} \quad (25)$$

Where ζ presents the surface layer stability parameter and defines as z/L. ϕ_x describes a non-dimensional flux profile which varies relied on the stability of the boundary layer forcing. The stability parameter used in this equation is

assumed to vary over the entire depth of the boundary layer in stable and neutral conditions. In unstable condition it is assumed only to vary though the surface layer which is defined as εh_{sbl} (where ε is set at 0.1). Beyond this depth ζ is set equal to its value at εh_{sbl}.

The flux profiles are expressed as analytical fits to atmospheric surface boundary layer data. In stable conditions they vary linearly with the stability parameter ζ as

$$\phi_x = 1 + 5\zeta \qquad (26)$$

In near neutral unstable conditions common Businger-Dyer forms are used which match with the formulation for stable conditions at $\zeta = 0$. Near neutral conditions are defined as $-0.2 \le \zeta < 0$ for momentum and $-1.0 \le \zeta < 0$ for scalar. The non-dimensional flux profiles in this regime are,

$$\phi_m = (1 - 16\zeta)^{1/4} \qquad (27)$$

$$\phi_s = (1 - 16\zeta)^{1/2} \qquad (28)$$

In more unstable conditions ϕ_x is chosen to match the Businger-Dyer forms and with the free convective limit. Here the flux profiles are

$$\phi_m = (1.26 - 8.38\zeta)^{1/3} \qquad (29)$$

$$\phi_s = (-28.86 - 98.96\zeta)^{1/3} \quad (30)$$

The shape function: The non-dimensional shape function $G(\sigma)$ is a third order polynomial with coefficient chosen to match the interior viscosity at the bottom of the boundary layer and Monin-Obukhov similarity theory approaching the surface. This function is defined as a 3rd order polynomial

$$G(\sigma) = a_0 + a_1\sigma + a_2\sigma^2 + a_3\sigma^3 \quad (31)$$

The interior scheme: The interior scheme of KPP estimates the viscosity coefficient by adding the effects of several generating mechanisms: shear mixing, double-diffusive mixing and internal wave generated mixing.

$$K_x(d) = K_x^s + K_x^d + K_x^w \quad (32)$$

Shear generated mixing: The shear mixing term is calculated using a gradient Richardson number formulation, with viscosity estimated as:

$$K_x^s = \begin{Bmatrix} v_0 & Ri_g < 0 \\ v_0\left[1-\left(Ri_g / Ri_0\right)^2\right]^3, & 0 < Ri_g < Ri_0 \\ 0 & Ri_g > Ri_0 \end{Bmatrix}, \quad (33)$$

Where v_0 is 5.0x10^{-3}, $Ri_0 = 0.7$

Double diffusive processes: The second component of the interior mixing parameterization represents double diffusive mixing. Form limited sources of laboratory and filed data parameterize the salt fingering case ($R_\rho > 1.0$)

$$K_s^d\left(R_\rho\right) = \begin{cases} 1\times 10^{-4}\left[1-\left(\frac{\left(R_\rho-1\right)^2}{R_\rho^0-1}\right)^3\right], \; for 1.0 < R_\rho < R_\rho^0 = 1.9 \\ 0, otherwise \end{cases} \qquad (34)$$

$$K_\theta^d\left(R_\rho\right) = 0.7K_s^d$$

For diffusive convection ($0 < R_\rho < 1.0$) KPP suggest several formulation from the literature and choose the one with the most significant impact on mixing.

$$K_\theta^d = (1.5^{-6})(0.909\exp(4.6\exp[-0.54(R_\rho^{-1}-1)]) \qquad (35)$$

for temperature. For other scalars

$$K_s^d = \begin{cases} K_\theta^d\left(1.85-0.85R_\rho^{-1}\right)R_\rho, 0.5 \le R_\rho < 1.0 \\ K_\theta^d 0.15R_\rho, otherwise \end{cases} \qquad (36)$$

Internal wave generated mixing: Internal wave generated mixing serves as the background mixing in the KPP scheme. It is specified as a constant for both scalars and momentum. Eddy diffusivity is estimated based on the data of Ledwell et al (1993). While Peters et al suggest eddy viscosity should be 7 to 10 times

larger than diffusivity for gradient Richardson number below approximately 0.7. Therefore, KPP use

$$K_m^w = 1.0x10^{-4} m^2 s^{-1} \quad (37)$$

$$K_s^w = 1.0x10^{-5} m^2 s^{-1} \quad (38)$$

2.3.3 Horizontal and vertical grid

The horizontal and vertical discretization used second-order finite-different approximation. The horizontal arrangement of variables equivalent to the well-known Arakawa "C" grid, and the vertical arrangement is well behaved with staggered vertical grid as shown in the Fig. 2.8.

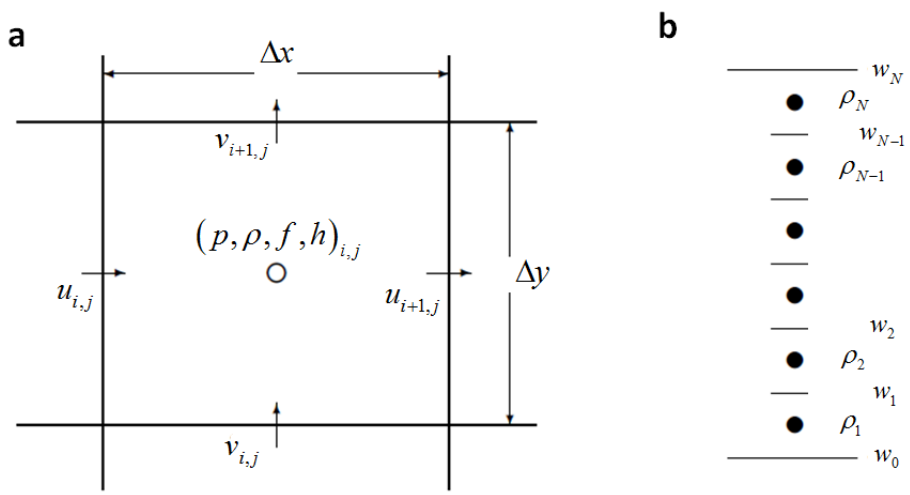

Figure 2.8 Placement of variable on (a) an Arakawa C grid in horizontal, (b) staggered vertical grid (Hedström, 2009).

CHAPTER THREE

3. EFFECT OF ERROR SOURCES ON THE RESULTS OF ORCMs.

3.1 Introduction

Due to the limited resolution of the Ocean Global Circulation Models (OGCM) to be applicable to the small regional domain, methods of downscaling from the OGCM to the Ocean Regional Circulation Models (ORCM) have been studied and developed over the several decades (Li et al. 2012; Herbert et al. 2014). However, the errors due to the differences in spatial and temporal resolution between two models are unavoidable. Therefore, the ORCMs are still suspicious because of bear a lot of aforementioned potential errors relate to downscaling technique causing the uncertainties results. Such errors may limit the application of ORCMs in the studying of local problem (Warner et al. 1997; Denis et al. 2002).

Nevertheless, there is not a standard method to assess how well information from the larger to the smaller domains can be assessed. In the traditional method, the simulated oceanic statistics are compared with observation data and OGCMs output. But this method cannot separate the errors whether they arise from model or observation limitations. Also, the OGCMs only support large-scale with rough resolutions, they, therefore, do not have small scales motions as in the ORCMs

simulates with higher resolutions (Denis et al. 2002). In this chapter, we presented the application of the BBE for the downscaling assessment of ORCMs which can eliminate errors from models errors and observation limitations. Therefore, they enable us to verify separately errors contributing from the nesting and downscaling technique. Further, based such separate errors assessment we proposed the optimal setup and evaluated the downscaling ability of the ORCMs.

3.2 Model set-up

The Big-Brother simulation, with 3 km × 3 km grid resolution, was performed over a large domain: 128.50°E to 133.50°E longitude and 36.10°N to 38.51°N latitude, equivalent to lengths of 450 km and 273 km, respectively, in the East Sea of Korea. The domain of the Little-Brother, embedded with the same resolution as the Big-Brother domain, extended from 129.90°E to 132.30°E longitude and 36.58°N to 38.19°N latitude, equivalent to 216 km and 183 km, respectively (Fig. 3.1). Bathymetries were extracted from ETOPO1, which is a global, integrated bathymetric, digital elevation model with a cell size of 1 arc-minute (Amante and Eakins, 2009). Both the Big-Brother and Little-Brother were run with 30 vertical layers of the *S*-grid, where *S* is a nonlinear function of the actual coordinates which can flexibly adjust the vertical depth resolution (Hedström, 2009).

For the open boundary condition, the radiation method was selected; it is specifically described in section 3.3.1. The model's turbulence closure scheme for

calculating eddy viscosities and eddy diffusivities is the K-profile parameterization (Large et al., 1994). The initial conditions were provided over the whole domain at the start of the integration and only the boundary conditions were updated at any given time. Both initial and boundary conditions of Little-Brother were filtered. The small scales depend on the resolution jump. The results were saved every 10 minutes in the Big-Brother simulations. The resolution jump is calculated as:

$$J = \frac{\ell_{BB}}{\ell_{LB}} \ , \qquad (39)$$

Here, ℓ_{BB} is the filtered wavelength in the coarser Big-Brother; ℓ_{LB} is the shortest resolvable wavelength in the finer Little-Brother. The shortest wavelength equals grid resolution multiplied by 2. For instance, from the original Big-Brother having the grid resolution of 3 km, if we want to have a new Big-Brother with a grid resolution of 9 km, the filtered wavelength in original Big-Brother ℓ_{BB} is 18 km; and if the Little-Brother grid size is 3 km, the ℓ_{LB} is 6 km; and then the resolution jump is J = 3. A low-pass filter of the Discrete Cosine Transform, which can control the choice of the wavelengths to be removed, was used to generate the Little-Brother ICs and LBCs. As stated earlier, the dynamic downscaling method we used is similar to that used by Denis et al. (2002a) in their atmospheric model. However, in our current work, the resolution of the ORCM is finer; hence the removed wavelengths are much smaller than those of Denis et al. (2002a). In addition, downscaling ability was tested for various domain sizes and resolutions of

the LBCs in order to identify the effects of error sources numbers 3 and 4 on the results of the ORCM. Those effects were also addressed in previous atmospheric studies (Leduc and Laprise, 2008; Leduc et al. 2011).

Most experiments simulated 30 days (from September 1st to September 30th) in 2011. The Big-Brother used oceanic information from the global hindcast HYCOM output, which is available on the web site of the Center for Ocean-Atmospheric Prediction Studies (COAPS, http://hycom.coaps.fsu.edu/thredds/catalog.html). Oceanic variables, including sea temperature, salinity, horizontal momentum and sea surface height are provided at every 1/12° × 1/12°(~ 9 km), discretized with 33 vertical layers (0 - 5.5 km) in the *z*-coordinate, and updated every 24 hours, as described in detail in COAPS and Metzger et al. (2008). The results of HYCOM were validated for currents, eddies and temperature by comparing with other model results and observations in the East Sea of Korea (Hogan and Hurlburt. 2006; Hurlburt et al. 2008). In the East Sea of Korea, the primary warm current flows northeastward through the Korea/Tsushima Straits (Chang et al. 2004; Hurlburt et al. 2008).

The annual mean volume transport rates of this warm current range from 0.5 to 4.2 Sv and seasonal variations of transport rate range from 0.7 to 4.6 Sv (Chang et al., 2004). The transported warm current splits into two main branches following the Japanese and Korean coasts. The first branch (Nearshore Branch) flows eastward along the northeastern northern coast of Japan. The second branch (East

Korean Warm Current) flows northward along the eastern coast of Korea. The second flow through the channel of the Korea/Tsushima Straits sometimes forms the Offshore Branch, which flows along the coast of Japan, following the continental slope (Teague et al. 2006). The annual volume transport through the Korea/Tsushima Straits was estimated at approximately about 2.74 Sv for year 2011, and the volume transport of the East Korean Warm Current was 1.62 Sv, with large seasonal variations (Takikawa et al. 1999; Chang et al. 2004; Teague et al. 2006).

Therefore, near the area of interest, the average current speeds are expected to be approximately 14.7 km/day in the winter and 21.6 km/day in the summer. Along with the hydrodynamic circulation patterns, sea surface temperatures and other oceanic variables show monthly variations. The coldest month is February, during which relatively strong vertical mixing occurs. The warmest month is August, when there is strong stratification, as suggested by previous studies (Chu et al. 2001a; and Liu and Chai, 2009). Thus, a simulation period of one month may be the minimum time scale for responses, as most signals and errors are not expected to take longer than 20 days to pass from a boundary to the opposite open boundary, over the area of interest. A possible exception may be when strong seasonal advection affects the estimation of numerical errors.

The atmospheric data were downscaled from the results of the NCEP final operational global analysis (NCEP-FNL), by using the Weather Research Forecast

(WRF) model. The NCEP-FNL supplies data at every 1° × 1° grid point and provides updates every 6 hours; it was downscaled to the same grid size as the ocean models. The main atmospheric variables include wind speed at 10 m, atmosphere pressure, relative humidity, atmosphere surface temperature, precipitation, and net short- and long-wave heat fluxes.

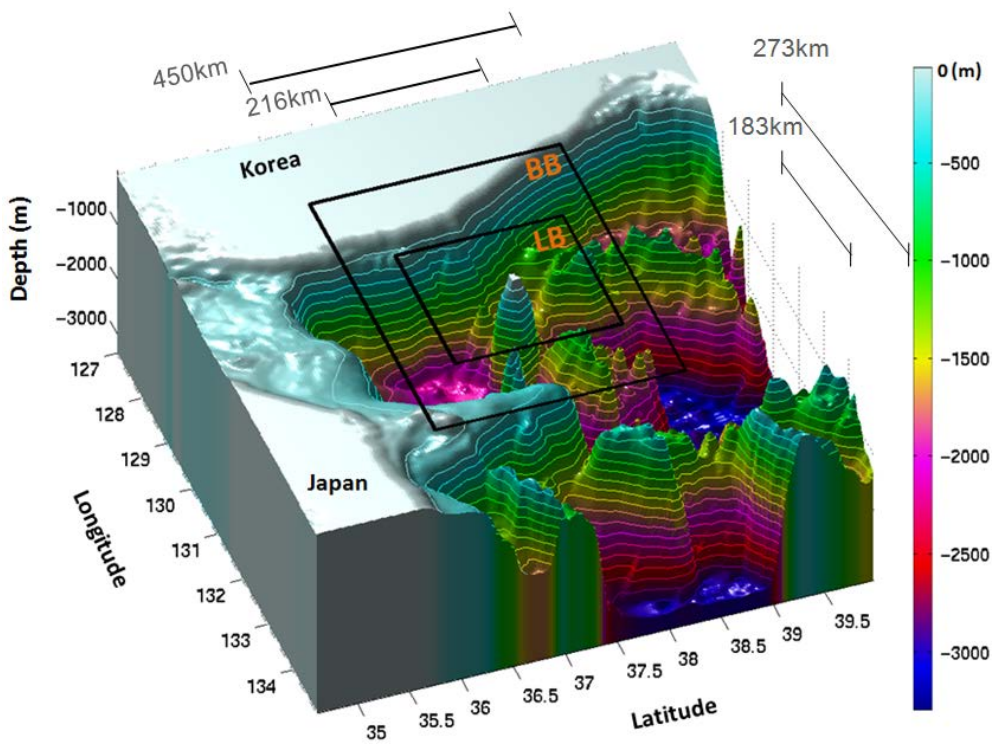

Figure 3.1 Geographical layout of the study area. The large and small rectangular areas, enclosed by solid lines, denote the simulated domains for the Big-Brother and Little-Brother.

3.3. Results

The BBE identified four among the six error sources, as discussed in the previous section. First, we evaluated the role of OBCs, which have a first order effect on solutions of ORCMs. Second, we analyzed spin-up effects, which cannot be avoided in implementation of initial conditions. Third, we studied the errors caused by the different spatial and temporal resolutions for the driving data and the nested model at the boundaries. In the fourth experiment, we assessed the effects of domain sizes associated with the propagation of errors produced at the boundaries. Finally, the pattern and magnitude reproductions by the ORCMs are discussed.

3.3.1 Boundary condition types

Defining and prescribing boundary conditions for artificial boundaries is a necessity in all the ORCMs, in order to close the system of equations and to obtain a well-posed problem (Blayo and Debreu, 2005). Ideal Open Boundary Conditions (OBCs) are to evacuate the outgoing information reaching the boundary without deterioration of the inner model solution, and to make the model solution compatible with the extra knowledge on incoming information. Over several decades, numerous methods to implement OBCs have been proposed (Chapman, 1985; Palma and Matano, 1998; Blayo and Debreu, 2005).

The OBCs have a first order effect on the solutions of the ORCMs. Therefore, the choice of reasonable OBCs is important but difficult, and has been

the subject of many studies. However, the selecting of OBCs seems to depend on the cases and conditions of the experiments. Then again, the appropriate implementation of OBCs is still in debate, as even the same OBCs have given different results in several comparative studies (Tsynkov, 1998; Marchesiello et al. 2001; Blayo and Debreu, 2005). We decided to test some popular OBCs, as summarized below.

Clamped: This is simple and widely used in both ocean and atmosphere modeling. However, its performance is still far from obvious. For example, Chapman (1985) and Durran (2001) commented that "clamped" OBCs need to be avoided as they perform poorly, because of a tendency to reflect outward propagating disturbances. In contrast, "clamped" OBCs were reported to provide good results in several comparative studies (Holloway, 1996; Katsumata, 2005; Carter and Merrifield, 2007 and Cailleau et al., 2008).

Flather: Flather (1976) proposed an OBCs for barotropic flow which can combine the Sommerfeld equation with a one-dimensional version of the continuity equation in case of outwardly normal direction at an open boundary.

$$\overline{v_n} = \overline{v_n^{ext}} - \sqrt{\frac{g}{h}}\left(\eta - \eta^{ext}\right), \qquad (40)$$

Where $\overline{v_n}$ is the normal component of the barotropic velocity, $\overline{v_n^{ext}}$ represents the external information and h is the local water depth.

In this equation, the differences between the external information and the local model are allowed to propagate out of the domain at the speed of the external gravity waves. The propagation is always outward so it does not need an adaptive scheme. Therefore, These OBCs itself can satisfy two necessary conditions for a hyperbolic system: (1) allow the perturbations which were generated inside the computational domain to leave freely without deterioration of the inner model solution, (2) provide consistency between external data and model solutions (Blayo and Debreu, 2005). This OBC performed well in many previous studies (Flather, 1988; Palma and Matano, 1998; and Palma and Matano, 2001). However, the "Flaher" restricts to the physical assumption that surface gravity waves should be dominant.

Raymond and Kuo Radiation (R-K radiation): The "radiation OBCs" based on the work of Raymond and Kuo (1984) and associated with an adaptive technique (Marchesiello et al., 2001) can work well for cases when waves approach the boundary at an angle. These OBCs mitigate errors due to reflections. The R-K radiation with adaptive technique can be written as:

$$\frac{\partial \phi}{\partial t} + c_x \frac{\partial \phi}{\partial x} + c_y \frac{\partial \phi}{\partial y} = -\frac{1}{\tau}\left(\phi - \phi^{ext}\right) \qquad (41)$$

$$c_x = -\frac{\partial \phi}{\partial t} \frac{\partial \phi / \partial x}{\left(\partial \phi / \partial x\right)^2 + \left(\partial \phi / \partial y\right)^2} \qquad (42)$$

$$c_y = -\frac{\partial \phi}{\partial t}\frac{\partial \phi / \partial y}{\left(\partial \phi / \partial x\right)^2 + \left(\partial \phi / \partial y\right)^2} \qquad (43)$$

Where ϕ is prognostic model variables, $\left(c_x, c_y\right)$ are projection of oblique radiation in the normal and tangential directions to the boundary in local Cartesian coordinates, τ represents the time scale for nudging, with $\tau = \tau_{out}$ if $c_x > 0$, $\tau = \tau_{in}$ if $c_x < 0$, $\tau_{out} \geq \tau_{in}$. During outward propagation, a weak nudging can prevent substantial drifts while avoiding over-specification problems. While during inward propagation, a strong nudging is applied but not so that it produces a data shock problem (Marchesiello et al. 2001).

Simulations with these three types of OBCs were performed and compared (Table 3.1), in J3 spatial resolution without temporal interpolation (not shown in Table 3.2). The simulations were set for both with and without sponge and nudging layers in order to assess their role on the results of the ORCMs. The 10 grid points set for the sponge and nudging layers always lay along the lateral boundaries. The time scale for nudging during outward propagation was set at 3 days and the time scale for nudging during inward propagation at 365 days.

The solutions from the “flather” method appear to be the best when supplementary methodologies of sponge/nudging are not applied (Table 3.1). In terms of the diagnostic variables associated with temperature and vorticity, the “flather” method has the highest CORs and smallest CRMSD, whereas the results

of “R-K radiation” are of poorer quality and just slightly better than the “Clamp” method. The performance of the three OBCs is not a surprise since the “flather” can, on its own, satisfy the requirement for OBCs in hyperbolic systems (Blayo and Debreu, 2005). Note that the “R-K radiation” method without sponge/nudging is similar to the clamped condition, in that the model solution at the boundary never departs significantly from the external data (Tréguier et al. 2001; Blayo and Debreu, 2005).

Table 3.1 COR and CRMSD of each field depending on the OBC method with/without setting sponge/nudging **(**Extracted from Pham et al., 2016**).**

Statistics	**Clamped OBC method**		**Flather OBC method**		**Radiation OBC method**	
	Tempera-ture (°C)	**Vorticity (s^{-1})**	**Tempera-ture (°C)**	**Vorticity (s^{-1})**	**Tempera-ture (°C)**	**Vorticity (s^{-1})**
Without sponge/nudging layer						
COR	85.2	74.3	91.6	92.4	87.6	80.5
CRMSD	0.101	0.177	0.054	0.069	0.084	0.135
With sponge/nudging layer						
COR	88.1	77.6	96.2	96.9	96.3	97.1
CRMSD	0.090	0.125	0.049	0.066	0.047	0.065

When supported by sponge/nudging, the quality of the results obtained increases significantly, especially for the “R-K radiation” results. The solutions from the “R-K radiation” method perform the best. The CORs are highest and close to 100% for both temperature and vorticity with the “R-K radiation” method. The CRMSDs between the Little- and Big- Brothers are smaller for the “R-K radiation” method than for the “flather” or “clamped” methods. It is believed that sponge/nudging provides most of efficiency for the “R-K radiation” method (Marchesiello et al. 2001). Although the “flather” is depth averaged and commonly used in barotropic models, suggesting that it may be appropriate for assessing downscaling ability, our comparisons show slightly better results with “R-K radiation” OBCs when the supplementary methodologies of sponge/nudging are employed. Thus, we chose the latter for the present study.

3.3.2 Error during spin-up time in generating small-scale structure

Initial and boundary conditions produced by coarser global models do not have small-scale fluctuations. Therefore, it takes spin-up time to generate sufficient small-scale fluctuations and it is necessary to assess the degree to which such under-specified small-scale motions raise the error of downscaling with the ORCM. The spin-up time needed to regenerate small-scale motions compatible with the Big-Brother simulation was studied with J3 spatial resolution, and the LBC was updated every 10 minutes. At first, to reduce the effects of smaller-scale randomness for analysis and to emphasize the main trends of changes of errors, 10

sets of 4-days integrations of the ORCMs were implemented to the Little-Brother domain, successively, beginning on September 1st. For example, the first 4-day integration was from the 1st to the 4th and the second 4-day integration was from the 2nd to the 5th.

Figure 3.2 (a) and (b) show the CRMSDs of the Little- and Big-Brother depth-averaged z-vorticity at 12 and 48 hours. At both times, CRMSD values at the boundaries are higher, and they seem to increase from 12 to 48 hours and propagate from the boundaries into the inner domain. After the first 12 hours (Fig. 3.2 (a)), CRMSDs show lower values over the sub-region of the domain compared with the case after 48 hours (Fig. 3.2 (b)). The errors due to the LBCs grow with time, whereas the errors generated by the ICs decrease as time passes. This is because the mean z-vorticity RMSDs of Little- and Big-Brother simulations are significantly reduced after 4 days of simulation (Fig. 3.2 (c)). Even though such results of initial periods are not practically important in operational research, this information can help us determine an optimized initial spin-up period. For example, Elía et al. (2002) found that the existence of small-scale fluctuations in the initial conditions can help reduce the discrepancies between BB and LB, more than the existence of small-scale fluctuations at LBC.

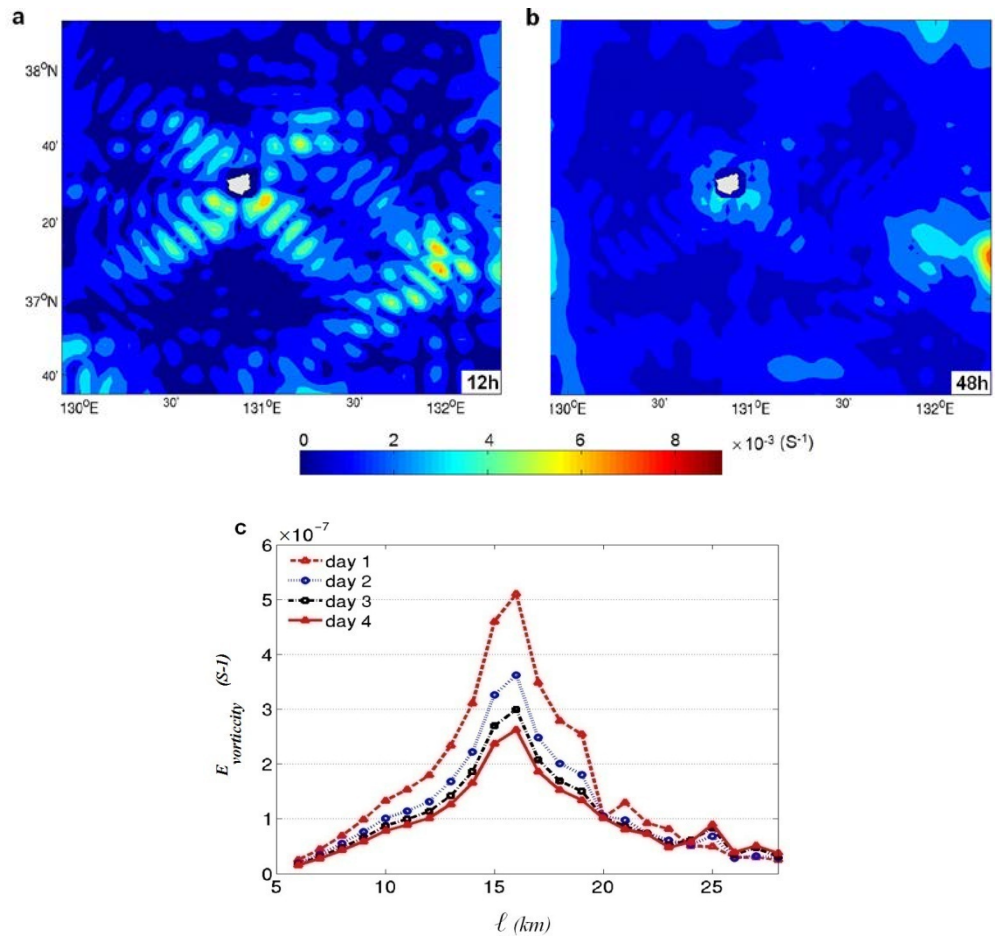

Figure 3.2 CRMSDs of the Little-and Big-Brother depth-averaged z-vorticity after (a) 12 and (b) 48 hours. And (c) the mean z-vorticity RMSD (*E*) of the Little-and Big-Brother in the sub-region of 186 km and 153 km, within 216 km and 183 km, for low level of wavelengths (Extracted from Pham et al. 2016).

In turbulent flows, larger eddies contain the most energy initially, and this energy cascades from larger to smaller scales (Tennekes and Lumley, 1997) at later times. In a similar way, after filtering out small-scale motions, larger scale motions produce smaller scale motions by non-linear energy cascades. Comparing kinetic

energies at the same wavelength in the Little- and Big-Brother simulations, we can determine whether small-scale motions in the Little Brother grow to similar magnitudes in the Big-Brother simulation. Kinetic energy (*KE*) at a given wavelength ℓ is given by

$$KE(\ell) = \frac{1}{N_z}\sum_{1}^{N_z}\frac{1}{N_x N_y}\sum_{1}^{N_x}\sum_{1}^{N_y}\frac{1}{2}\left(u(\ell)^2 + v(\ell)^2\right), \qquad (44)$$

Where N_x and N_y are the respective number of longitudinal and latitudinal grids; N_z is the number of vertical layers; and $u(\ell)$ and $v(\ell)$ are the momentum components in the *x* and *y* directions, respectively. The ratio of the kinetic energies at the given wavelength is

$$R_{KE}(\ell) = \frac{KE_L(\ell)}{KE_B(\ell)} \times 100, \qquad (45)$$

Where $KE_L(\ell)$ and $KE_B(\ell)$ are the average kinetic energies of the Little-Brother and Big-Brother simulations, respectively.

Figure 3.3 (a) and (b) present the ratio of kinetic energies of the averaged results of 10 runs of the Little-Brother, depending on the wavelength during the first 18 hours. Initially, all small-scale perturbations with wavelengths smaller than 18 km are removed by the low-pass filter in the Little-Brother simulation. After 10 minutes, these perturbations grow to around 50% of the Big-Brother amplitudes at the smaller scales ($\ell < 12$ km). The Little-Brother needs 50 minutes to recover 80% of the *KE* of the unfiltered Big-Brother in the range of 6 km $< \ell <$ 12 km (Fig. 3.3

(a)) and only 60% was recovered at the smallest scale. After 6 hours, as shown in Fig. 3.3 (b), the Little-Brother *KE* grows over the Big-Brother for all smaller scales and starts to decrease and at around 15 hours is just slightly smaller than the Big-Brother *KE* for all wave numbers. After that, between 15 and 18 hours, the *KE* ratios do not change significantly (Fig. 3.3 (b)).

The *KE* is proportional to the vorticity (Fig. 3.3 (b) and (c)). Therefore, the increase of *KE* could be commensurate with increasing the vorticity. In other word, the increase in *KE* is interpreted as the growth of small-scale motions, which are produced by the energy cascade from larger scales through the process of breaking from the larger vorticities (larger eddies) to smaller vorticities (smaller eddies). The energy of small-scale motions increases and exceeds that of Big-Brother after 3 hours of simulation. When there is a lack of small–scale fluctuations, the *KE* is not efficiently dissipated and *KE* accumulates at the larger scale. Energy dissipation is most efficient at the smallest scale even though the energy reaches a maximum at the largest scale. After 3 hours, when the *KE* at the smallest scale of $\ell = 6$ km (Fig. 3.3 (b)) becomes 100 % of the Big-Brother energy, and dissipation becomes most efficient, *KE* begins to decrease.

Compared with the original Big-Brother simulations, the Little-Brother simulations have fewer small-scale fluctuations that dissipate energy efficiently from the initial time onward. After 3 hours, small-scale fluctuations develop completely and play more significant roles in dissipating. After 15 hours, *KE* at the small-scales remains at a steady state and the model may achieve a threshold at the

equilibrium state. Assuming that the achievement of equilibrium is a spin-up level, 15 hours could be a spin-up time for producing small-scale motions, which may exist before filtering.

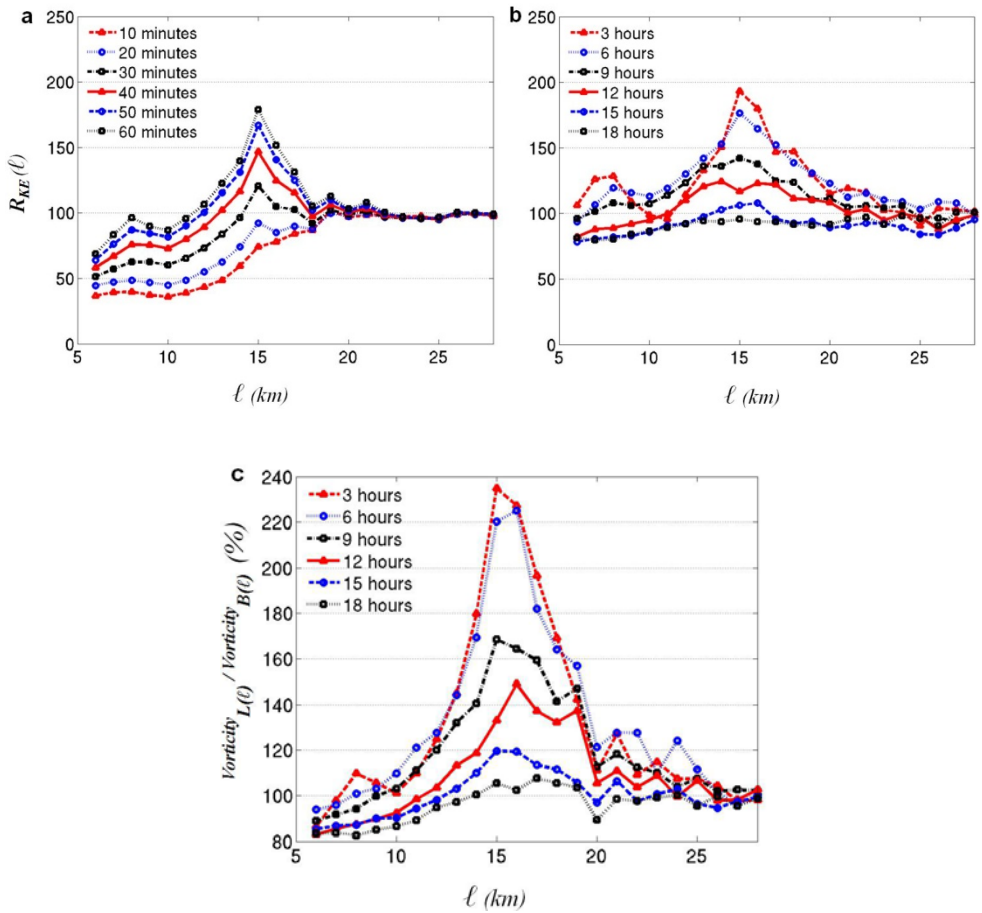

Figure 3.3 Ratio of kinetic energies and vorticities of averaged results of 10 running times of the Little-Brother to Big-Brother; (a) the comparison of *KE* during shorter and earlier times, (b) the comparison of *KE* during longer times, and (c) the comparison of vorticities during longer times (Extracted from Pham et al. 2016).

However, it should be noted that 15 hours of spin-up time is required only when the Big-Brother is filtered at a wavelength of 18 km. Consequently, as the grids of the global model are coarser than this, it will take longer to achieve equilibrium. Denis et al. (2002a) showed that the spin-up time for generating climatic filtered scale motions that are less than 500 km is 12 hours in the atmosphere. In our study, 15 hours of spin-up time were required for generating oceanic filtered scale motions of less than 18 km, which is a much smaller scale than Denis et al.'s, because atmospheric climate phenomena occur more quickly than oceanic phenomena.

3.3.3. Effects of lateral boundary

The errors driven by LBCs are unique and they are unavoidable aspects of the nesting process. These errors can significantly affect nested model results (Warner et al. 1997; McDonald, 1999; Denis et al. 2002). As noted in the previous section, the errors produced by LBCs tend to grow and propagate into the inner domain, degrading the solution of the nested model. Here, we separate and individually evaluate such effects caused by the spatial resolution and the updating period of the LBCs and the domain size or distance from the LBCs to the interested area, by assessing one-month "oceanic statistics". Moreover, the performance of these one-month "oceanic statistics" helps us determine the model bias or oceanic drift after the regional model has run for a long time.

3.3.3.1. Experimental set-up for lateral boundary resolution

Table 3.2 summarizes all the experimental cases in assessing the effect of the diverse LBCs' resolution on the results of ORCMs. The rows are for studying the effect of the temporal updating of the LBCs. Five cases were chosen: U1, U6, U12, U16 and U24, which correspond to the intervals for updating the old LBCs with new LBCs from the Big-Brother simulation every 1, 6, 12, 16 and 24 hours, respectively. The Little-Brother requires LBCs every 10 minutes, so the Big-Brother data need to be temporally interpolated. For example, the U6 data should be interpolated linearly at 10 minute intervals for 6 hours and provided as LBCs to the Little-Brother.

The columns are for studying the effect of the spatial resolution jump ratio between LBCs and the Little-Brother. Seven cases were selected, including J1, J3, J6, J9, J12, J18 and J24. The resolution jump (J) is the ratio between the spatial resolution of the Big-Brother driver and that of the nested Little-Brother model (Denis et al. 2002a). Here, J is purely the horizontal resolution jump. Vertical resolution may affect the results of ORCMs because of inconsistencies and imbalances between driving data and the driven model, as pointed out by Caya and Laprise (1999) and Denis et al. (2002a). However, the assessment of the impact of the vertical resolution as well as the mutual effects between horizontal and vertical resolutions are not covered here, as the variations of the resolutions of vertical layers are generally not as diverse as horizontal ones.

Table 3.2 The set of performed experiments. 'J' presents the jump ratio. For example, J3 means the jump ratio is 3. 'U' means updating period. For example, U6 indicates that data were updated every 6 hours. Simulated cases are marked "○", non-simulated cases are marked "×".

Updating Interval (hour) / **LBC Interval (km)**	**1**	**6**	**12**	**16**	**24**	**Spatial case name**
3	○	○	○	○	○	**J1**
9	○	○	○	○	○	**J3**
18	○	○	○	○	○	**J6**
27	○	○	○	○	○	**J9**
36	○	○	○	○	○	**J12**
54	○	×	×	×	×	**J18**
72	○	×	×	×	×	**J24**
Temporal case name	**U1**	**U6**	**U12**	**U16**	**U24**	

Based on these previous studies, the range of jump ratio was determined. For the nesting from the large to very fine scale, Barth et al. (2005) implemented a triple cascade of embedded domains to cover the whole of the Mediterranean Sea and suggested resolution jump ratios from 3 to 5 at each nesting step. Spall and Holland (1991) concluded that the nested domain reproduced results reasonably well with grid ratios up to 7, and Blayo and Debreu (2005) mentioned that the ratio between driving data and driven models typically ranges from 5 to 20. If one wants to simulate a regional coast with ORCMs with a grid resolution of 0.5 km by

downscaling from the global model, for example HYCOM with resolution of 9 km, the resolution jump is 18. If this ratio seems to be too large, then multiple nesting "cascades" should be considered. Therefore, to address all the effects of LBC spatial resolution on nested results, we chose resolution jump ratios covering the aforementioned range.

3.3.3.2. Effect of LBC spatial resolution

The effects of errors on the nested results were examined in the diverse LBC resolutions. The LBCs were produced by linear interpolation of the hourly data from the filtered Big-Brother simulation. The interpolated data for LBCs were updated at 10 minute intervals in all cases to exclude errors due to the temporal updating scheme. Therefore, all cases were the U1 category (Table 3.2), excepting the J1 case. The LBCs of J1 were originally obtained from every 10 minutes of the unfiltered Big-Brother simulation, in order to avoid the inconsistent small scale effect which was produced by linear interpolation of the hourly data from the unfiltered Big-Brother. The original unfiltered Big-Brother was used as a reference and taken as representing real values.

Figure 3.4 presents Taylor diagrams of temperature and vorticity. When the relative CRMSDs are evaluated by;

$$\mathrm{CRMSD}_{relative} = \sqrt{\frac{\mathrm{CRMSD}^2}{\mathrm{SDS}_B^2}} \times 100\ (\%)\ , \qquad (46)$$

As the jump ratio increases from 1 to 24, the relative CRMSDs increase and the CORs decrease in temperature and vorticity in both months (Fig. 3.4). Therefore, as we expected, the quality of reproduction by the nesting becomes better as the jump ratios become smaller. This is because of two reasons: (1) the higher resolution jump causes more loss of driving information at the LBCs, and therefore degrades the solution of the ORCMs; (2) the discontinuity at the open boundaries between the driving data and driven model is increased with the higher resolution jump. Therefore, it causes larger wave transfer back to the inner domain and generates larger errors.

From a seasonal perspective, while the vorticities were reproduced slightly better in summer than in winter, the temperatures in summer appeared a little worse than in winter. It is because the temperatures vary seasonally, having high temperature with strong stratification in the summer, and low temperature with strong mixing in the winter. In summer, temperature decreased sharply from the surface (22 °C) to a depth of 200 m (2 °C) with a strong thermocline. In other words, the jump ratio could affect the temperature field more significantly in summer because of strong stratification (Fig. 3.4 (b)). In contrast, in winter, due to strong mixing, the temperature does not change from the surface to a depth of 80 m (10 °C), below which it gradually decreases with increasing depth. Therefore, a change in the resolution jump ratio does not affect the temperature results in the winter as much as in the summer (Fig. 3.4 (a)).

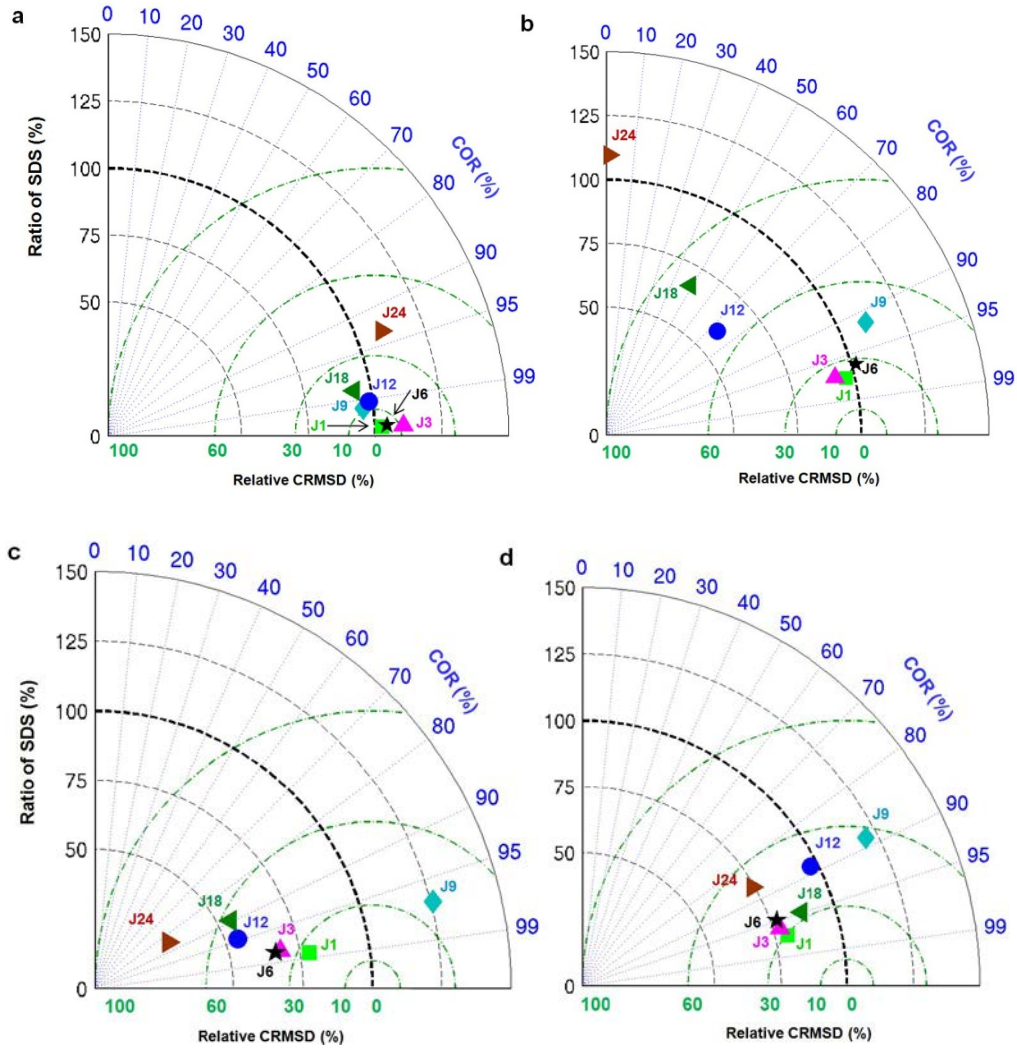

Figure 3.4 Taylor diagrams for the U1 case after 4 days: (a) temperature in February, (b) temperature in September, (c) *z*-direction vorticity in February, and (d) *z*-direction vorticity in September **(**Extracted from Pham et al. 2016**)**.

As the spatial resolution increases, the downscaled *z*-direction vorticity improves during the first 4 days. After that, the results are similar in all the

resolved cases. This means that after the spin-up, small-scale motions recover in the momentum fields (Fig. 3.4 (c) and (d)). Moreover, roughly resolved LBCs do not always decrease the quality of the vorticity. So, we suspect that errors accumulate in the inner domain. For instance, J18 provides better results than J9 and J12 (Fig. 3.4 (d)). However, the acceptable resolution jump ratio must still be 3, with approximately 97.0 % of the COR after spin-up time.

3.3.3.3 Effect of temporally updating the LBCs

Due to the spatial spin-up of fine scales and horizontal interpolation error, the LBCs generate errors whenever they are updated. To investigate the effect of updating the LBCs, at the various temporal resolutions, numerical simulations were performed similar to those described in the previous section. These simulations are summarized in Table 3.2. The LBCs are reconstructed by linear interpolation between the updating times, to synchronize with the regional temporal time step. For example, in the case of U6, two data sets of initial and final time steps, 6 hours apart, are interpolated, producing data every 10 minutes to feed LBCs for the Little-Brother simulations. The results of each Little-Brother simulation are compared to the unfiltered original Big-Brother as a reference. In this experiment, all cases have the same spatial resolution as the original Big-Brother, and this can help separate the errors from the spatial interpolations.

Figure 3.5 displays the results of the comparison between the unfiltered original Big-Brother and Little-Brother simulations, with different updating of the

LBCs in both February and September. As shown by Figure 3.5 (a) and (b), shorter updating times did not always improve the quality of the reproduced salinities. In winter, salinity shows no variation (Fig. 3.5 (a)) but in summer, shorter updating does not guarantee better results (Fig 3.5 (b)). In summer, cases U1, U6 and U12 have almost similar correlation values of about 90% and U16 and U24 have 80% and 40%, respectively (Fig. 3.5 (b)). While the correlation coefficient increases as the updating interval decreases, the relative CRMSD pattern and the SDS are not improved. For example, in the case of U12, for which the LBCs were updated every 12 hours, relative CRMSD and SDS are smaller than for U1, which rapidly updates the boundary conditions. However, the difference between U1 and U12 is too small ($O(10^{-4})$) to say that one or the other has better performance.

The difference between the SDSs of U1 and U12 is approximately 30% and the relative CRMSD difference between them is 25%. Unlike salinity, vorticity is reproduced better from all three perspectives for cases with short updating intervals (Fig. 3.5 (c) and (d)). As updating becomes more frequent, the reproduction seems to become better. The Taylor diagram for temperature is not presented here since it behaves very similarly to (and is not significantly different from) that of salinity.

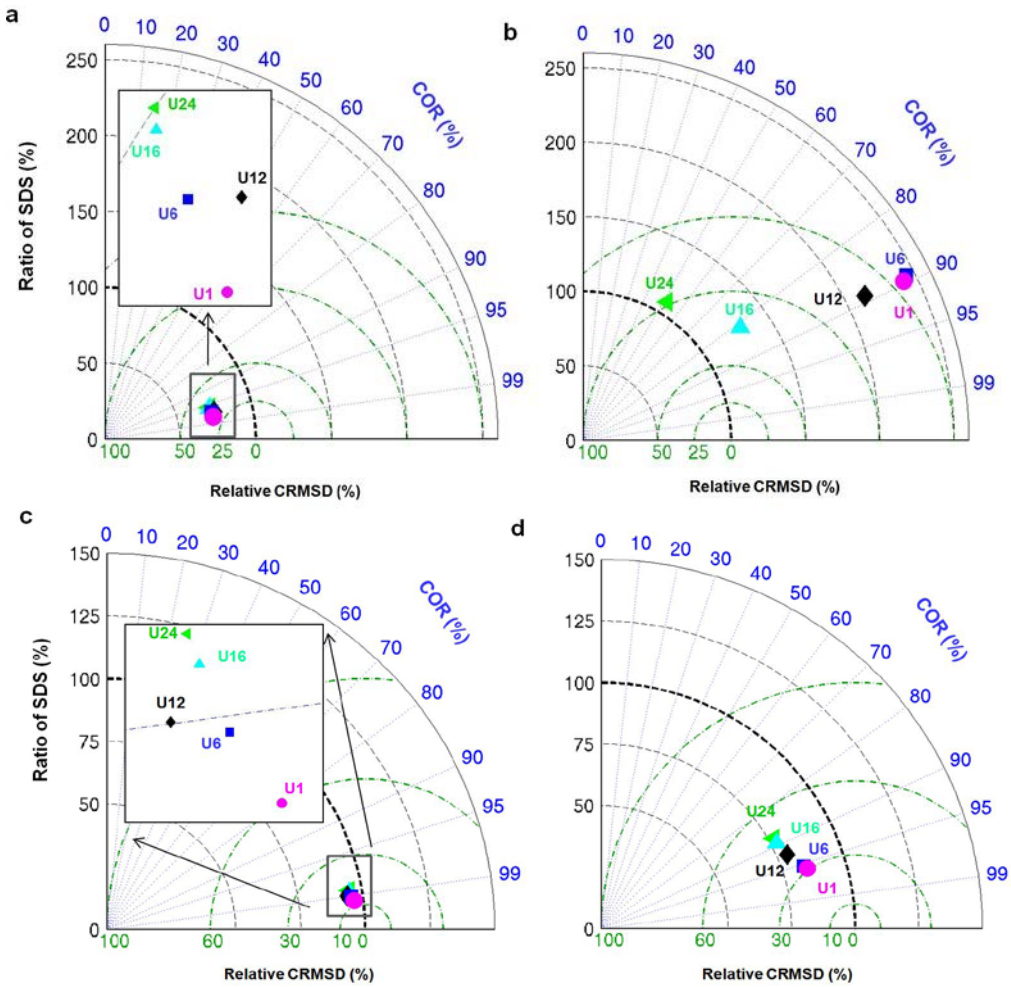

Figure 3.5 Taylor diagrams for the J1 case, showing the effect of updating time on each field: (a) salinity in February, (b) salinity in September, (c) *z*-direction vorticity in February, and (d) *z*-direction vorticity in September (Extracted from Pham et al., 2016).

We could not find significant differences of any variables in each field when we compared U1, U6 and U12 for the J1 case. U12 seems, overall and in

terms of salinity, to show better SDS and relative CRMSD compared to U6. But U1, U6, and U12 do not show significant differences in the salinity field or in the temperature field (not shown here). In terms of vorticity, U1 and U6 agree well with the original Big-Brother data, but even U12 shows reasonable prediction levels for all three variables. Overall, U1 and U6 perform similarly. Hence, we can choose U6 as the recommended time interval since U6 requires less storage than U1.

In the previous section, J3 was selected as the optimized resolution when the interval was set at U1. Therefore, we tested whether these results are still valid for the U6 case and tested the effects of spatial resolution in this case. The cases of J6 and J9 with U6 were also performed for comparison. Table 3.3 shows that J3 agrees better than the other cases for all variables. Even though J6 has slightly better COR in terms of temperature, J3 has almost twice the COR for vorticity, when compared to J6. The selected J3 is in good agreement with previous research studies in which such a jump ratio has been imposed in many applications with different purposes.

We may extend all the cases in Table 3.3 by using the “flather” method to compare the error contributed by using different OBCs. If this is done, we see that the variance in error due to the changing boundary resolution is quite similar to that obtained by using the “R-K radiation” method with sponge/nudging. However, the quality of solution is slightly smaller (not shown). Therefore, it is clear that the error contribution that arises due to using different OBCs is not as much as the

error caused by varying boundary resolution (Table 3.1 and Table 3.3). Results from a nested ocean model always performed well with the application of J3 when dealing with simple idealized or complicated real cases with different grid resolutions (Spall and Holland, 1991; Barth et al. 2005). Performance was also good when testing for both 'barotropic' and 'baroclinic' modes (Spall and Holland, 1991), using different numerical ocean models (Laugier et al. 1996; Barth et al. 2005), and examining a variety of boundary conditions as well as a diversity of ocean dynamics scenarios provided by the LBCs (Laugier et al. 1996; Nash and Hartnett, 2014). Moreover, the optimal resolution performance of the LBCs (J3-U6) with a high value of COR for all diagnostic variables including temperature, salinity and vorticity (Table 3.3), has shown that Little-Brother does not show significant bias or drift from Big-Brother.

Table 3.3 CORs of all fields for the cases J3, J6 and J9 with updating frequency U6 (every 6 hours)

Case	February			September		
	Temperature	**Salinity**	**Vorticity**	**Temperature**	**Salinity**	**Vorticity**
J3	98.9	95.6	98.0	91.7	87.7	91.5
J6	98.6	95.2	97.1	94.3	82.8	43.1
J9	98.4	93.9	96.8	88.6	87.1	46.2

3.3.4. Error propagation and domain size

Errors produced at the boundary propagate into the interior of the domain as time passes. To study this phenomenon, the LBC grid ratio was set to 3, the J3 case, the LBCs were updated every 10 minutes, and the size of the Little-Brother domain was 306 km × 246 km (Fig. 3.6).

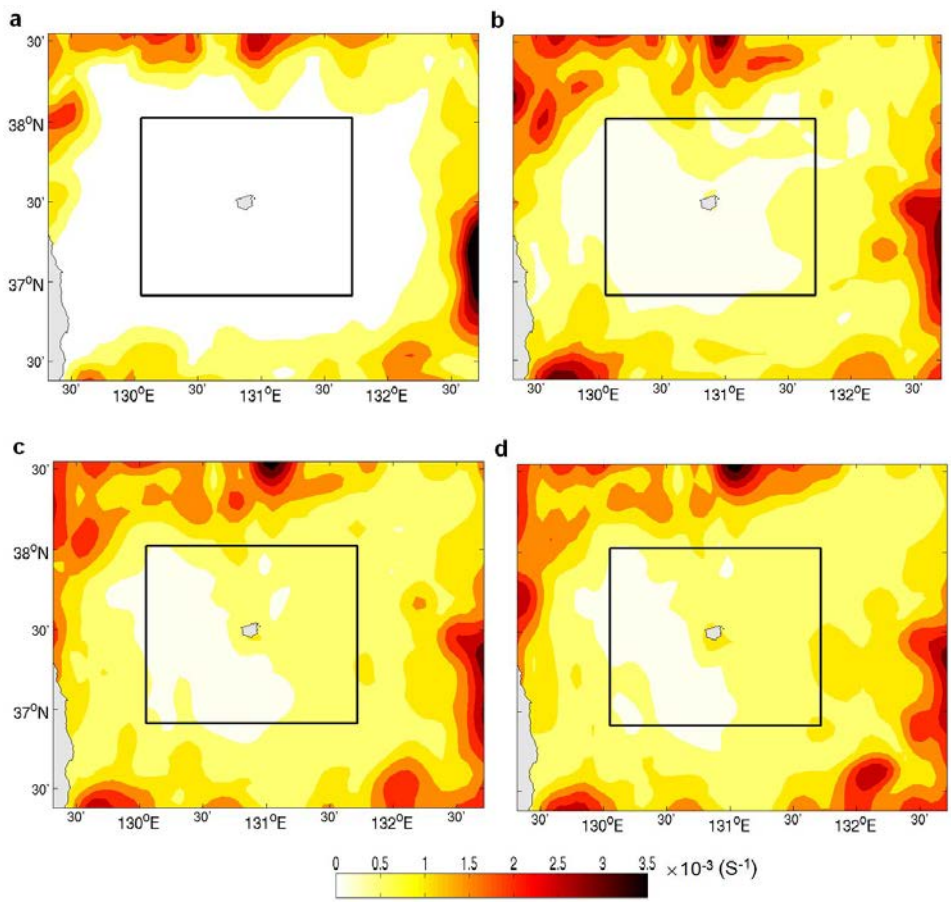

Figure 3.6 CRMSD of depth-averaged vorticity between the large and small domains after (a) 1 day, (b) 10 days, (c) 20 days and (d) 30 days **(**Extracted from Pham et al., 2016**).**

After depth-averaging the vorticities in the domains of the Little- and Big-Brother simulations, the CRMSD values for the differences between them were obtained. After the first day, some errors (red or yellow areas in Fig. 3.6 (a)) prevailed along the boundaries and decreased toward the center (the color becomes whiter in Fig. 3.6 (a)). Furthermore, no distinct error appeared inside the domain of interest enclosed by the black rectangular line in Fig. 3.6 (a). After 10 days, errors (yellow colored area in Fig. 3.6) spread into the domain of interest (Fig. 3.6 (b)) and gradually their magnitudes increased, as seen clearly on the 20^{th} and 30^{th} days (Fig. 3.6 (c), and (d)).

Therefore, the space between the boundaries of each domain and the area of interest can help reduce the propagation of errors from the LBCs. The extra space can play a role as a buffer, providing a further distance for errors to pass through. If there is enough distance, then LBCs are refreshed before errors reach the domain of interest. In other words, the distance for buffering or the domain size can be another factor determining downscaling ability.

To examine the effects of domain size on the errors, the Big-Brother simulation was constructed on a 168 × 126 point 6 km × 6 km grid. The experimental set consisted of four experiments with different numbers of grid points (different domain size) but with the same resolution as the Big-Brother simulation (6 km × 6 km). The cases were named LB1, LB2, LB3 and LB4 and they had, respectively, 25 × 21, 51 × 41, 78 × 64 and 125 × 104 grids (Fig. 3.7).

The updating time of the LBCs from the Big-Brother was every 10 minutes, which was the same as the interval time of these four Little-Brothers. All four cases have the same resolution, are embedded in the Big-Brother domain and are nested there with the same jump ratio. This experiment had the same spatial and temporal resolutions in all four cases, so the only errors were those produced by the specific formulation of the LBCs. The Big-Brother results were degraded to a lower resolution by filtering small-scale signals, those that were less than 36 km, and the resolution jump ratio between the Big-Brother and the four domains was set at 3.

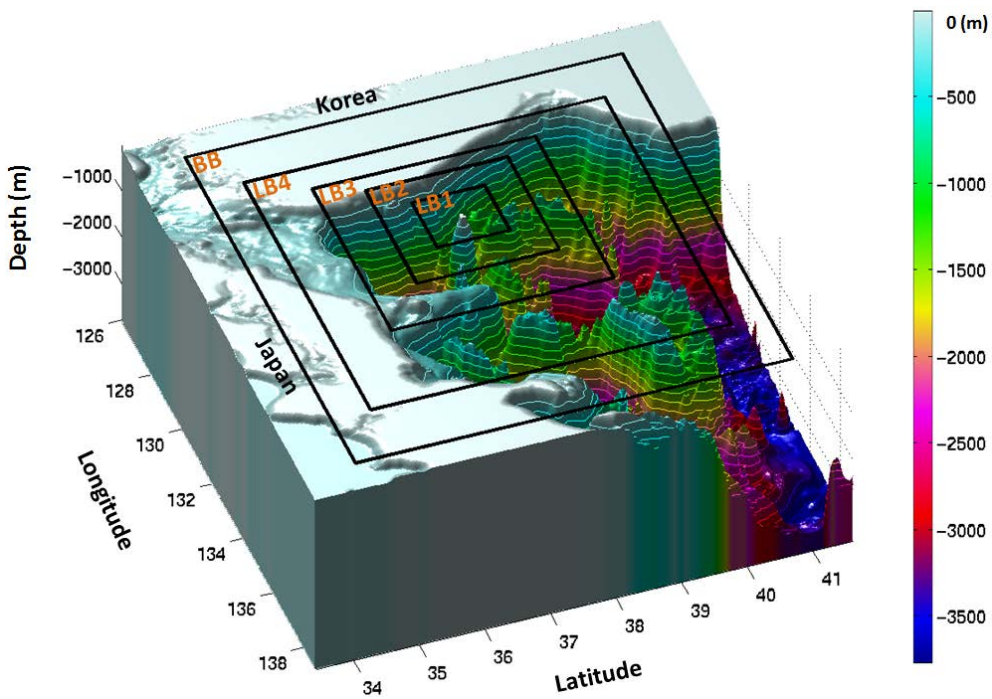

Figure 3.7 Geographical layout of the Big-Brother and experimental domains for LB1, LB2, LB3, and LB4.

In all experiments, the area of interest can have the same domain size as LB1. We can also simulate this area of interest by adding some extra space as a buffer distance. Such extra distance from the LBCs to the edge of the area of interest can prevent the errors generated at the LBCs from propagating into the area of interest.

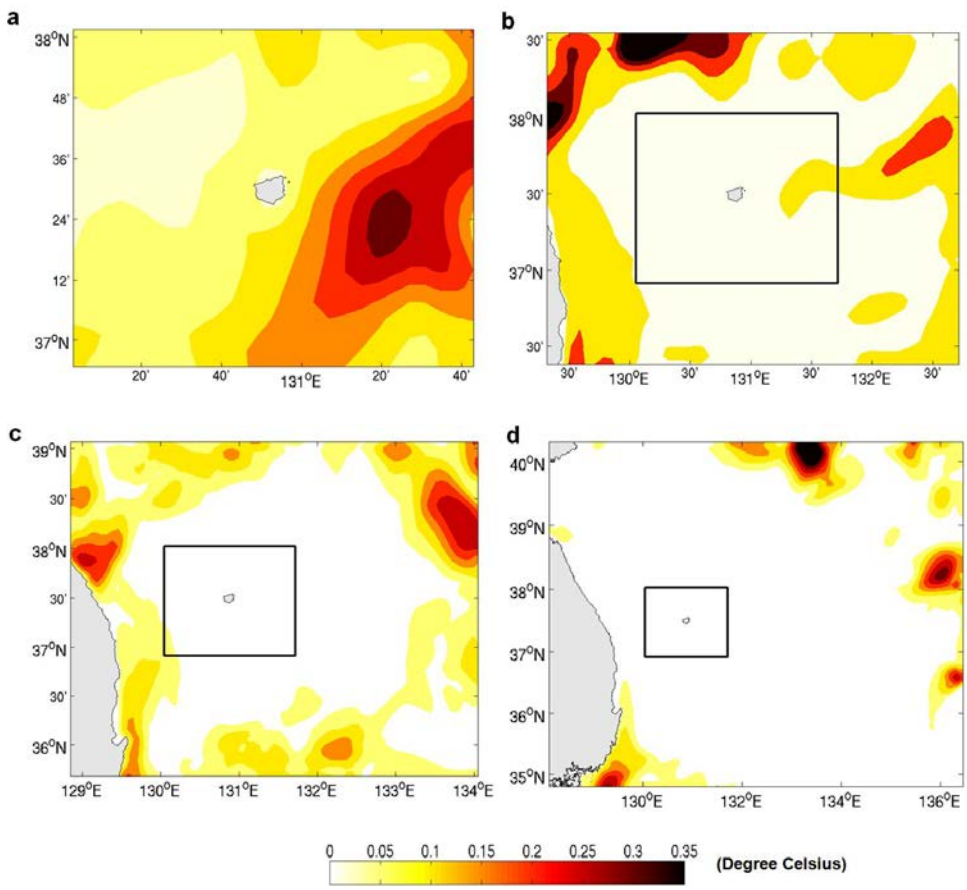

Figure 3.8 CRMSD of depth-averaged temperatures, after 30 days, between the Big-Brother and four different domains: (a) LB1, (b) LB2, (c) LB3 and (d) LB4 **(**Extracted from Pham et al., 2016**)**.

For example, in the unfiltered experiment cases, in each domain the areas bounded by solid lines in Fig. 3.8 are the areas of interest, which are all the same size as LB1. In the case of LB1, the nested domain has the same area as the area of interest, so LB1 has no buffer distance to prevent errors from propagating into this area of interest (Fig. 3.8 (a)). As the domain size increases from LB1 to LB4, the area affected by the LBC errors (colored yellow) becomes smaller within the solid-outlined area of interest (Fig. 3.8 (b), (c) and (d)). Finally, in the case of LB4, the errors from the LBC do not reach the edge of the boundary of the area of interest (Fig. 3.8 (d)). Similar effects were observed and discussed by Warner et al. (1997) and Vannitsem and Chomé (2005).

As the size of the domain increases, ORCMs produced better results for all diagnostic variables (Fig. 3.9). So, larger domains have higher CORs and smaller relative CRMSDs, as we expected. LB1 and LB2 have CORs of 90% and 70% respectively, smaller than that for LB3, which performs well qualitatively, producing correlation coefficients of over 97% for all fields. LB4 shows the best results, as expected LB4 is better than LB3, but the improvement of performance seems to be meaninglessly small, and requires 1.4 times more grid points. Hence, LB4 costs more in terms of CPU time and output memory requirements than LB3.

In summary, LB3, which has an area around 9.5 times larger than the area of interest, and an average buffer distance of approximately 140 km from the open boundaries to the area of interest, is recommended as an optimal domain.

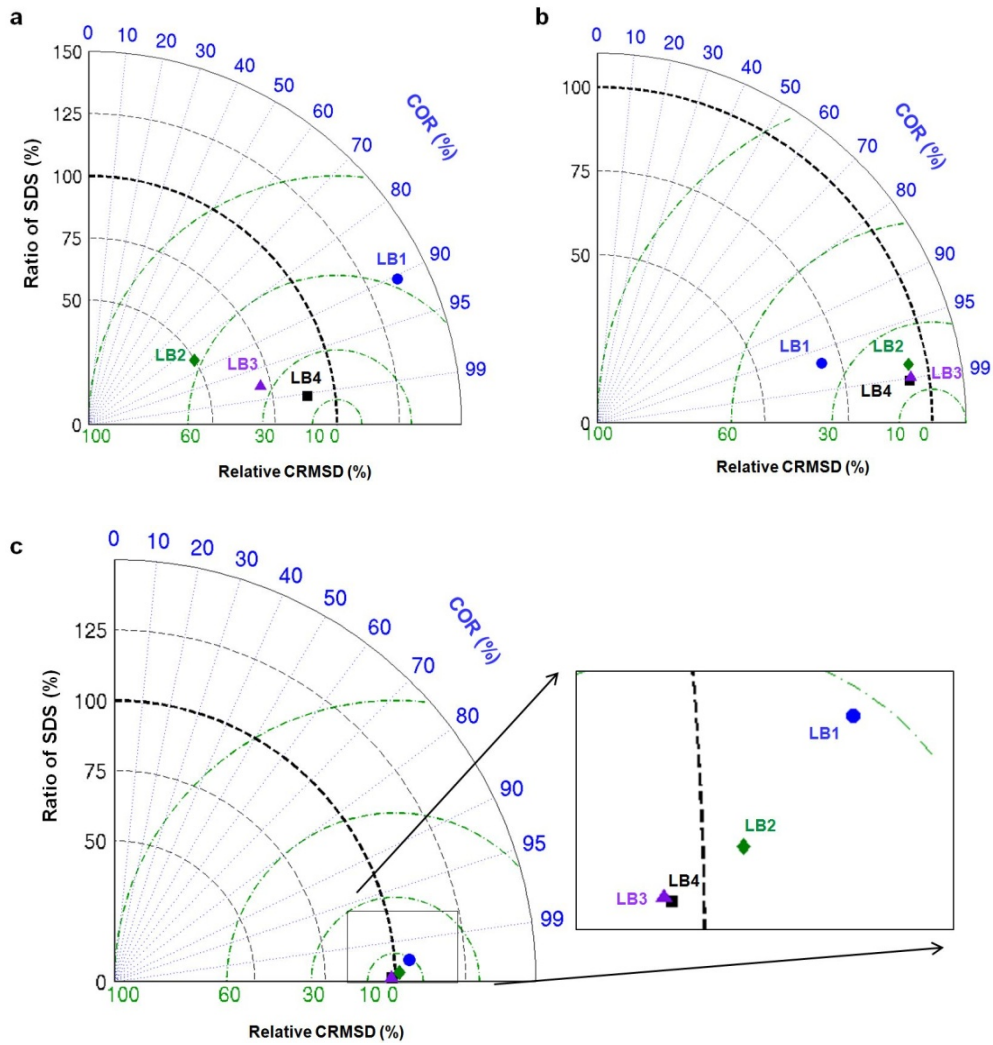

Figure 3.9 Taylor diagrams of unfiltered cases (winter season) showing the effect of domain size on (a) mean salinity fields, (b) mean vorticity fields, and (c) mean temperature fields **(**Extracted from Pham et al. 2016**)**.

Leduc and Laprise (2008) suggested that an optimal size should be not too large, but their recommendation was for the atmospheric research. But, as our area

of interest is blocked by several islands and continents, we could not extend the buffering distance further to confirm whether their finding holds for oceanic studies as well. If the optimization is performed for the wider open ocean, then the optimal size might be found to be neither too large nor too small.

3.3.5. Downscaling ability

After identifying optimal nesting conditions by the above method, as the second step, the overall downscaling ability was quantified by modifying a method used by Denis et al. (2002a). Each variable consists of small and large spatial components, as follows

$$\phi = \phi_{ls} + \phi_{ss}, \tag{47}$$

where the subscript *ls* means *large spatial* component and the subscript *ss* means *small spatial* component, as determined by the filter wavelength. Putting Equation (47) into Equation (8) and squaring, yields:

$$\overline{\phi^2} = \overline{\phi_{ls}^2} + 2\,\overline{\phi_{ls}\phi_{ss}} + \overline{\phi_{ss}^2} + \overline{\phi_{ls}'^2} + 2\,\overline{\phi_{ls}'\phi_{ss}'} + \overline{\phi_{ss}'^2}\,. \tag{48}$$

The first and third terms on the right hand side are related to the stationary properties of each large- or small-scale feature. Therefore, those two terms are referred to as the large- and small-scale stationary variables. Once those terms are measured, the results are used to calculate the spatial correlation coefficients

(SCOR) between them to find how similar the Little- and Big-Brothers are. For a given arbitrary two-term variable, the SCOR is determined by:

$$\mathrm{SCOR} = \frac{\sum_{N}\left(\overline{\phi}_{L} - \left\langle\overline{\phi_{L}}\right\rangle\right)\left(\overline{\phi}_{B} - \left\langle\overline{\phi_{B}}\right\rangle\right)}{\sum_{N}\left(\overline{\phi}_{L} - \left\langle\overline{\phi_{L}}\right\rangle\right)^{1/2}\left(\overline{\phi}_{B} - \left\langle\overline{\phi_{B}}\right\rangle\right)^{1/2}}. \qquad (49)$$

These SCORs can give us some indications of the pattern of agreement between the Little- and Big-Brother simulations. More detailed descriptions of the equation can be found in Denis et al. (2002a). To propose a method to find optimal downscaling ability, the combinations J3-U1 and J3-U6 were compared (Tables 3.4 and 3.5). In the last section, the recommended spatial jump was 3 times larger than the original grid size and updating frequency was every 6 hours, even though hourly updating produced slightly better results. Therefore, the combination of J3-U6 was most appropriate for the present simulation and J3-U1 was used for reference. In the Taylor comparison, there was no significant difference between J3-U1 and J3-U6. In this experiment, domain size effects are not considered since larger domains will show better results, once the spatial jump ratio and updating period are optimized.

3.3.5.1. Pattern reproduction

For the large and small stationary components, the SCORs in all cases were high enough to tell us that the original patterns were reproduced well (Table 3.4). As expected, in all fields, J3-U1 shows slightly better results than J3-U6. For

the large scale, temperatures in the two cases are nearly the same. For the small scale, the temperature SCORs between J3-U1 and Big-Brother and between J3-U6 and Big-Brother are 96.1% and 89.3%, respectively (Table 3.4). As the updating time increased, small-scale motions generally became less correlated. For the large scale, the salinity SCOR between J3-U6 and Big-Brother is 89.3%, which is slightly better than that of J3-U1, 84.2% (Table 3.4). The SCOR of the small-scale components of the salinity fields between Little-Brother and Big-Brother are 83.1% and 84.2% for J3-U1 and J3-U6, respectively.

Table 3.4 SCOR of domain-averaged stationary large-scale and small-scale variances for temperature, salinity and vorticity.

	Temperature	**Salinity**	**Vorticity**
Large scale (J3-U6)	96.1	89.3	82.4
Small scale (J3-U6)	89.3	83.1	79.2
Large scale (J3-U1)	96.1	84.2	97.3
Small scale (J3-U1)	96.1	84.2	68.1

The large-scale stationary components of vorticity also show good agreement with Big-Brother and the SCORs are approximately 82.4% for J3-U6 and 97.3% for J3-U1 (Table 3.4).The small-scale vorticity SCOR results were 79.2% for J3-U6 and 68.1% for J3-U1, slightly smaller than the other cases and fields, but the numbers still indicate that the model reasonably reproduced the patterns of the original signals. Even though J3-U1 can produce better results than J3-U6, we did

not find significant differences in errors between the two cases. Therefore, to reduce storage requirements, J3-U6 can be generally recommended, depending on the computational capabilities, as already suggested.

3.3.5.2. Magnitude reproduction

We assessed, as variance ratios, whether sufficient amounts of overall variables were regenerated, in a manner similar to that of Denis et al. (2002a), except that we applied it to salinity, temperature and vorticity. They called the magnitude reproduction rate “downscaling ability”. Longer-time-scale signals can be regarded as “stationary” and treated as mean values in calculations. The stationary variance ratios can be calculated as

$$\Gamma_{ss}^{stat} = \frac{\left\langle \overline{\phi_{ss}^{2}} \right\rangle_{L}}{\left\langle \overline{\phi_{ss}^{2}} \right\rangle_{B}}. \qquad (50)$$

Temporally fluctuating signals are defined as having “transient” variance ratios and are calculated as

$$\Gamma_{ss}^{tran} = \frac{\left\langle \overline{\phi_{ss}^{'2}} \right\rangle_{L}}{\left\langle \overline{\phi_{ss}^{'2}} \right\rangle_{B}}. \qquad (51)$$

Table 3.5 gives the ratios of variances calculated with equations (49) and (50). We first compare the J3-U1 cases to the Big-Brother results. Temperatures are well reproduced in both stationary (1.04) and transient ratios (0.91). While the stationary variances of salinity are regenerated well, the transient ratio is only 0.62. Stationary and transient ratios of vorticity are 0.86 and 0.80 respectively, indicating that the model seems to reproduce the original signals well, even though the values are all smaller than those of Denis et al. (2002a). Since water is more viscous and denser than air, the response time for the ocean circulation is longer than that for the atmospheric models. Therefore, once small-scale fluctuations are filtered out, it will take a longer time in the ocean than in the atmosphere to regenerate the same amount of fluctuation. Nevertheless, the downscaling ability of the present optimized method seems reasonably able to reproduce the overall regional scale motion.

When the J3-U6 case is compared with Big-Brother, the results are once again reasonable (Table 3.5). Although the stationary temperature ratio is 5% larger in the nested results, the model still reproduces the temperature field well overall. In the case of salinity, as in the J3-U1 case, the stationary part reproduces well but the transient part is still below the appropriate level. Comparing the transient parts of the J3-U1 and the J3-U6 cases for salinity, slower updating shows a slightly better result than updating with shorter time scales (such as 1 hour). However, we could not observe such trends for temperature and vorticity and so checked the orders of magnitude for the stationary and fluctuating parts of temperature and

salinity. While the stationary parts of temperature and salinity are of similar order ($O(1)$), the stationary part of the salinity being only 2 to 3 times larger than that for temperature, the fluctuating part of the salinity is $O(10^{-5})$, which is two orders of magnitude lower than for temperature($O(10^{-3})$). Therefore, the calculations of smaller scale salinity fluctuations could be more limited than corresponding calculations of temperature. Such small discrepancies in both salinity and temperature do not tell us that U6 is better than U1. Overall, it can be said that both U1 and U6 predict with similar accuracies.

Table 3.5 Ratio of domain-averaged stationary and transient small-scale variances for temperature, salinity and vorticity.

	Temperature	**Salinity**	**Vorticity**
Stationary (J3-U6)	1.05	0.99	0.81
Transient (J3-U6)	0.87	0.67	0.73
Stationary (J3-U1)	1.04	0.99	0.86
Transient (J3-U1)	0.91	0.62	0.80

Furthermore, the predictability with the recommended temporal and spatial resolutions also seems reasonable based on the assessments of the correlations and the variance ratios. In particular, an LBC that is three times larger still produces reasonable results, from all perspectives. After temporal updating, the results of simulations have somewhat smaller than expected stationary and transient variances. However, updating the boundary conditions every 6 hours reproduced,

reasonably well, the mean, stationary and transient small-scale behavior of the original Big-Brother results.

3.4. Summary

The use of one-way nested regional models produces highly resolved information from poorly resolved observations or OGCMs (Denis et al. 2003; Li et al. 2012; Herbert et al. 2014). However, downscaling procedures degrade the quality of predictions through many sources of error. Such sources of error are generally unavoidable and affect the ORCM results. These error sources can combine during simulation and synergistically degrade the ORCM solution. The sets of Big Brother Experiments used here separated the sources of errors and quantified the error magnitudes, with analyses following and combining those of Leduc and Laprise (2008) and Denis et al. (2002a). Through a framework of error assessment, we are able to assess quantitatively the contribution of each error source to the nesting and downscaling procedures. Finally, optimal combinations of grid resolution, updating time, and domain size are proposed. From the results discussed in the previous sections, the main findings are summarized as follows:

The error sources associated with downscaling technique including (1) boundary condition types; (2) Error during spin-up time to generating small-scale features; (3) effect of LBC resolution; and (4) Error propagation and domain size were unavoidable during downscaling procedure due to the different in grid sizes and updating intervals between coarse reference and nested model. They degrade

the results of ORCMs in different aspects and levels. The OBCs construct a first order effect on the ORCMs solution. Difference of applied OBCs gives different results of ORCMs. The OBCs often combines with supplementary methodology e.g. sponge/nudging to improve the solution quality. The “R-K radiation” combination with sponge/nudging show the best selection in the experiment. During the spin-up of time to generate small-scale features, the lacking small scales in the coarse reference were regenerated over the whole domain. It took over 15 hours to become fully saturated. Such small scale fluctuations contribute much to kinetic energy and dissipation rate.

The results of ORCMs are strongly sensitive to the resolution of lateral boundary condition. The lacking driving information and the discontinuity at the open boundaries between the driving data and driven model generate errors. Such errors tend grow and propagate to inner domain, then degrade the ORCMs solution. The quality of ORCMs solution increases with reducing the spatial resolution jump ratio and increasing the updating frequency. The consistent use of external data is ≤ 3 for spatial resolutions jump and every 6 hours for LBC updating period. The errors generating from the LBCs can be mitigated when increase the domain size. The extra space gives rise the distance between the area of interest and the LBC, therefore, retard the errors from the LBC propagate into. The optimal numerical setup of ORCMs with spatial resolution jump ≤ 3; LBC updating period at every 6 hours and domain size larger 10 times of interested performs a good downscaling ability in term of magnitude and pattern reproduction.

Our current work is limited in terms of generalizing optimal values, because we have considered only one special domain location, which may be critical in determining the quality of the simulation results. As Chen et al. (2007) and Huang et al. (2008) have pointed out, errors during dynamic downscaling also depend on the types of regional ocean models. However, despite limits imposed on the present conclusions, our assessment method could be applied as a framework for finding an optimized combination of grid size ratio, updating interval and domain size in downscaling at different locations with other regional ocean models. Even though bottom bathymetry, shape of domain, tidal influence, extreme weather, period of simulation time, etc. could generate significant errors, those sources are not covered here, as this work focuses on downscaling influences for climate change impact assessment rather than real operational forecasting.

CHAPTER FOUR

4. SMALL SCALE-ADDING BOUNDARY TECHNIQUE

4.1 Introduction

Generation of small scale motions, which are absent from the large scales of coarse reference, is one of important issue of dynamical downscaling technical. The small scales can be generated due to separate or combination of different sources at homogeneously in time and space. Therefore, in a real domain, it is really a big challenge in addressing the characteristic of small scales motions associating with separate sources in dynamical downscaling technical. In this part, the Big-Brother method one again was applied in designed experiments with ideal domain. The advantage of BBE in separating the effect of stimulated sources with ideal domain gives us deeply identify the roles of sources contributing to the small scale generations. The chapter first started with description of Model set-up, then presenting the results with identifying the role of stimulated sources to the generating small scale motions. Following that diversified experimental cases showed comprehensively sensitivity of small scale generation to the levels of stimulated sources.

Two kinds of stimulated sources including “advection producing shearing” (type 3) and “island making wake” (type 1) were experimented. The normal case, which has not any stimulated source presented, also was implemented. It is considered as a basic case for comparison of smalls-scale development with those in case of presenting sources. Besides, we also examined effect of adding small scales to boundary condition on small scale generation and development.

4.2. Set-up mode in ideal domain

In the ideal designed experiment, the Big-Brother and Little-Brother are in homogeneous depth of 145 m. The Big-Brother simulation has grid resolution of 3 km × 3 km. It performed over a large domain with lengths of 990 km in x direction and 880 km in y direction. The Little-Brother embedded and had the same resolution as the Big-Brother domain. It’s domain has lengths of 400 km in x direction and 312 km in y direction, respectively (Fig. 4.1). Both of the Big-Brother and Little-Brother were run with 30 vertical layers of the *S*-grid. However, in this implemented experiment, the spatial resolution between Big-Brother and Little-Brother is J5. It means that all the wave length scales smaller than 30 km were filtered.

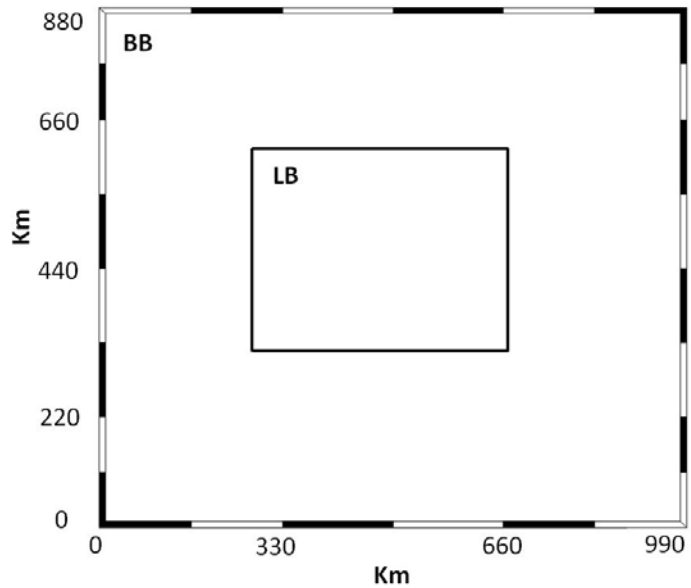

Figure 4.1 Geographical layout of ideal grid domain with constant depth of 150m. Resolution of both Original Big-brother and Little-Brother is 3 km.

4.3. Results

In the Figure 3.3 (a) and (b), we already observed how the small scales motion generated and grew up. During first 18 hours of simulation, there some peaks which over 100% of Litle-Brother kinetic energy. The generation of such small scales can be affected of combination of sources during dynamical downscaling technical in a real domain. Therefore, in this section, we did experiment with ideal domain to separately identify the separate stimulated sources which play important role to small scales generation and development, and re-observe how small scale generate in the simple case of ideal domain.

4.3.1. Contribution of adding advection to small scale generation and development

The initial and boundary condition are imitated from the East Seat of Vietnam. The initial conditions were set only one time at the beginning of the integrated simulation with the averaged current speed in Big-Brother around 0.04 m/s and flow direction was in eastward (from left boundary to right boundary). In order to establish an adding advection (AD_10), high speed of current was added at 10 grid of middle western boundary of Big-Brother with speed of 0.4 m/s (10 times higher than inner current speed of inner domain) as shown in the Figure 4.2. Velocity filed at boundaries was update in every 2 minutes which is equated to time step on Big-Brother. For simplicity, temperature and salinity are constant with value of 28.76 (Degree Celsius) and 33.03 PSU, respectively. There is no interaction with atmosphere in order to eliminate their effect on the results.

The Little-Brother started 2 days later than Big-Brother in order to discard the short time scale spin-up phenomena. For example, The Big-Brother starts to run from 1st, The Little-Brother begins to run from 3st. The time step of both Big-Brother and Little-Brother is 2 minutes.

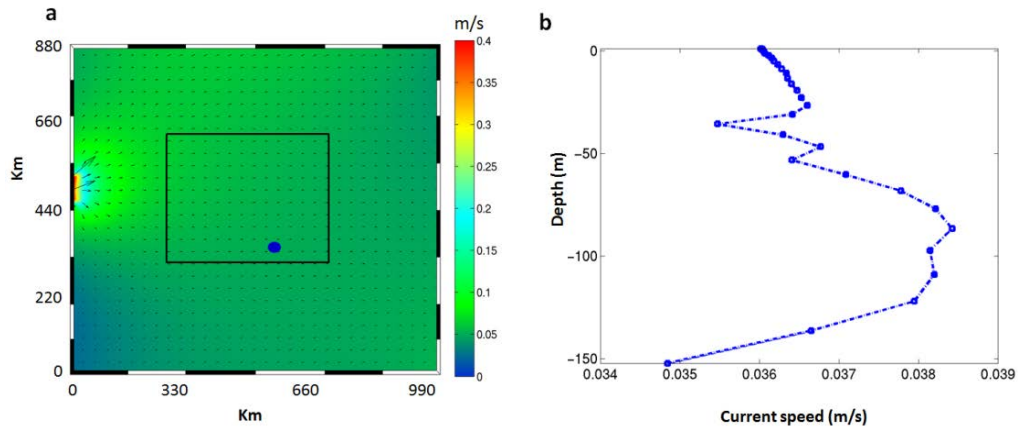

Figure 4.2 Initial condition of current speed. (a) in horizontal, the speed current at added advection is greater than 10 times than the inner region, and (b) vertical profile of current speed extracted from the blue dot location. The large domain is Big-Brother and the small black rectangular is Little-Brother

Firstly, we take into account with the energy spectrum of the Big-Brother and Little-Brother within 40 minutes of simulation (Fig. 4.3). The energy has high value at largest scale and gradually reduces at smaller scales. The energy slope of Big-Brother is nearly -5/3. At beginning, all small scales perturbations having wavelengths smaller than 30 km were filtered in the Little-Brother. Therefore, the Little-Brother does not have energy at these scales, while its energy is the same to Big-Brother with larger scale having wavelengths greater 30km. At first step of simulation, the filtered small scale perturbations in Little-Brother grow. As a results, their energy increase. The energy at the smallest wavelength grow first, the energy development of consecutive wavelength slightly retards. It is interesting that they form as a wave shape (noting that it is fluctuation of energy, not a real wave)

oscillating around the energy line of Big-Brother amplitude with first node at the smallest wavelength and the final node at the wavelength of 30 km. This wave looks like the development of a wave running upward to a gentle slope with gradually increase of the length of wave and amplitude. After coming to the final node at 12 minutes, the wave reflects downward with slightly reduces its amplitude. As time goes pass, undergo the same process, the wave disappears and there is not many change of kinetic energy of wavelength smaller than 30 km of Little-Brother after 3 hours of simulation (now shown). At this state, it can be consider the Little-Brother gets equilibrium.

Slightly similar to kinetic energy spectrum, dissipation, which is calculated as in the equation (52), also increases at first few time steps. However, in difference to KE, the dissipation ratio of Little-Brother does not fully reach the Big-Brother level. It means that in smaller scale energy is not fully dissipated efficiently, and it helps accumulate energy in this region (Fig. 4.4 (a) & (b)).

The dissipation (ε) at a given wavelength ℓ is calculated as bellow

$$\varepsilon(\ell) = \frac{1}{N_x N_y} \sum_{1}^{N_x} \sum_{1}^{N_y} \nu \frac{\partial u_{(\ell)}}{\partial y} \frac{\partial v_{(\ell)}}{\partial x}, \qquad (52)$$

Where $u\ (\ell)$ and $v\ (\ell)$ are the momentum components in the x and y directions, respectively. The ratio of the dissipation at the given wavelength is

$$R_{\varepsilon}(\ell) = \frac{\varepsilon_L(\ell)}{\varepsilon_B(\ell)} \times 100, \qquad (53)$$

Where $\varepsilon_L(\ell)$ and $\varepsilon_B(\ell)$ are the average dissipation of the Little-Brother and Big-Brother simulations, respectively; v is kinematic viscosity v=1.5x10^{-6} m^{2}s^{-1}.

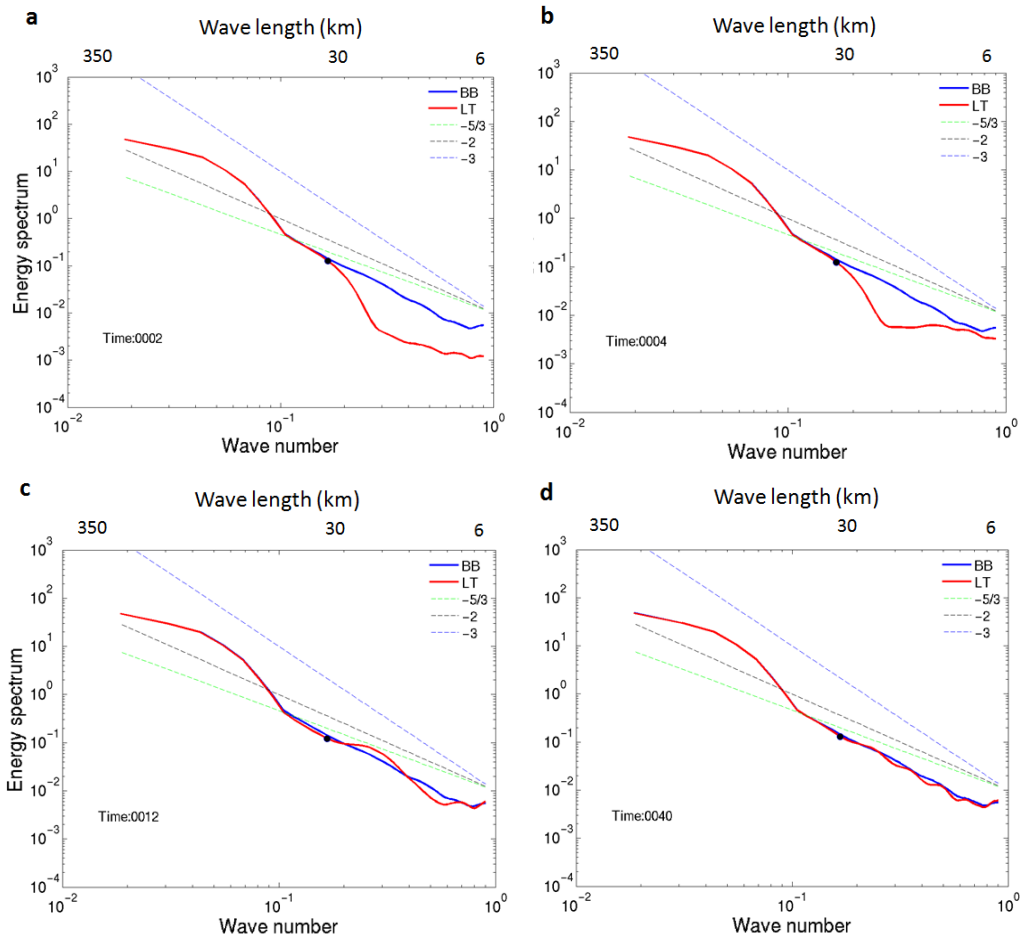

Figure 4.3 Surface energy spectrum of Big-Brother (blue lines) and Little-Brother (red lines) of AD_10 case. (a) after 2 minutes, (b) 4 minutes, (c) 12 minutes and (d) 40 minutes. The black dot describes location at wavelength of 30 km where all small scales were filtered.

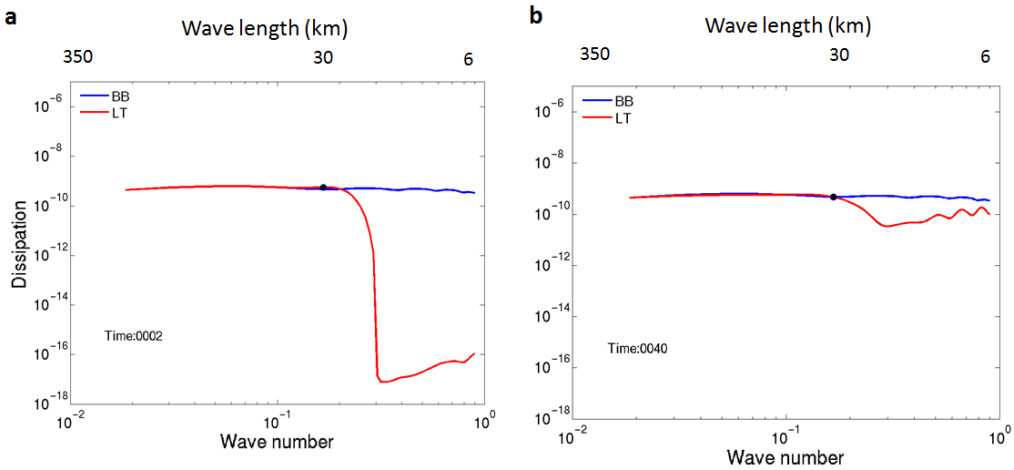

Figure 4.4 Surface dissipation spectrum Big-Brother (blue lines) and Little-Brother (red lines) of AD_10 case. (a) after 2 minutes and (b) 40 minutes

The development of small scale motions were deeply described with the ratio of kinetic energy of Little-Brother within wave length of 50 km. We first look at small scale development of normal case (NC) which has the same model setup with AD_10 case except no adding advection at western boundary. The current speed at initial condition of NC case is constant with value of 0.04m/s. The current flows from southwest to northeast (Fig. 4.5 (a)). The filtered small scales of Little-Brother in NC case grow in monotonic fashion with smaller scale having higher speed during first 4 minutes of simulation. After 12 minutes, its small scales energy only gets 60 percent of Big-Brother, and never keep Big-Brother level as time goes pass (Fig. 4.6 (a)). However, in case of AD_10, just after 8 minutes filtered mall scales recovered nearly 100%, and over level of Big-Brother with 145% (Fig. 4.6 (b)). This proves that adding advection producing shearing can significantly

stimulate the development of small scale through hydrodynamic instabilities as mentioned in (Denis et al. 2002a).

Base on the growth of Little-Brother's kinetic energy, it is an interesting that, during the increase 12 minutes of simulation, the total energy of filtered small scales increases, while the energy of unfiltered larger scales (ranging from 30 to 50 km) monotonic decrease from larger wavelength at 50 km to smaller wavelength at 30 km. This gives a sign of transferring energy from large scales to smaller scales in order to make the filtered small scales develop (Fig. 4.6 (b)).

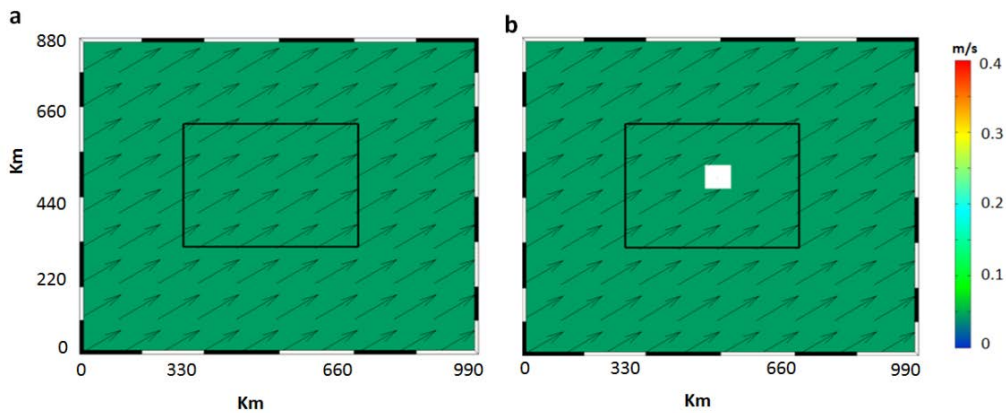

Figure 4.5 Initial condition of current speed. (a) case of NC and (b) case of IS. The initial current speed of both cases are 0.04m/s. In the case of IS, the island is added at the middle of both Big-Brother and Little-Brother domain.

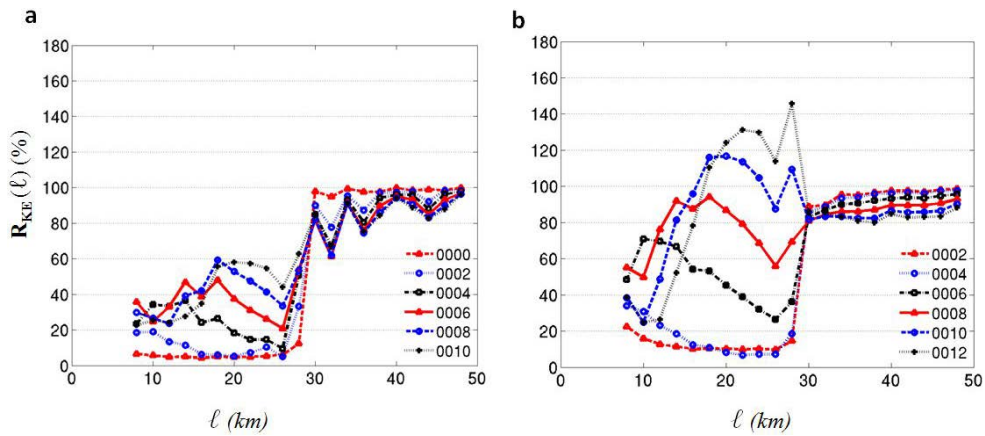

Figure 4.6 Ratio of surface kinetic energy of the Little-Brother to Big-Brother during short time of simulation. (a) case of no adding advection (NC), (b) case of adding advection

Figure 4.7 shows the CRMSD between Little-Brother and Big-Brother of vorticity after 2 and 10 minutes of AD_10, the errors appear in whole domain especially in a regional close to the western boundary where the source is located. It again proves that adding advection producing share generate more disturbance near source. When time goes pass, such boundary errors strongly develop and propagate to the inner domain.

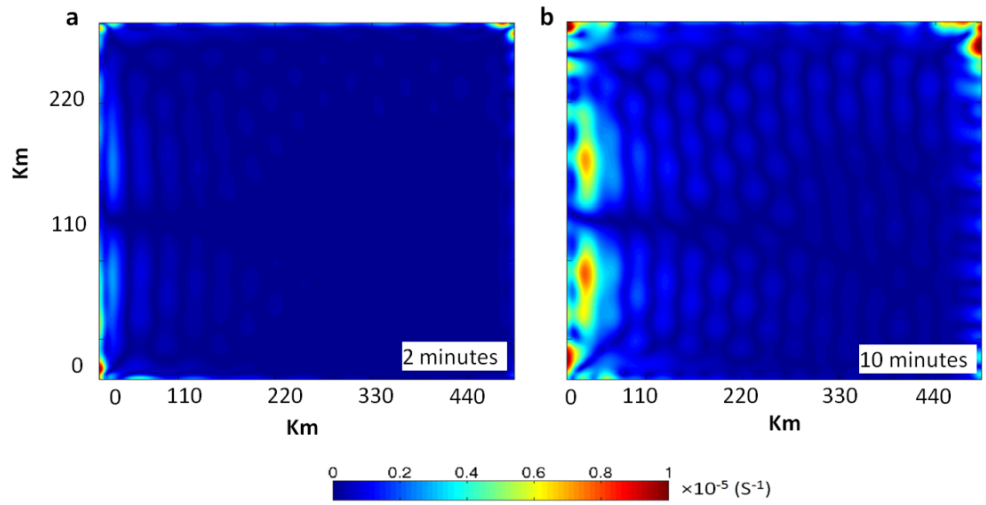

Figure 4.7 Center root mean square different of depth averaged z-vorticity between Little-Brother and Big-brother. (a) and (b) case of AD10 at 2 and 10 minutes.

The evidence in the Figure 4.6 has shown that, adding advection producing shearing is one of a factor significantly affect to the small scale generation. It accelerates the development of small scale perturbation and increases the spin-up time of generating small scale process. However, it raises a question that whether the small scale generation and development is depended on amplitude of adding advection. Therefore, we implemented more experiment with different amplitude of adding advection including 0.08 m/s (we call AD_2, it means that current speed of adding advection higher than inner domain 2 times), 0.2 m/s (AD_5), and 2 m/s (AD_50).

The results of increasing the speed of current at adding source are from 2 times to 50 times as shown in the Figure. 4.8. In case of increasing current speed 2 times (AD_2), it is not strong enough to affect to generate small scales motion (Fig. 4.8 (a)). It is totally similar to the case of not adding source (NC) (Fig. 4.6 (a)). The reason is that the distance from the Big-Brother to Little-Brother is far enough, therefore jet flow from the source cannot reaches to Little-Brother.

However, when increasing the current speed to 5 times (AD_5), the effect shows obviously. The filtered small scale perturbation grows faster, and reaches 100% of Big-Brother amplitude after 10 minutes. The tendency kinetic energy development is the same to the case of AD_10 (Fig. 4.8 (b)). However, the energy amplitudes of most unfiltered small scales are smaller than AD_10 except at the scale of wavelength 28 km. It is interesting that, when increasing current speed higher than 10 times, the unfiltered small scale perturbations do not keep continuously growing. The energy amplitude of most unfiltered small scales of case AD_50 is event smaller than AD_10. But there is not appearance of wave number at the wavelength 26 km.

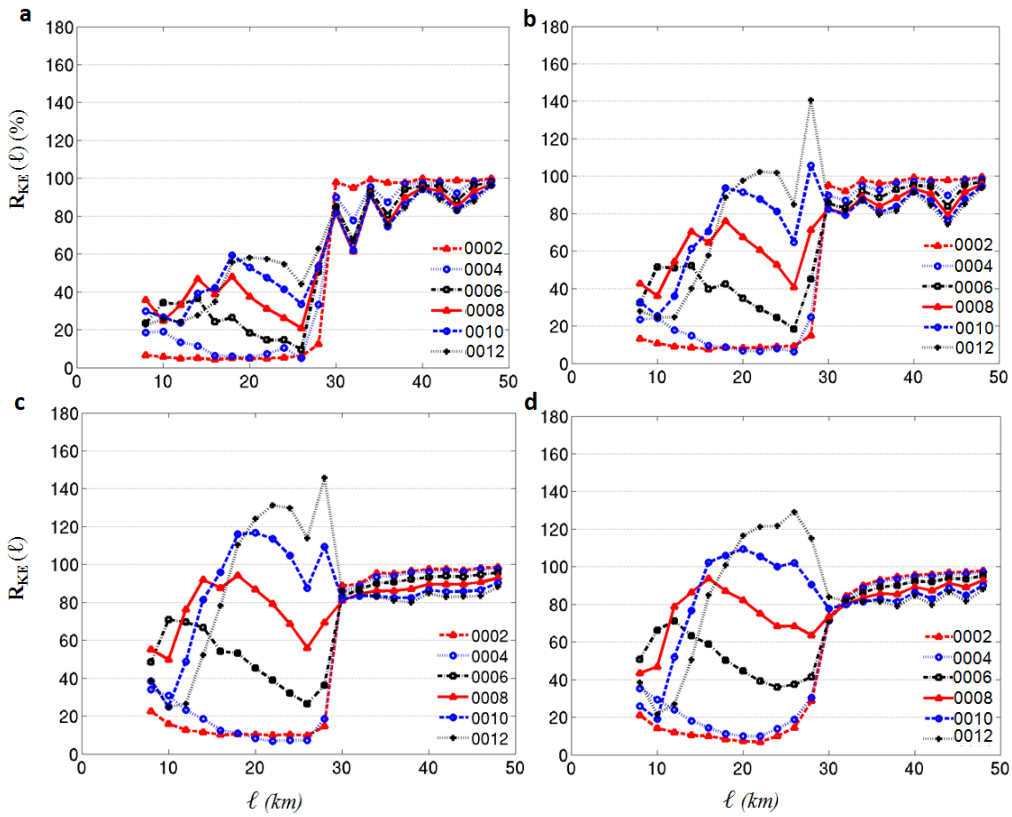

Figure 4.8 Ratio of surface kinetic energies of the Little-Brother to Big-Brother during shorter and earlier times. (a) 2 times (AD_2), (b) 5 times (AD_5), (c) 10 times (AD_10) and (d) 50 times (AD_50).

The energy transport from the lateral boundary and adding advection into inner domain is intensively described in the Figure 4.9. Here, we reduce the domain size of Big-Brother with size of domain in 200 km × 200 km. The adding advection was added directly at the western boundary of Big-Brother with value of 0.4 m/s and the current speed gradually decrease far from the boundary.

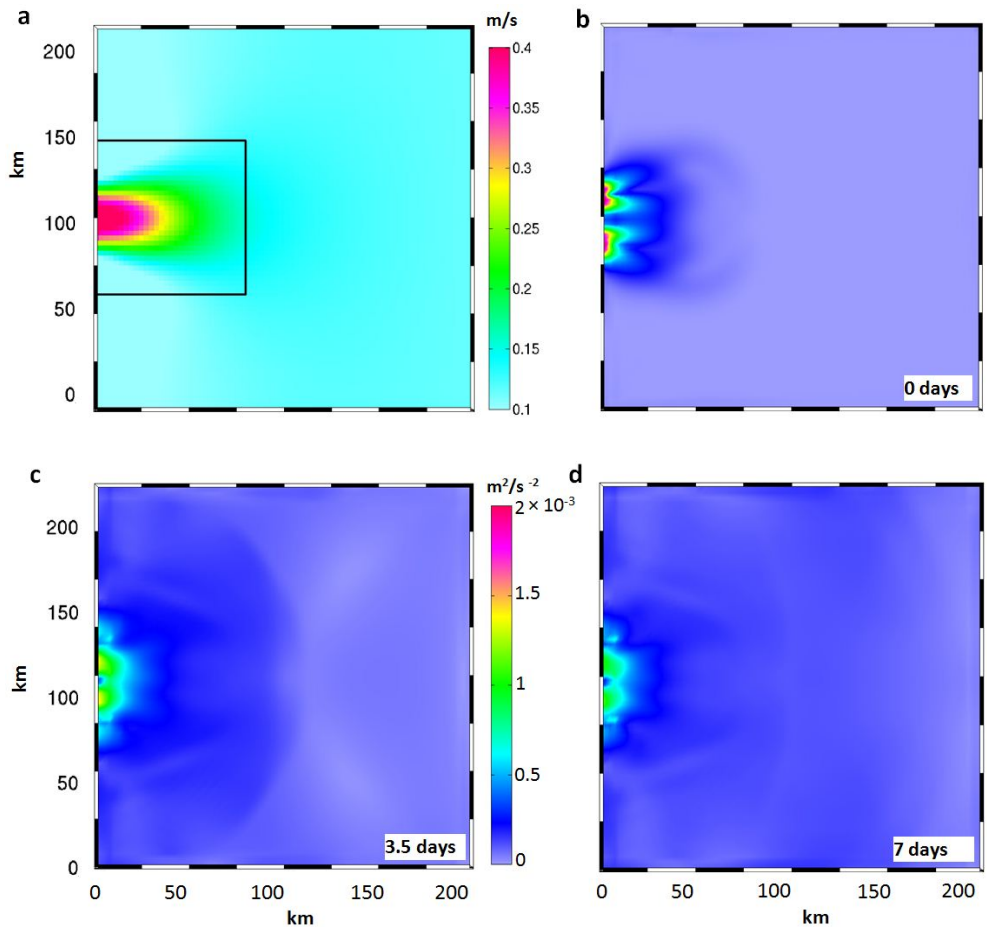

Figure 4.9 (a) is current speed in case of adding advection at west boundary of Big-Brother. (b), (c) and (d) are CRMSD of kinetic energy of fluctuated velocity at surface layer between BJ1 and BJ5 at 0 days, 3.5 days and 7 days, respectively

The Big-Brother was run for 30 days and first 15 days were discarded to be sure it achieves equilibrium; this reference is called BJ1 (Fig. 4.9 (a)). BJ1 simulation is then filtered small scale smaller 30 km to construct IC and BC for BJ5. Figure 4.9 (b) to (c) show the relative CRMSD of kinetic energy of

fluctuated velocity at different simulated time. At initial stage, high value of errors occupied at area around advection source. Such errors propagated to the left with decreasing amplitude as far as source as time goes pass. After 3.5 days these errors come to center of domain and reach eastern boundary after 7 days.

Figure 4.10 shows kinetic energy of fluctuated velocity at surface layers after 14 simulated days for two cases. In the case of BJ5, kinetic energy of fluctuated velocity equate zero because all small scales were filtered at initial stage. As soon as simulating, disturbance at source significantly generate and develop. As a results, IKE-BJ5 strongly increase to keep up original BJ1 level ((Figure 4.10). Similar to IKE-BJ5, OKE-BJ5 also increase as soon as time goes pass, however its amplitude is much smaller. The increase value of OKE-BJ5 at just several first step of simulation is not come from advection source propagate to. They should come from disturbance generating in area near out boundaries (north, south and east) during the spin-up time of small scale generation. OKE-BJ5 keeps continue to increase when kinetic energy from advection source propagates to north and south boundary, and get highest value when KE from advection source reach the east boundary after 7 days.

In case of adding small scale at west boundary and source (Figure 4.10) (BJ5R), initial kinetic energy of BJ5R equates to a half of BJ1. As time goes pass, IKE-BJ5R significantly increase and over the level of BJ1, then very slowly increase onward. Similar to OKE-BJ5, OKE-BJ5R at initial state also equates to zero and then significantly increase as time goes pass. However, its value is much

higher. Such higher OKE-BJ5R is much contributed from disturbance which added at west boundary, propagate to north and south boundaries. The OKE-BJ5R get highest value earlier than that of in OKE-BJ5. This kinetic energy perhaps is contributed from disturbance combining from both west boundary and adding source, propagate to north and south boundaries. After 7 days, OKE-BJ5R has second smaller peak that is the same time to the peak of OKE-BJ5. Therefore, it highly confirm that after 7 days, disturbance from advection source propagate to eat boundary.

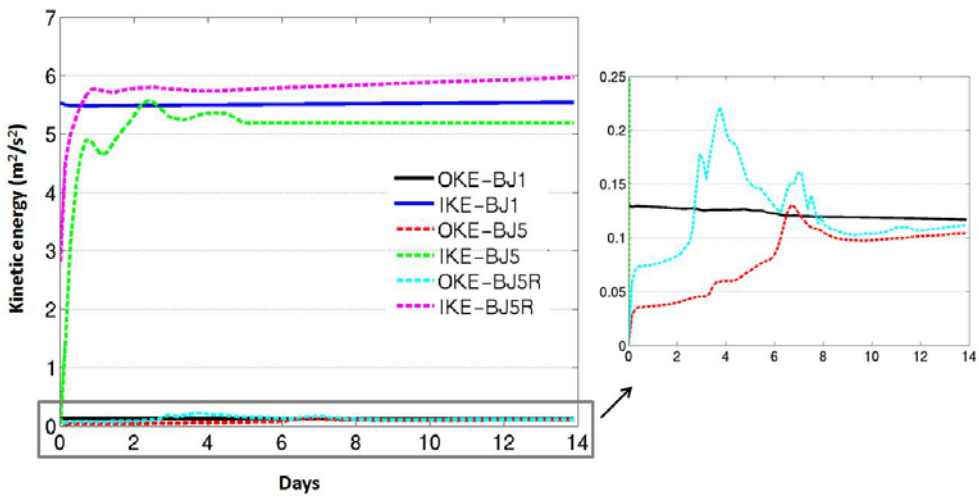

Figure 4.10 Time series of kinetic energy of fluctuated velocity at surface layers after 14 simulated days. IKE denotes kinetic energy calculated at adding advection (inside the rectangular in Figure 15 (a)), and OKE denotes sum of kinetic energy calculated at three out boundaries including south, north and east.

4.3.2. Contribution of island to small scale generation

Island case is a type of source number 1 (Denis et al. 2002a) which can make weak around island shape and accelerate the development of small scales. The model set up of island case (IS) is similar to NC except adding island in the center of domain. The shape of island is a white area in the Figure 4.5 (b).

The generation of filtered small scales in island case (Fig. 4.11 (a)) has totally different shape with those in AD (Fig. 4.6 (b)). While the smaller filtered small scales grow first, then shift the speed of growing energy to larger filtered scale in the case of added advection after first 4 minutes. In the case of IS, larger filtered scale develops first, then shifts the energy speed to smaller filtered scales. It is worth to pay attention that, the smaller filtered scales keep grow and over 140% of Big-Brother amplitude after 12 minutes whereas, such filtered small scales just reach 80% in maximum in AD.

In term of CRMSD, the errors in case IS only have high value around the island which is white area in the middle of domain, while there is no error along the boundary or inner domain far from the island. Such errors long the island strongly grows in value and broadens in space as time goes pass. Therefore, such kind of source dramatically affect to generation of small scale perturbation (Fig. 4.11 (b) & (c)). The error will reduce as the corner of island become smoother.

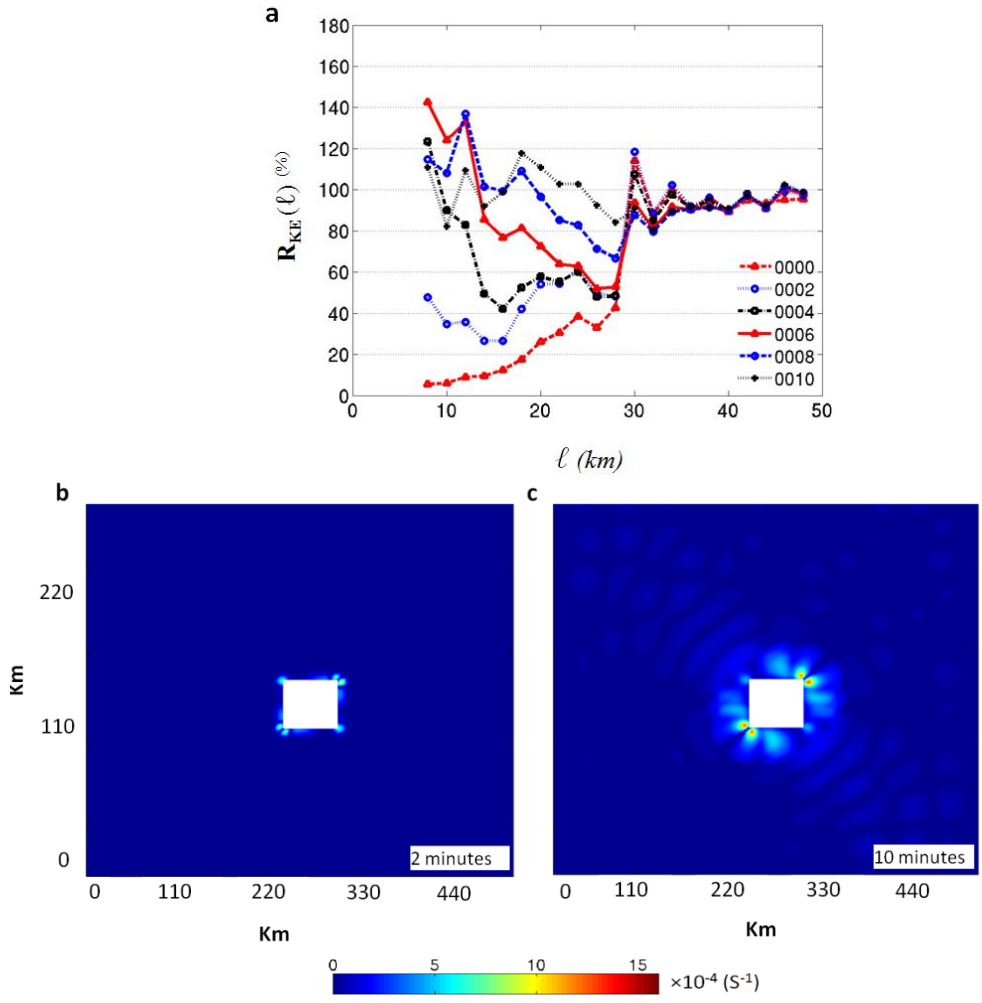

Figure 4.11 (a) is ratio of surface kinetic energy of the Little-Brother to Big-Brother during short time of simulation. (b) and (c) are CRMSD of z-vorticity between Little and Big-Brother after 2 and 10 minutes. White area is shape of island.

4.3.3. Benefit of adding random small scale at boundary condition

We already observed that, normal case (NC) have no any source supporting for generation and development of small scales. Therefore, although energy of filtered small scale generate and develop, it's never keep up and just get 60% of Big-Brother amplitude. However, in cases of AD and IS, it quickly get over 100% of Big-Brother amplitude. Therefore, in this part we will observe how adding random small scales affect to the generation and development of small scales. We implemented cases base on the NC case with adding random small scales at only boundary condition. The current speed of NC in this experiment is changed to 0.4 m/s. The small scales at initial condition were totally filtered. The small scales adding boundary starts updating from second time step of simulation.

Figure 4.12 shows energy spectrum at surface layer of Big-Brother and Little-Brother with of original normal case (J5) and case of after adding small scales at left boundary condition (J5R). The red line is original normal case. After a days of simulation, kinetic energy of J5 is still under estimation comparing with that of Big-Brother and never reach original Big-Brother's level when running for longer time of simulation. As we discussed before, although kinetic energy at filtered small scales are transferred from larger scales for development, such support is not large enough to help it reaches level of original Big-Brother. Whereas, kinetic energy of J5R nearly fits to original Big-Brother's level. In other word, small scales with wavelength smaller than 30 km were recovered after 1 day.

This is reasonable since current speed is 0.4 m/s so adding small scales at boundary can travel around 34 km a day.

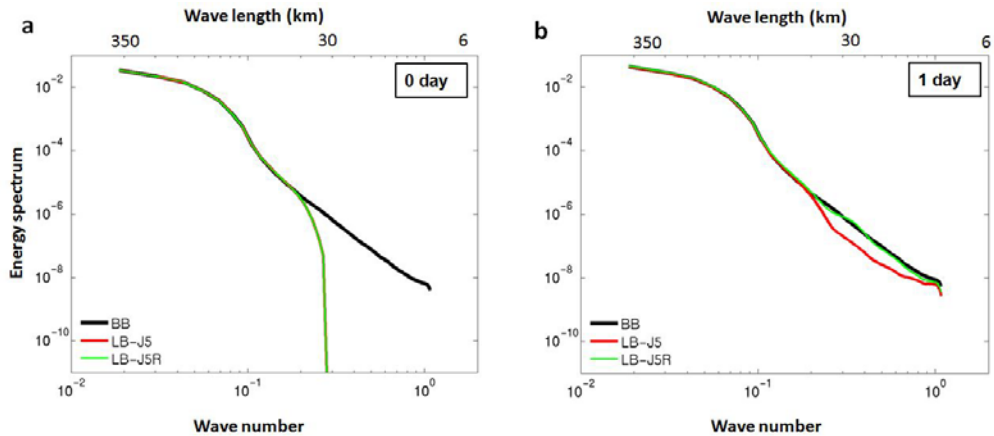

Figure 4.12 Energy spectrum at surface layer of Big-Brother and Little-Brother before and after adding random small scale at boundary condition of NC case with current speed of 0.4 m/s. (a) at initial state, (b) after 1 day of simulation

We also implemented experiment for IS case which can itself stimulate small scale develop. Similar to normal case, small scales only are added at the left boundary and they are started to update from second step of simulation. The kinetic energy of case before and after adding small scales at boundary are described in the Figure 4.13. It is interesting that, filtered kinetic energy at small scales is in winding shape which is totally different to smooth shape of NC and AD. This perhaps is caused by island rectangular shape with diameter of 30 km. Such winding shape will become smoother if the corner of island become smoother or in circle shape.

Kinetic energy of J5 grows up and nearly keeps up to original Big-Brother's level after 3 days of simulation. Kinetic of J5R grows up faster than J5 and exactly reaches the level of original Big-Brother's level after 3 days. It can interpret that, IS case is kind of source number 1, it can stimulate the development of small scales. Therefore, it itself can help small scales reach the level of Big-Brother's.

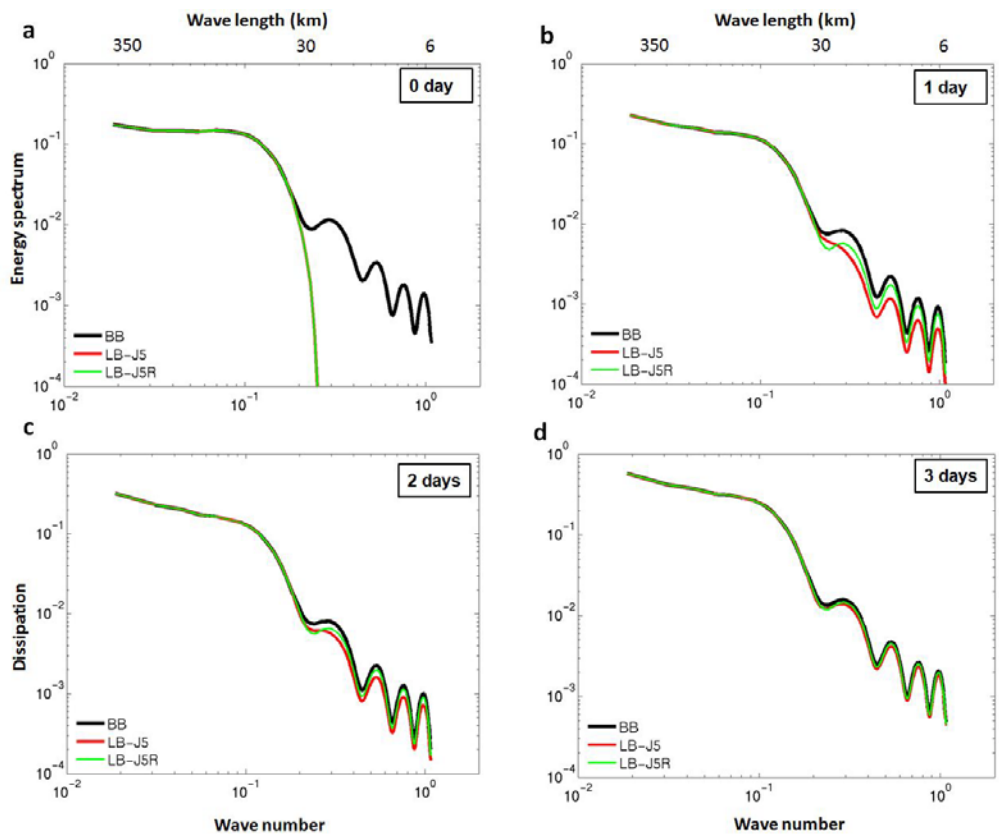

Figure 4.13 Energy spectrum at surface layer of Big-Brother and Little-Brother before and after adding random small scale at boundary condition of IS case. (a) at initial state, (b) after 1 day, (c) 2 days and (d) after 3 days of simulation.

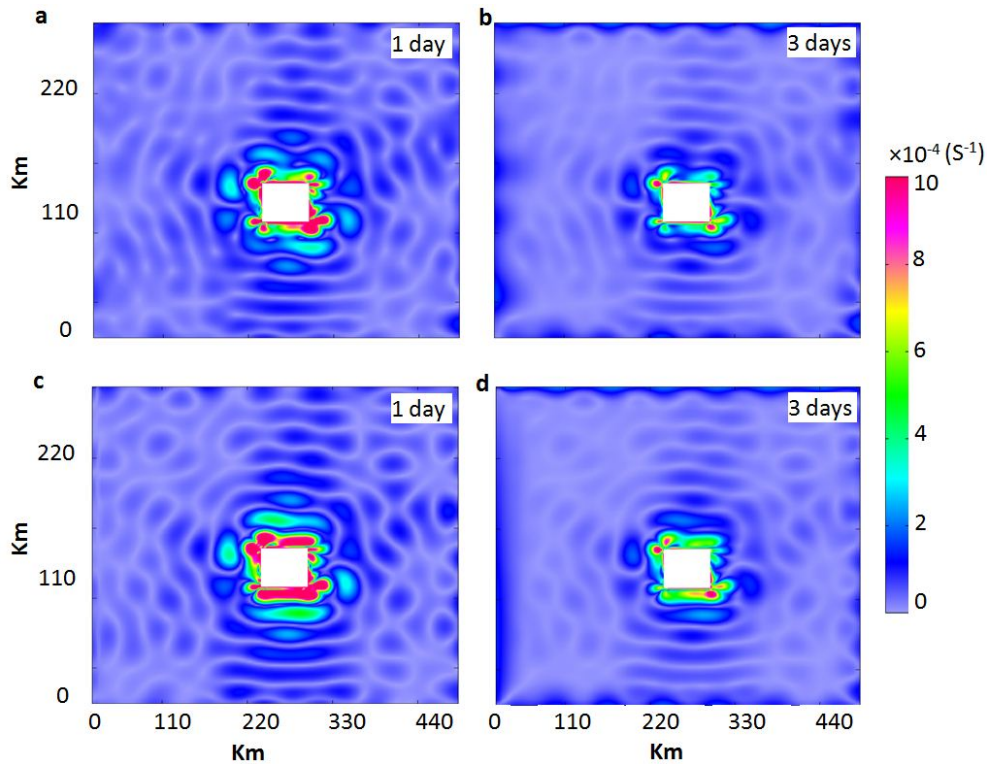

Figure 4.14 Center Root Mean Square Different depth averaged of z-vorticity between Little-Brother and Big-Brother after 1 day and 3 days of simulation. (a) and (b) before adding small scale, (c) and (d) after adding small scale at boundary condition

When adding small scales at boundary condition, such small scales develop faster and quicker recover the Big-Brother's level (Fig. 4.13). Laprise. (2008) pointed out that spatial spin-up time of fine scale development from the lateral boundary whenever updating is very important. In other word, fine scales take a place or need a distance from the lateral boundary to develop before they reach their equilibrium amplitude at each time of updating large scales at lateral

boundary. Therefore, adding small scales at boundary condition can help fine scales reach their equilibrium amplitude quicker and reduce such small scale developing distance from the lateral boundary. As a result, it helps to reduce spatial spin-uptime. As shown in the Figure. 4.14, adding small scales at boundary condition (J5R) can reduce more errors, especially in the region near left boundary (Fig. 4.14 (c) & (d)) when comparing to those of J5 case (Fig. 4.14 (a) & (b)). We name technique “small scale-adding boundary technique”.

4.4 Summary

This chapter investigated characteristic of small scales generation which associated with downscaling technical. With support of Big-Brother Experiment advantage, the role of sources and some factors affect to the generating small scales were intensively examined. From the discussed results let us have some summary as bellow:

1. The adding source and complex bathymetry significantly affect to the generation of small scales. The effect of each source on the small scales generation is in different way. The adding advection mostly impact on the larger filtered scale with forming a wave oscillating around the Big-Brother amplitude. Adding advection producing sharing stimulates disturbance in development near the source, they then transport to the inner domain. While the island can make weak strongly influence to smaller filtered scales. These wakes occur around the corner of island, and reducing the amplitude as corner become smoother.
2. Small scale generation is quite sensitive to the adding source change. The acceleration of small scale development increase with increasing the adding source levels. The forming wave in all adding source levels are the same but their amplitude is different. They reduce with decreasing the levels.
3. The generation of small scales also strongly sensitize to the adding small scale in the boundary condition. Adding small scales in case of lacking supporting

stimulated sources such will stimulate small scales grow up faster and quickly keep up with Big-Brother level (Fig. 4.12).

CHAPTER FIVE

5. ENHANCEMENT OF PREDICTABILITY IN ONE-WAY NESTED PROCEDURE

5.1 Introduction

There are a number of studies have shown skill of RCM in the small scale generation with right amplitude and spatial distribution (Warner et al. 1997; Denis et al., 2002). However, others recognized an interested matter that, although RCM successfully generated the smaller-scale features, kinetic energy on the large scales was lost (Castro et al. 2005; Feser et al. 2011), and this has not been reconfirmed so far. In this aspect, we suspect characteristic of small-scale generation are one of reasons contributing to the loss of kinetic energy on the large scales.

Moreover, Winterfeldt et al. (2010) and Feser et al. (2011) mentioned that dynamical downscaling does not generate small scales in a region which was not present of small scale generating sources. Denis et al. 2002a also experienced this matter when finding underestimation of nested small scale relative vorticity at 500 hPa where small scale dynamics are in free atmosphere. Therefore, based on all aforementioned issues, this part will focus on how small scales generate when lacking supporting stimulated sources in the domain; how much they affect to large scales, and then degrade the RCMs results; and then how to develop small scales in such case and improve the quality of solution.

5.2 Experimental setup

The Big-Brother simulated over a large domain with grid resolution of 9 km × 9 km, extended from 101.00°E to 111.00°E longitude and 5.00°N to 12.00°N latitude, equivalent to lengths of 1089 km and 774 km, respectively, in the southeast sea of East Sea of Vietnam. The Little-Brother simulation, with the same resolution as the Big-Brother, was performed over a smaller domain, and embedded in the Big-Brother domain: 103.50°E to 108.50°E longitude and 6.98°N to 10.70°N latitude, equivalent to lengths of 554 km and 418 km, respectively (Fig. 5.1). The bathymetry established in the study was extracted from ETOPO1. Total vertical layers of both Big-Brother and Little-Brother were 30 layers in S grid. S grid is a nonlinear function of the actual coordinates. It is similar to σ grid but can more flexibly adjust the resolution of vertical depth (Hedström, 2009).

Open boundary condition selecting in the work was Raymond and Kou Radiation (R-K radiation) with supported by sponge/nudging. As suggested in Pham et al. (2016), R-K radiation can mitigates errors cause by reflections from the LBCs for case of outgoing flow. For calculating eddy viscosities and eddy diffusivities, K-profile parameterization was selected. It is efficient model's turbulence closure scheme in simulating for regional domain (Large et al. 1994). Moreover, it is the same as scheme used in driving model (HYCOM) in order to mitigate errors due to the physical parameterization inconsistencies as mentioning in Denis et al. (2002a), and Pham et al. (2016).

Most experiments simulated 25 days (from September 1st to September 25th) in 2014. The global hind-cast HYCOM output, which is freely available on the web site of the Center for Ocean-Atmospheric Prediction Studies (COAPS, http://hycom.coaps.fsu.edu/thredds/catalog.html) was used to construct ICs and BCs for the Big-Brother. This global dataset includes sea temperature, salinity, horizontal momentum and sea surface height. Their horizontal resolution is at every 1/12° × 1/12°(~ 9 km) with discretized with 33 vertical layers (0 - 5.5 km) in the *z*-coordinate. The update frequency is at every 24 hours, as described in detail in COAPS and Metzger et al. (2008).

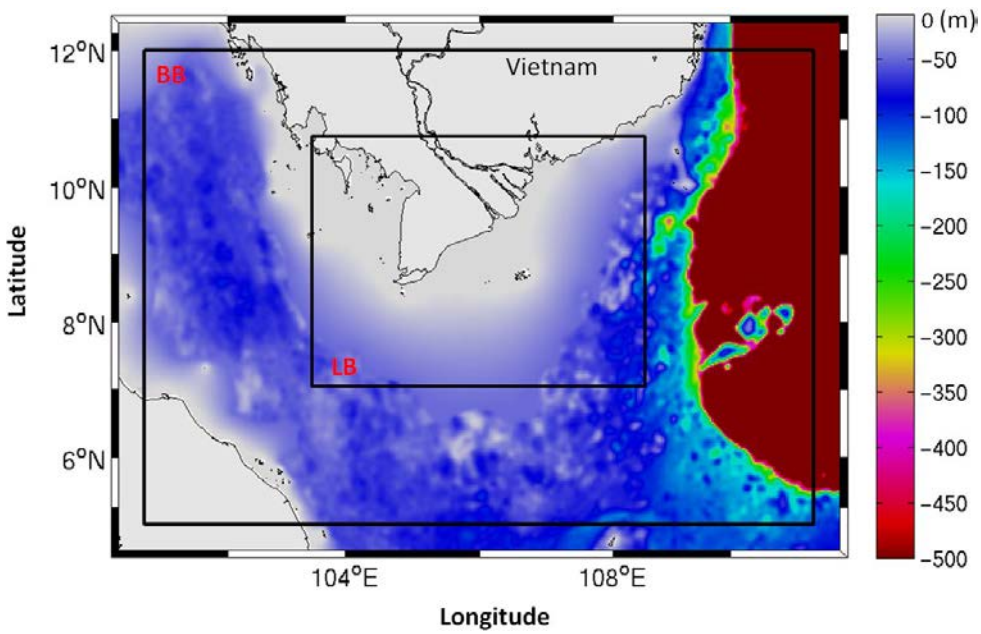

Figure 5.1 Geographical layout of the study domain. The large and small rectangular areas denote the simulated domains for Big-Brother and Little-Brother, respectively.

For providing atmospheric data including wind speed at 10 m, atmosphere pressure, relative humidity, atmosphere surface temperature, precipitation, and net short- and long-wave heat fluxes, the Weather Research Forecast (WRF) model was used to downscale from the results of the NCEP final operational global analysis (NCEP-FNL). The NCEP-FNL is global data set at every 1° × 1° grid point and supplies updates every 6 hours. The spatial resolution of WRF is the same as to the ocean models.

Table 5.1 The design of performed experiments. 'J' describes the jump ratio. For example, J3 means the jump ratio is 3. Simulated cases are marked "○", non-simulated cases are marked "×".

Experimental cases with real domain	**Viscosity /diffusivity (m^2/s) in sponge layer**					
	0	***40***	***80***	***300***	***800***	***1200***
No filtering small scales: J1 (0km)	○	○	○	○	○	○
Filtering small scales: J3 (54 km), J6 (108 km), and J9 (162 km)	×	×	○	×	×	×
Adding small scales: J3, J6, and J9	×	×	○	×	×	×

In the BBE, Big-Brother guides Little-Brother with only the large and medium scale oceanic information. The spatial small scale features from Big-Brother output were filtered out with a low-pass filter of the Discrete Cosine Transform, which is suitable for non-periodic signal data and flexible in controlling the choice of the removed wavelengths (Denis et al. 2002b). These filtered datasets were used to construct initial conditions as well as lateral boundary condition for Little-Brother. The initial conditions were established only one time at the start of the simulation. While boundary conditions were updated at every time steps of Little-Brother. Table 5.1 describes the experiment with different cases in setting up viscosity/diffusivity of sponge layer in columns, and different resolution jump (J) which is ratio of the spatial resolution between Big-Brother driver and the nested Little-Brother model (Denis et al. 2002a; Pham et al. 2016).

5.3 Results

The core of the work is to identify characteristic of generating small-scales and their effect to the large scale in nested procedure using ocean regional circulation model. However, in downscaling procedure, there are many factors such as domain size, type of boundary conditions and even ORCMs itself, can degrade the downscaled results (Warner et al. 1997; Denis et al. 2002a; Pham et al. 2016). Therefore, as a first step of work, we validated ability of ORCMs with given factors. Second, we accessed how small scale generation impacts on the large scale,

then degraded the quality of ORCM's results, and investigated the original reasons behind that. Finally, we proposed and practiced new idea to improve the quality of solution in such cases.

5.3.1. The role of sponge layer in improving quality of ORCMs results

It is well known that the open boundary conditions were developed base on hyperbolic equations (Marchesiello et al. 2001). Therefore, the method to mathematically treat LBC to averaged Navier-Stock equation is an ill-post problem (Palma and Matano. 1998). It means that, in case of flow moving in the domain one must only specify boundary conditions, but when flow is directed outward no physical boundary condition is required, and still prescribed boundary conditions will cause ill-posed problem due to an over-specifying boundary conditions. Such over-specification will lead to inconsistence between specified boundary conditions with that of in interior domain, generate reflect waves back at lateral boundary and then cause large deterioration in the interior solution (Palma and Matano. 1998; Giorgi and Mearns. 1999; Marchesiello et al. 2001; Bayo and Debreu. 2005).

Therefore, open boundary condition plays an important role in dynamic downscaling. It is a first order effect on the ORCMs solution (Pham et al. 2016). Over several decades, numerous OBC from simple to sophisticated such as "Clamp", "Flather" and "Raymond and Kuo Radiation". According to Roed and Cooper (1986), a good open boundary should permit the perturbations generated inside interior domain to freely leave out the boundary without causing any change

to inner solution. However, there are still no perfect OBC can solve this problem (Bayo and Debreu. 2005). According to practical experience, the numerical behavior of any particular OCB not only strongly depends on its numerical implementation, the general characteristic of the model, but also the nature of the problem to be identified (Palma and Matano. 1998).

In order to mitigate their limitation, OBCs are often used with supported from supplementary methodology (sponge/nudging) (Palma and Matano. 1998; Giorgi and Mearns. 1999; Marchesiello et al. 2001; Bayo and Debreu. 2005). Pham et al. 2016 pointed out that, solution of ORCM changes with different OBC when combining with supplementary methodologies. The sponge layer is a simple relaxation technique but it can efficiently improve the of interior numerical model solution (Marchesiello et al. 2001). Sponge layer has been widely used in numerous studies and shown the ability to restrict the error cause by discontinuity near the open boundaries.

The principle behind sponge layer is that, increasing horizontal viscosity in the model interior region near the open boundary, to absorb disturbances and suppress computational noise generated by the inconsistency between external and internal solutions, in particular for case of flow going out of domain (Palma and Matano. 1998; Marchesiello et al. 2001; Oddo and Pinardi. 2008). Generally, the sponge layer width is about 10 grid points (Giorgi and Mearns. 1999) and maximum sponge viscosity/diffusivity can up to 0.1 × horizontal resolution in meter. For instance, resolution of LB is 9 km, the sponge layer width is 90,000 m,

and maximum sponge viscosity/diffusivity is up to 900 m^2/s. Since the range of sponge viscosity/diffusivity value is too large, it is very difficult to select a suitable value. Therefore, in this work we tested nested procedure with employing difference of sponge viscosity/diffusivity value ranging from 0 to 1200 m^2/s as shown in the Table 5.1. The *Raymond and Kuo Radiation* (*R-K radiation*) with supplementary methodologies of sponge/nudging which are deserved highly believable as suggested by Pham et al. 201, are employed in this work.

The time scale for nudging when flow going out was set at 3 days and the time scale for nudging during flow moving in the domain was at 365 days. All cases of different sponge viscosity/diffusivity were simulated at spatial resolution at *J1*. It means that there are no any removing small scales, in other word all scales of Big-Brother specify at ICs and BCs for Little-Brother. Also, update frequency at LBC is at 10 minutes, same to time steps of Little-Brother in order to avoid effect causing by inconsistency of LBCs resolution (Denis et al. 2002; Pham et al. 2016).

First, we look at kinetic energy spectrum calculated at the surface layer of Big and Little-Brother without supporting of sponge layer, in other word sponge viscosity/diffusivity was set 0 m^2/s after 20 days of simulation (Fig. 5.2 (a)). In general, energy most reserved at large scales, and gradually decreased amplitude in smaller scales. Little-Brother captured well large scales of Big-Brother. On the energy spectrum, they nearly fitted together. However, at medium and small scales (scales in the red rectangular), energy of Little-Brother was distorted.

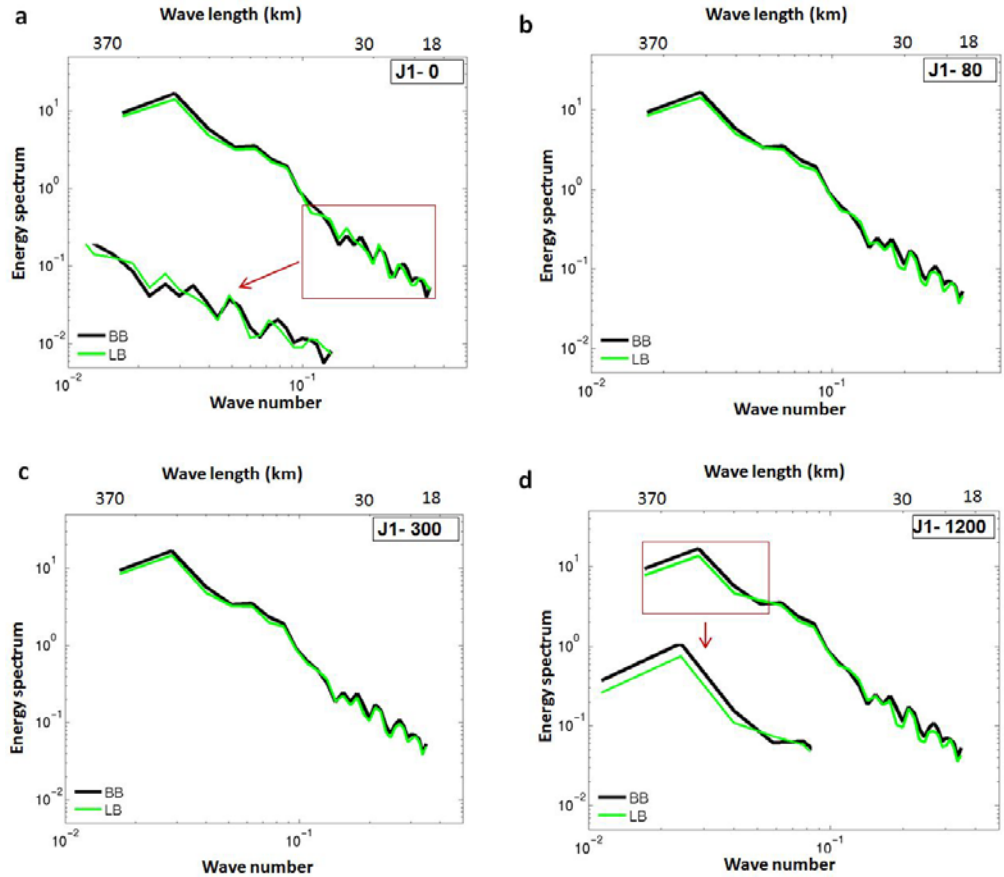

Figure 5.2 Energy spectrum at surface layer after 20 simulated days of Big-Brother and Little-Brother of case J1 with different viscosity/diffusivity value. (a) to (d) are cases of viscosity/diffusivity from 0 to 1200 m^2/s.

At some parts of scales, energy spectrum of Little-Brother is in different trend with that of Big-Brother. This can understand that, because of without supporting from sponge layer, disturbance and noise generated due to discontinuities between internal and external information during outward propagation, were not suppressed from sponge viscosity/diffusivity along region near open boundaries. They therefore, caused reflection back to interiors domain,

then deteriorated the inner model solution (Marchesiello et al. 2001). Whereas, large scales can freely leave the domain, and disturbance and noise due to discontinuities at the open boundary too small to make any effect to large scales, but may cause the change in the consecutive medium scales.

When employing sponge layer, disturbances and noise along the region near boundaries were highly absorbed, and reflection of disturbances from boundary were substantially reduced (Marchesiello et al. 2001; Oddo and Pinardi. 2008). Therefore, we can observe significant mitigation of distortion at small scales of Little-Brother (Fig. 5.2 (b) & (c)). The energy spectrum of Little-Brother was quite similar with value of sponge viscosity/diffusivity were set at 40 (not shown), 80 and 300 m^2/s.

However, when setting sponge viscosity/diffusivity at 800 (not shown) and 1200 m^2/s, both energy of small and large scales was distorted and underestimation. This perhaps is a caution of sponge layer in setting suitable value of sponge viscosity/diffusivity. Sponge layer may also absorb the income waves. Therefore, if sponge viscosity/diffusivity is high enough it may damp also damp large scales. Moreover, too high value of sponge viscosity/diffusivity may produce reflections of outgoing waves (Oddo and Pinardi. 2008), then make small scale distort as observing in Figure. 5.2 (d).

In overall, regional model ROMS has a good ability in reconstruct all scales from driving dataset specified at boundary conditions. The nested performances in term of energy spectrum of cases J1-40, J1-80 and J1-300 are

pretty good with high correlation coefficient of 99.9%. They only deviate from Big-Brother about 5%, and get error of 3% in comparing to Big-Brother. Thus, in this work we chose sponge viscosity/diffusivity with value of 80 m^2/s for further study.

5.3.2. Small scale generation effect on the large scales

Since ocean regional circulation model downscale coarse dataset of ocean global circulation model by supplied large-scale forcing at the lateral boundaries, it must have ability in both simulate large-scale circulation without biases and can generate meaningful finer scale features that absent in the LBCs. Such skills of ORCMs have been proved by numerous previous studies (Denis et al. 2002a; Pham el al. 2016). Of course, simulating in different factors such as resolution jump, domain size, type of boundary conditions and even different ORCMs, downscaled results can differ.

In the last section, The ORCMs has also confirmed how well reproducibility of the features of Big-Brother when Little-Brother were forced by time variables conditions at all scales. This research will not prove downscaling ability of ORCMs again. Here, we just concentratively identify dynamical small scale generations on a special aspect of lacking the support from stimulated sources which can stimulate the small-scales generation and development.

The given domain, in the southwest Sea of East Sea of Vietnam, is suitable for this circumstance. The surface circulation pattern in the research area is quite

complicated with combination of many currents and eddies. Stable current coming from Karimata Strait flows to northwest ward along the eastern coastal of Vietnam. Such current merges with strong anti-cyclonic eddy appearing in the southeast of Vietnam and unstable current from Gulf of Thailand to become a main circulation along the eastern coastal of Vietnam (Hu et al. 2000; Liu et al. 2008; Fang et al. 2014).

The simulated period of time is from September 1st to September 25th which is in summer season with strong stratification often happens. Therefore, there is no buoyancy which is type source number 3 in developing small scales occurring in the region. Also, although there is a Mekong river with a mean annual discharge into the East Sea of Vietnam of 13,000 m^3/s (Botkosal. 2009). However, with resolution of 9 km × 9 km this river seems to do not take any effect to the current and does not produce shearing as one of type source number 3. In the region, there is no island (type 1) which can make wake and stimulate small-scale development.

Figure 5.3 shows energy spectrum of case J3 and J6. We first look at J3 which is the optimal case of spatial resolution jump as suggested in Pham el al. 2016, all small scales less 54 km were filtered in ICs and BCs as shown in Figure 5.3 (a). After 5 days of simulation, Little-Brother energy of filtered scales increase a lot, but they still cannot reach the amplitude of Big-Brother (Fig. 5.3 (b)). This interprets that, filtered small scales in Little-Brother regenerate and develop. However, such growth is still not large enough to fully recover the level of Big-

Brother due to lack sources which can increasingly develop small scales. After 10 simulated days, energy at consecutive larger scales (scales larger than 54 km) decrease. The energy at largest scales significantly decrease after 20 days (Fig. 5.3 (c) & (b)). This gives a sign of large scales transfer energy for small scales development through interactions of internal dynamics processes as classified in source type number 2 (Denis et al. 2002). However, this energy transfer of process is also not big enough to make filtered small scales reach level of Big-Brother. Therefore, larger scales gradually lose their energy and step by step become more negative bias as time passes.

At the higher spatial resolution jump of J6 (Fig. 5.3) and J9 (not shown), its negative bias at large scales are larger than that of smaller resolution jump of J3, and the interested thing is that, speed of losing energy at the part of largest scale is much higher than in the medium scales. After 20 simulation days, deflection of energy in J6 at large scale is much greater than that of small scales. These can prove that, small scales generation without support from stimulated source may significantly affect to large scales part, and make large scales strongly biases comparing to driving dataset. They then degrade quality of nested solution. Such contamination increase with increasing resolution jump. For example, J3 is in better agreement of coefficient correlation with Big-Brother and has smaller error than J6 (Fig.5.5).

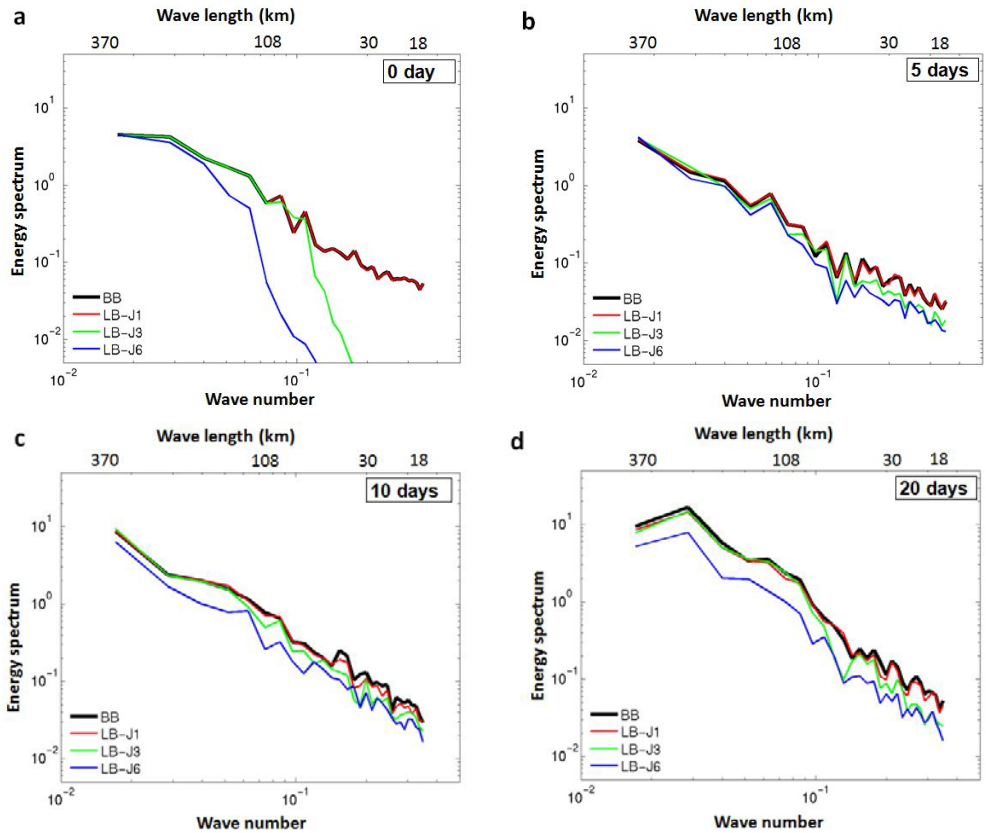

Figure 5.3 Energy spectrum at surface layer of Big-Brother and Little-Brother with different spatial resolution jump. (a) is at initial state, (b) to (d) are at 5 days, 10 days and 20 days, respectively.

Figure 5.4 shows the time series and statistic terms of elevation in different resolution jump. J1 which is case of without filtering small scales is also presented here for easily comparison. The elevation of J1 totally fits to Big-Brother's with correlation coefficient almost 100%, CRMSD is nearly zero and standard deviation is exactly same to Big-Brother's. Whereas, elevation of case J3 and J6 deflect from the Big-Brother's as time go passes, especially after 5 days of simulation. The

amplitude of deflection increases with increasing the resolution jump. For example, J3 has correlation coefficient around 95%, 30% of errors and 5% of standard deviation. While correlation coefficient of J6 reaches only 85%. Its error is also higher than J3 with value of 55% and standard deviation is around 10% (Fig. 5.4 (b)).

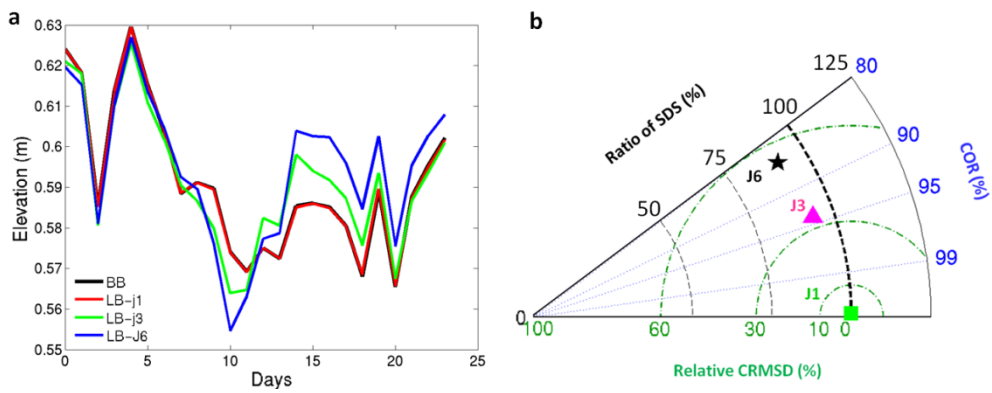

Figure 5.4 (a) time series of elevation in different resolution jump after 20 days of simulation. (b) is their statistic terms presenting on Taylor diagram.

Similar to elevation, with higher resolution jump quality of amplitude horizontal velocity increases. As shown in the Figure 5.5, amplitude horizontal velocity of J1 is the best. It almost fits to Big-Brother's. The amplitude horizontal velocity of J3 is worse. The uJ3 has correlation coefficient only of 97%. It deflects nearly 5% and gets 27% of error. The amplitude horizontal velocity of J6 is the worst with correlation coefficient of 96% and value of error and standard deviation of uJ6 are higher than uJ3.

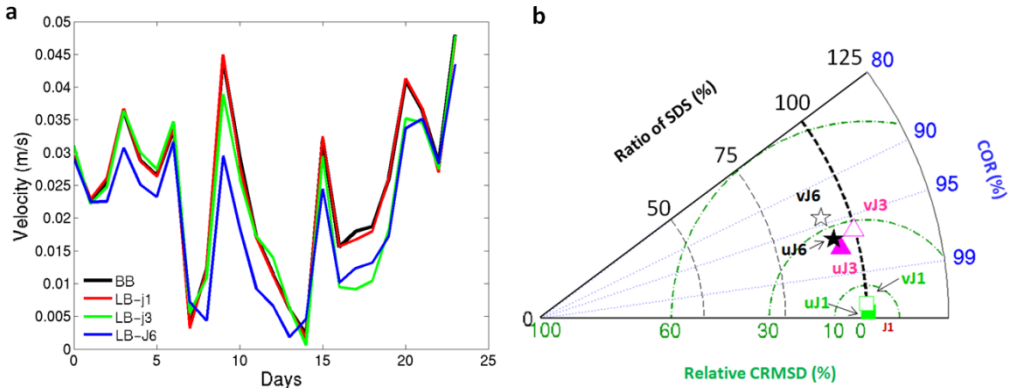

Figure 5.5 (a) time series of mean amplitude velocity in y direction of different resolution jump after 20 days of simulation. (b) Taylor diagram showing the effect of different resolution jump on the mean horizontal amplitude velocity. u is velocity in x direction, and v is velocity in y direction.

5.3.3. Enhancement of predictability

We already observed small scales which are absent at ICs and BCs do not fully recover during the nested process at the region where stimulated source are unavailable. Such small scales underestimation cause energy of larger scale in negative bias to Big-Brother. While in case of J1, Little-Brother reproduced well the features at all scales driving from Big-Brother (Fig. 5.2 (b) & (c)).

Base on that, it let us have an idea to add small scales at both ICs and BCs in nested procedure. Added small scales should depend on the shortest resolvable wavelength in the Little-Brother and spatial jump ratio. For example, in case of J3, the shortest resolvable wavelength in the Little-Brother is 18 km, and spatial jump ratio is 3. Therefore, added small scales should be from 18 km to 54 km. However,

small scales adding in J9 must be greater than in J3, from 18 km to 162 km. This approach is somehow similar to specifying values of the kinetic energy k at initial in the turbulence model k-ε or k-ω. In such turbulence model, beside specifying values of turbulence variables at initial in order to avoid "division zero" because of equations using k values in the denominator part of fractions, its main purpose behind that is to make turbulence quickly become full development (Sullivan et al. 1994; Franklin et al. 2004; Rao and De Bruyn Kops. 2011).

The same to that aim in the turbulence model k-ε or k-ω, adding small scales at boundary condition in nested model help finer small-scales rapidly achieve full development. As a result, it can reduce their spin-up time in generating of fine-scale features. Here, the spin-up time is time needed for fine-scale features reach their equilibrium amplitudes (Denis et al. 2002a; Laprise. 2008; Pham et al. 2016).

In order to find out small scales existing in the IC or BC can help to improve the quality of nested solution, the many different experiments with different presenting small scales in the IC and BC were implemented as described in the Table 5.2.

Table 5.2 The set of performed experiments with difference of setting small scales at initial and boundary condition of J6 . Simulated cases are marked "○".

cases	J6 (Filtering small scale ≤ 108 km)
J6: Filtering all small scales at both IC and BC	○
J6IO: Keeping small scales at IC, filtering small scale at BC	○
J6O: Filtering small scale at IC, keeping small scale at BC	○
J6R: Filtering small scale at IC, adding random small scale at BC (*adding small scales at BC from J*6). BC were updated from second time step	○

In the Figure 5.6, the result of case J6 which is both filtering small scales at IC and BC, is the worst. The energy spectrum of J6 significantly deflects to Big-Brother's with standard deviation of 10% and getting 15% of error. In case of keeping small scales at IC but filtering small scales at BC (J6IO), the quality of J6IO is just slightly better than J6. It is clear that existing small scales at IC does not much improve quality of nested solution.

Whereas, when removing small scales at IC and keeping small scales at BC (J6O), its result quality significantly improves. The energy spectrum nearly fits to Big-Brother level with correlation coefficient up to 99.7%. Its standard deviation is only 7% and error is also at 7%. Similar to J6O, the J6R which is a case also removing small scales at IC but adding random small scale at BC after removing

small scales at original BC, has high quality of results, even slightly better than that of J6O. This significantly proves the benefit of existing small scales at BC.

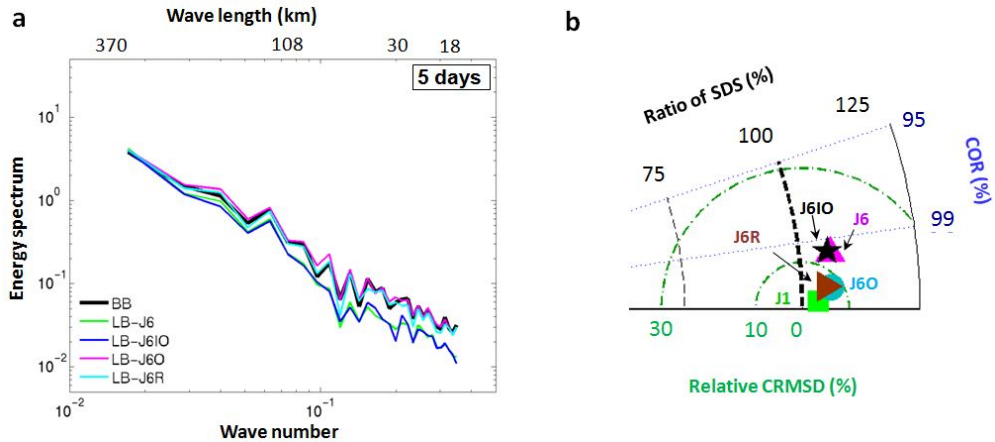

Figure 5.6 (a) energy spectrum at surface layer of Big-Brother and Little-Brother for J6 with different scenarios with ICs and BCs after 5 days of simulation. (b) is their statistic terms presenting on Taylor diagram.

The improved quality of nested results by existence small scales at BC than IC is reasonable. Pham et al. 2016 pointed out that small scales which are absent at IC, were recovered after 18 hours with resolution jump of 3 and this spin-up time of small scale generation may be longer when resolution jump increases. As a result, errors causing by small scales scale generation before reaching full development will be significantly reduce after this spin-up time. Whereas, small scales which are absent from BC continuously were generated. So they continuously generate error, propagate into the inner domain and degrade the quality of solution at every time of updating BC. Therefore, having small scales at

BC can stimulate quickly the small scales develop and reduce the spin-up time and error from small scales generation from BC (Fig. 5.7).

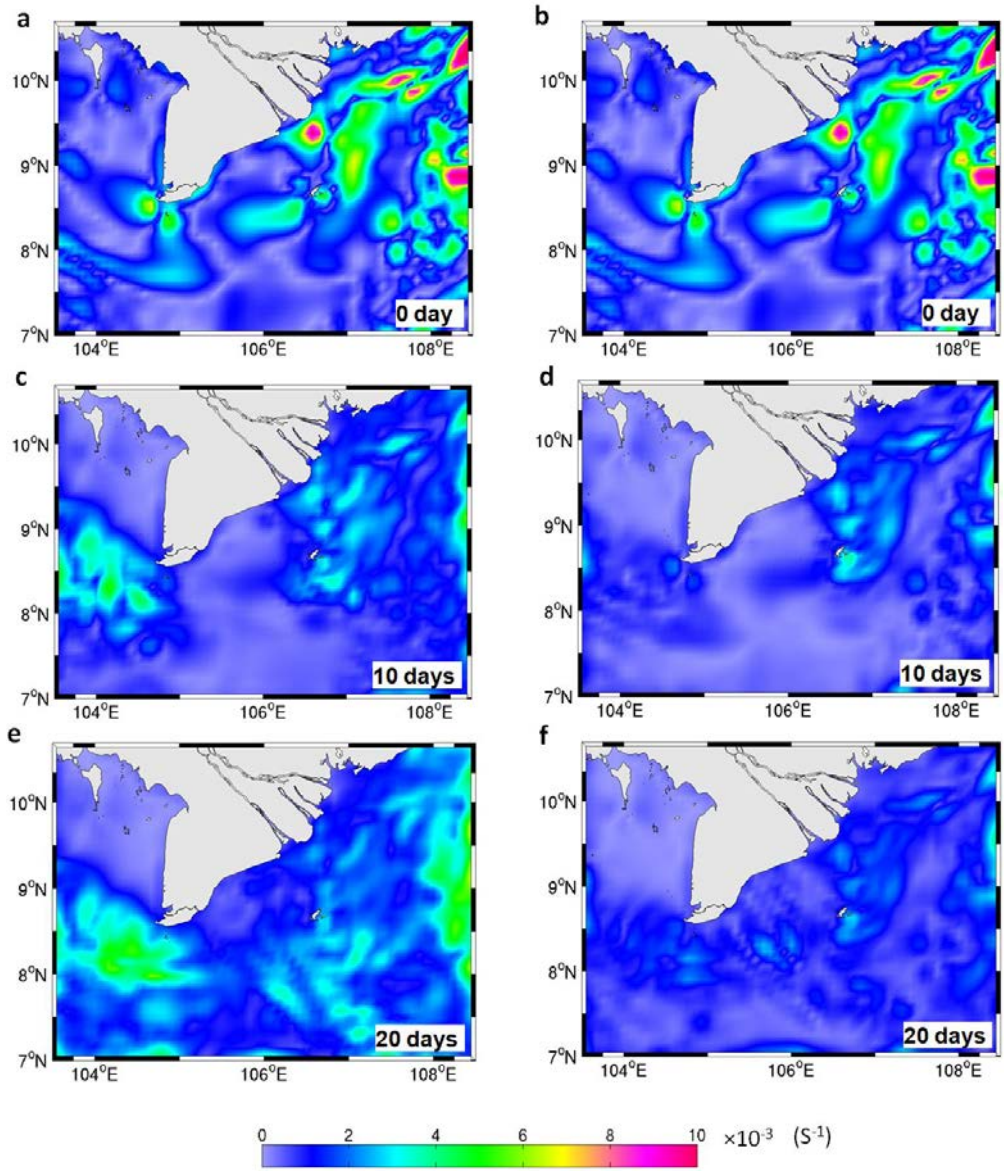

Figure 5.7 Center Root Mean Square Different of depth averaged z-vorticity between Little-Brother and Big-Brother. (a), (c) and (e) are of **case J6** after 0, 10 and 20 days, respectively. (b), (d) and (f) are of **case J6R** after 0, 10 and 20 days, respectively.

Figure 5.8 show the energy spectrum of J3 and J9 before and after adding small scales at initial state and after 5 days of simulation. The energy spectrum of J1 also was shown for easily comparison. It is easy to recognize that in original J3 and J9, all small scales were filtered at initial and boundary conditions, After 5 days of simulation such filtered small scales had a sign of recovery (Fig. 5.8 (a) & (b)).

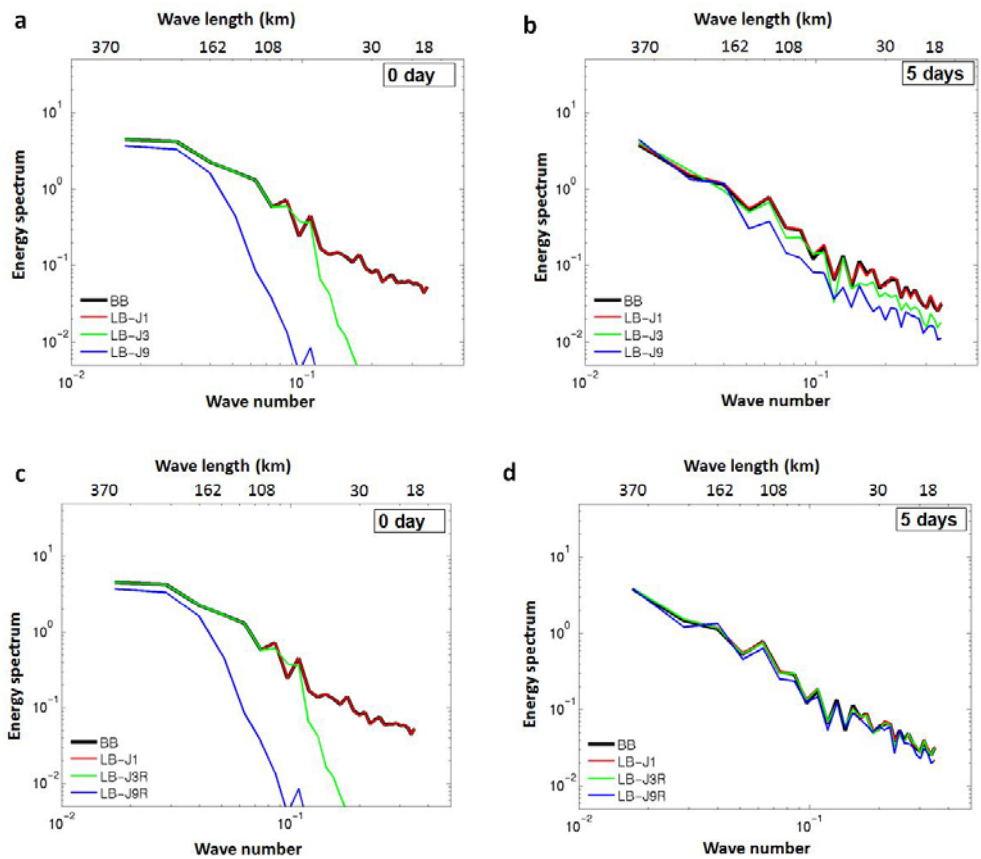

Figure 5.8 Energy spectrum at surface layer after 5 simulated days of Big-Brother and Little-Brother with different spatial resolution jump before and after adding small scales. (a) and (b) are original, (c) to (d) are cases of after adding small scales.

However, they still did not reach the right amplitude of Big-Brother. With higher resolution jump, level of underestimation of filtered small scales is larger. For instance, J3 with filtered small scales of 54 km, their small scales reproduced closer to Big-Brother level than J9. After adding small scales at BCs for J3 and J9 as shown in Figure 5.8 (c), the recovered energy of small scales at all filtered wavelength of both J3R and J9R become very close to Big-Brother amplitude after 5 days. However, although quality of J9R significantly improved, it is still not good as in the J3. This is reasonable, because larger wavelength of filtered scales in J9R will find harder to recover than smaller filtered scales.

Some statistic terms of energy spectrum after 5 days of cases J1, J3, J6 and J9 were calculated and described in the Taylor diagram as shown in Figure 5.9. As the jump ratio decreases from J9 to J1, the correlation coefficient increases, relative CRMSDs decrease and standard deviation is closer than to the Big-Brother. Therefore, as we expected, the quality of reproducibility by nested procedure becomes better as the jump ratios become smaller. This is also in agreement with conclusions in Denis et al. (2002a) and Pham et al. (2016). Pham et al. (2016) mentions two main reasons causing degradation of ORCM's solution as jump ratios become higher. They should be the losing more driving information at the LBCs and increasing discontinuity at the open boundaries between driving data and nested model. This guy also points out that the nested one would take longer to achieve equilibrium as resolution of the global model is coarser of spatial jump ratios increased. In other word, the spin-up time in reproducing small scales need

more time to reach full development with right amplitude and may significantly contaminate the quality of nested solution. Therefore, adding small scales at BC will reduce the loss of driving information and discontinuity at the LBCs, and then help to cut down spin-up time in generating small scales and improve the quality of ORCMs resolution.

After adding small scales, all simulated quality of these cases significantly increase. Performance of J9R is better than J6 and nearly as same as J3, while J6R is better than J3, and J3R has good quality of results as same as J1. The good performance of cases J3R to J9R in term of some statistic terms are as a clear evidence for benefit of adding small scales.

Furthermore, Pham et al. (2016) pointed out that optimal spatial resolution jump between driving data and the nested mode is J3. If this ratio is too large, one should use multiple nesting, or also called multiple "cascade" (Denis et al. 2002; Bayo and Debreu. 2005; Pham et al. 2016). For instance, if resolution of the global model is 81 km, we want to analyze interested area with resolution of 9 km. It is necessary to implement 3 times of nesting. The first nesting step is to downscale from 81 km (J9) to 54 km (J6), and then continues to downscale from J6 to J3 of 29 km in resolution. Finally, continuously nest from J3 to J1 with resolution of 9km. Such multiple nesting will take more time and computational cost to ensure the quality of ORCMs results. However, even following multiple nesting procedure, one still have unwanted errors at each step of nesting. Therefore, with adding small scales instead of multiple cascade, one can run only one nesting with J9R.

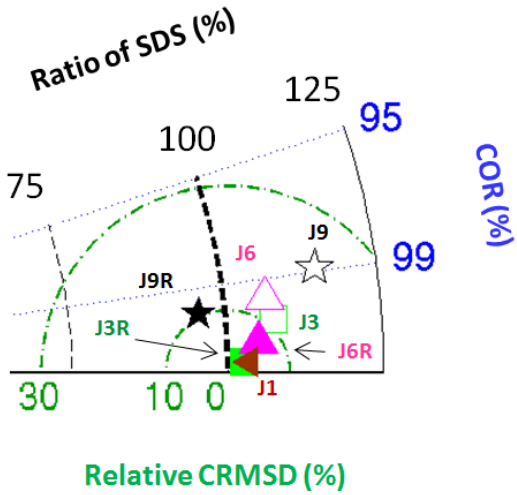

Figure 5.9 Taylor diagram of energy spectrum for different spatial resolution jump before and after adding small scales

Figure 5.10 presents Taylor diagrams of mean relative vorticity after 20 days. We chose to show the relative vorticity field because it is a fundamental quantity in fluid motion and is a higher order variable with regard to velocity (Lam. 2015). Moreover, relative vorticity strongly highlights the small scales of the flow (Denis et al. 2002) and is strongly sensitive to small scale generation during spin-up time (Pham et al. 2016). Figure 5.10 (a) & (b) shows time series of the square relative vorticity averaged over the domain before and after adding small scales of case J1, J3 and J9 after 20 days of simulation, and Figure 5.10 (c) shows their statistical terms presenting on the Taylor diagram. As we can see, J1 was generally quite good in reproducing features of Big-Brother with high correlation coefficient of 95%. Relative vorticity deviates from Big-Brother just only 10 % and has relative CRMSD of 30% (Fig. 5.10 (a) to (c)).

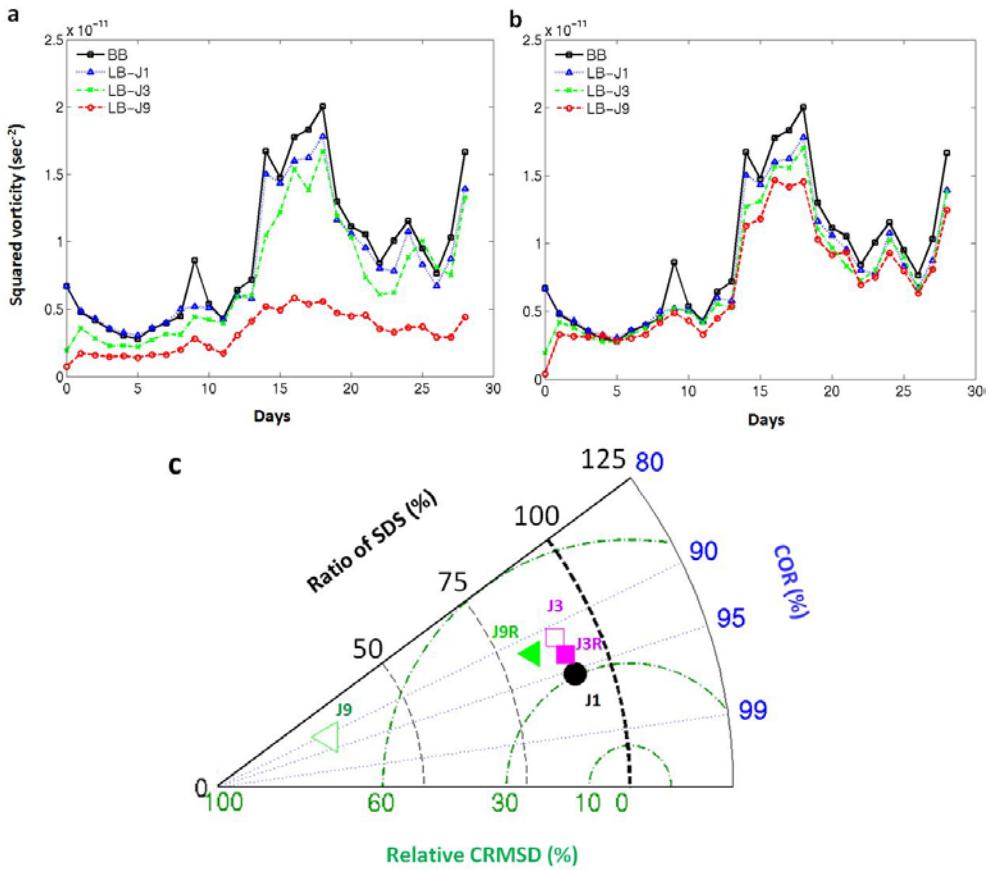

Figure 5.10 Time series of spatial-averaged squared relative vorticity after 20 days of simulation. (a) original cases, (b) after adding small scales cases, and (c) is their statistic terms presenting on Taylor diagram

Relative vorticity of J3 although has negative bias all of time, it does not drift significantly from Big-Brother. However, in J9, relative vorticity significantly deviates and bias from Big-Brother with ratio of SDS of nearly 80%, and getting high relative CRMD up to 70%. Its bad performance is not surprised since resolution jump between Big-Brother and Little-Brother of J9 is too high, and it is

necessary do with multiple nesting as suggested by (Denis et al. 2002; Bayo and Debreu. 2005; Pham et al. 2016).

However, after adding small scales for cases of J3 and J9, their quality of relative vorticity significantly improves. Especially in case of J9R, although it's relative vorticity still under-estimate, its deflection sharply reduces with ratio of SDS of 23% and relative CRMSD is only 35%. The relative vorticity of J9R even is better than J3 in term of correlation coefficient and relative CRMSD.

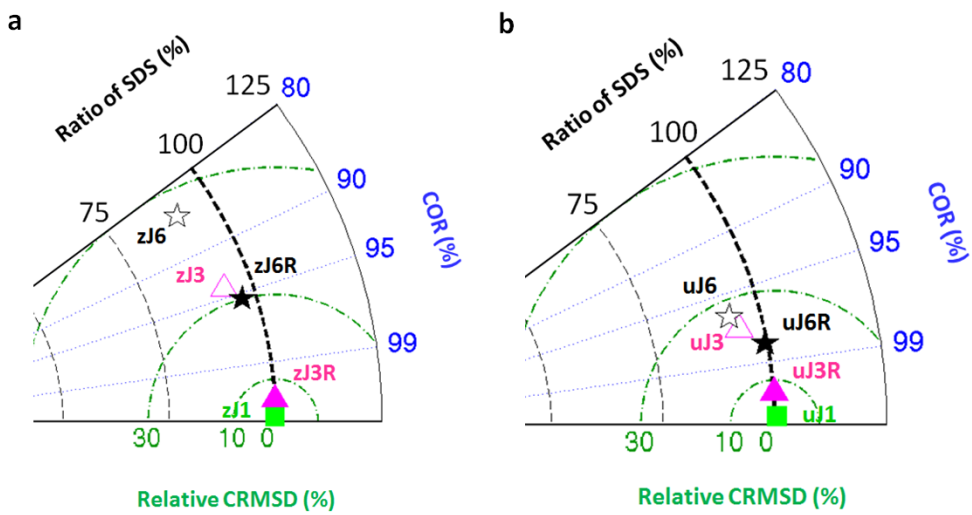

Figure 5.11 Taylor diagram showing the enhancement of results after adding small scales. (a) mean elevation, and (b) mean horizontal velocity in x direction.

The enhancement of downscaling ability by adding small scales at boundary conditions for elevation and velocity are described in the Figure 5.11. After adding small scales, quality of elevation significantly increases. For example, zJ6R increases correlation coefficient approximately 12%. Its SDS and relative

CRMSD all decrease about 6% and 26% respectively. zJ6R is even better than zJ3 and quality zJ3R's result is close to zJ1 (Fig. 5.11 (a)). Similar to elevation, result of velocity also improves. However, speed of improvement is not high as elevation. For instance, uJ6R only increase 4% of correlation coefficient and reduces 15% of relative CRMSD. This once again proves profit of adding small scales at BCs in nested procedure.

5. 4. Conclusions

One-way nested ocean circulation regional model is efficient tool used to achieve high resolution oceanic data from coarse information of global models. The ORCM takes the large-scale information specified from global model output at the LBC and incorporate with local forcing to generate the finer-scale features (Denis et al. 2002; Herbert et al. 2014 Pham et al. 2016). The generation and development of small scales features significantly rely on the stimulated sources (Denis et al. 2002; Fiser et al. 2011).

Though a framework of Big-Brother Experiment, which can significantly minimize errors associated downscaling technique and separate stimulated sources in developing small-scale generation, we can assess the effect of small scale generation to the larges scales as well as nested solution in case of un-sporting from sources. Base on that, an efficient method is proposed to reduce such effect. Finally, we identify role of separate stimulated sources contributing to characteristic of small-scale generation and development. Form the all the discussion in the previous section, the main results are as follow:

1. Small-scale generation and development strongly rely on the stimulated sources. Lacking such stimulated source, nested model cannot generate small-scales in right level with more negative bias of kinetic energy as time pass. Such under-estimation of kinetic energy increase with increasing ratio of spatial resolution between driving information and driven model. The negative bias of kinetic energy makes

large-scale significantly loose kinetic energy, and then degrades the quality of ORCMs results.

2. The proposed technique in adding small-scales boundary condition in case of lacking stimulated source can help small-scales significantly develop to the right level. Therefore, it can avoid the under-estimation of kinetic energy at small-scale part. As a result, it keeps large-scale kinetic energy in stable, and increase the quality of nested solution. Moreover, this method can help to run one-way nested model with higher spatial resolution different between the driver and the nested model. Instead of previous optimal resolution jump of 3, we can the nested model with spatial resolution difference up to J9.

The conclusions have been drawn from only a framework of specific Big-Brother Experiment configuration. However, the result of ORCMs may vary with different parameters such as geographical domain, update frequency of LBC, spatial resolution jump between driving data and nested model. Nevertheless, despite limits on the presenting conclusions, our finding on the role of source to small-scale generation and development, and proposed method on adding small scales at boundary condition could be applied in nesting procedure to increase quality of nested solution and reduce the different spatial resolution different between driver data and nested model.

CHAPTER SIX

6. SUMMARY AND RECOMMENDATIONS

6.1 Summary

Over several decades, one-way nested procedure using ORCMs have modeled coastal seas in a variety of domains (e.g., Kourafalou and Tsiaras, 2007; Costa et al., 2012) and have operationally forecasted sea weather on regional scales (e.g., Lim et al. 2013; Rowley and Mask, 2014). It has been demonstrated to be an effective approach for both operationally forecasted sea weather on regional scales and projections of future climate change and its impact on the ocean. However, there are there main issues associated with dynamical downscaling which require much attention from the numerical community. They include (1) error sources associated with dynamical downscaling technique; (2) small scale generation and development; and (3) effect of small scales generation on the large scale and quality of solution.

Among these issues, error source is the most important. They degrade the quality of predictions through many sources of error. Such sources of error are generally unavoidable and affect the ORCM results. These error sources can combine during simulation and synergistically degrade the ORCM solution. In compared with the many “atmospheric climate” studies of downscaling capabilities, the errors produced by the nesting with Ocean Regional Circulation Models

(RCMs) (Spall and Holland. 1991), have not yet been studied well. Many previous studies with RCMs have focused on optimizing RCMs to reduce errors from the nesting; but no standard method to identify, assess and reduce those errors has so far been published.

As a first step for assessing the oceanic dynamical downscaling feasibility in an RCM, we employed Big Brother Experiments which can separate the sources of errors and quantified the error magnitudes, with analyses following and combining those of Leduc and Laprise (2008) and Denis et al. (2002a). Through a framework of error assessment, it enables us to assess quantitatively the contribution of each error source to the nesting and downscaling procedures. Base on that, proposing optimal combinations of grid resolution, updating time, and domain size, and evaluating the downscaling ability of one-way nested using ORCMs.

The second issue with small scale generation and development also is very important. Since the regional model is essentially a method to dynamically downscale the low spatial resolution of global model to obtain greater resolution on a regional scale. The regional models should have ability in not only simulating the regional fields consist with and depends strongly depending on the realism of the large circulation provided from the LBCs but also generating meaningful fine-scale structures (IPCC. 2007). Therefore, generating small scale motions absenting from the large scales of global model reserved high attention. There are stimulated

sources (Denis et al. (2002a)) and factors can stimulate development of small scales. Each stimulated source and factor affect differently on the small scale generation and development. However, this issue has not been study well. In doing experiments with ideal domain using Big-Brother method to separate the effect of them on the small scales generation in dynamical downscaling process, we can address the role of each source and factor to small scales as well as figure out characteristic of small scales generation and development associated with each source and factor.

The final issue has been observed from several atmospheric studies. Castro et al. (2005) and Feser et al. (2011) pointed out that, although RCM successfully generated the smaller-scale features, kinetic energy on the large scales was lost, and this has not been reconfirmed so far. Moreover, Winterfeldt et al. (2010) and Feser et al. (2011) mentioned that dynamical downscaling does not generate small scales in a region which was not present of small scale generating sources. Denis et al., 2002 also experienced this matter when finding underestimation of nested small scale relative vorticity at 500 hPa where small scale dynamics are in free atmosphere. However, this point has not been reconfirmed so far.

The main results of this work involve the error sources associated with dynamical downscaling technique; small scale adding boundary technique; and enhancement of predictability are as follow:

1. Error sources associated with the downscaling technique including boundary

condition type, error during spin-up time of small scale generation, resolution of lateral boundary condition and domain main size significantly affect to the results of ORCMs. Such errors are generally unavoidable. They can combine during simulation and synergistically degrade the ORCM solution.

- The ORCMs solution changes when different OBCs are used and supplementary methodology (sponge/nudging) significantly improves the solution quality. The OBCs combined with supplementary methodologies, e.g. sponge/nudging are important level to improve the solution quality of the ORCMs. The “flather” and “R-K radiation” methods used in combination with sponge/nudging, can be good OBCs for the ORCMs.
- By isolating errors from different sources and preventing them from interacting with each other, the optimal ratio of spatial resolutions between the original data and the nested model appears to be ≤ 3. This recommendation means that LBC grids can be 3 times larger than the ORCM grids. Such an optimal spatial resolution jump ratio has been successfully applied and shown to be a reasonable selection in a great number of previous research studies even in cases of very different configurations (idealized or realistic), numerical models, domain sizes and grid resolutions (Spall and Holland, 1991; Laugier et al. 1996; Barth et al. 2005).
- Even though more frequent LBC updating results in more realistic reproduction, when we take into consideration storage and calculation time the recommended LBC updating period is every 6 hours in the experimental domain used here. Although the errors generally decrease as the jump ratio decreases, shorter

updating intervals do not guarantee higher accuracy. Since temporal updating requires some spin-up time initially, updating too often produces more error (immediately after each updating).

- Domain size also significantly affects the ORCM results. The errors produced at the boundaries propagate into the center of the nested domain as the simulations run for longer times. As the size of the ORCM's domain becomes larger, the extra space gives rise to a greater distance between the area of interest and the updated LBCs. So, the results exhibit patterns which are more highly correlated with the OGCMs. Therefore, the optimal domain size of the ORCMs could range from 1/10 to 1/2 of the OGCMs' domain size, depending on the computational cost.
- Among error sources which associated with downscaling technique during the one-way nesting procedure, the "spatial and temporal inconsistencies between lateral boundary condition of the nesting and nested models" extremely affect to nested resolution. Such error source is unavoidable and significantly depends on selection of spatial resolution ratio between given driving data and the nested model.

2. Based on the investigation of error sources, we suggest an optimization set-up for numerical model to mitigate such effect of error sources: The "flather" and "R-K radiation" methods used in combination with sponge/nudging, can be good OBCs for the ORCMs; spatial resolution jump between driving data and nested model can be 3; LBC updating frequency is every 6 hours for real domain with resolution of 3 km; and domain size of the ORCMs could be larger than interested area are about 10 times, depending on the computational cost. The optimization set-up helps to

mitigate the effect of aforementioned sources and improves the results of ORCMs. The results of presenting work within optimization set-up perform well with correlation coefficient of all diagnostic variables higher than 87%.

3. ORCMs show the good ability in down scaling from large scale information from global model. Within the optimization set-up, results of ORCMs perform well for all diagnostic variables in term of standard deviation, center root mean square difference, and correlation coefficient. Also, the pattern and magnitude reproduction for both stationary and transient variance are in good agreement with Big-Brother. The spatial correlation coefficient of domain averaged stationary large-scale and small scale variances for all diagnostic variables are higher than 82%.

4. Small scale generation and development must depend on the stimulated sources. Characteristic of small scale generation is in different with different stimulated source. The adding advection mostly impact on the larger filtered scale with forming a wave oscillating around the Big-Brother amplitude. Adding advection producing sharing stimulates disturbance in development near the source, they then transport to the inner domain. While the island can make weak strongly influence to smaller part of filtered scales. Such sources can stimulate the development of small scales to help them reach the level of Big-Brother.

5. Lacking such stimulated sources, although large scales transfer energy for small scales development through interactions of internal dynamics processes. However,

this energy transfer from this process is not big enough. Therefore, nested model cannot generate small-scales in right level with more negative bias of kinetic energy as time pass. Such under-estimation of kinetic energy increase with increasing ratio of spatial resolution between driving information and driven model. The negative bias of kinetic energy makes large-scale significantly loose kinetic energy, and then degrades the quality of ORCMs results with standard deviation deflecting 20% and giving 23% errors in case of J9.

6. The proposed technique in adding small-scales at boundary condition in case of lacking stimulated sources can help finer smalls scale quickly develop and achieve full development. In other word, it can reduce the spin-up time in generating and developing fine scale feature whenever updating from lateral boundary. Therefore, it can avoid the under-estimation of kinetic energy at small-scale part. As a result, it keeps large-scale kinetic energy in stable, and increase the quality of nested solution. Moreover, this method can help to run one-way nested model with higher spatial resolution different between the driver and the nested model. Instead of previous optimal resolution jump of 3, one can do the nested model with spatial resolution difference up to J9.

6.2 Recommendation

The present work was based on only a framework of specific Big-Brother Experiment configuration to address error source associated with dynamical downscaling technique, the characteristic of small-scale generation and development, and assess impact of small-scale generation on the large-scales, and then degrade ORCMs solution for specified regional domain. As mentioned from numerous studies (Warner et al., 1997; Denis, et al. 2002; Huang et al. 2008; Pham et al. 2016), quality of nested regional model depends on various parameters such as the driving information of global model, local forcing, geographical domain, season, horizontal resolution jumps, update frequencies from LBCs and nested model itself, etc. Therefore, results of nested model may perform very distinctly for many aforementioned parameters. We recommend further experiments need to perform for addressing the impact of various aforementioned parameters on the one-way nested ORCMs results.

REFERENCES

Ådlandsvik, B., Bentsen, M., 2007. Downscaling a twentieth century global climate simulation to the North Sea. Ocean Dyn 57:453-466. DOI 10.1007/s10236-007-0125-2.

Amante, C., Eakins, B.W., 2009. Etopo1 1 arc-minute global relief model: procedures, data sources and analysis. NOAA Technical Memorandum NESDIS NGDC-24. http://www.ngdc.noaa.gov/mgg/global/global.html.

Antic. S., Laprise. R., Denis.B., Elia.R,D., 2004. Testing the downscaling ability of a one-way nested regional climate model in regions of complex topography. Climate Dynamics. 23, 473-493.

Barth, A., Azcarate, A.A., Rixen, M., Beckers, J.M., 2005. Two-way nested model of mesoscale circulation features in the Ligurian Sea. Prog. Oceanogr., 66, 171-189.

Blaas, M., Dong, C.M., Marchesiello, P., McWilliams, J.C., Stolzenbach, K.D., 2007. Sediment transport modeling on southern Californian shelves: AROMS case study. Continental Shelf Research, 27, 832-853.

Blayo, E., Debreu, L., 2005. Revisiting open boundary conditions from the point of view of characteristic variables. Ocean Modelling. 9, 231-252.

Botkosal, W., 2009. Establishment of local river basin organization to promote water governance. Cambodia national Mekong committee. Conference on

New thing on water governance 2-3 July 2009, National University of Singapore.

Cailleau, S., Fedorenko, 5., Barnier, B., Blayo., Debreu, L., 2008. Comparison of different numerical methods used to handle the open boundary of a regional ocean circulation model of the Bay of Biscay. Ocean Modelling, 25, 1-16.

Cambon, G., Marchesiello, P., Penven, P., Debreu., L., 2014. ROMS_AGRIF User Guide.http://www.romsagrif.org/index.php/documentation/ROMS_AGRIF-User-Guide

Camerlengo, A.L., O'Brien, J.J., 1980. Open boundary condition in rotating fluids. J. Comput. Phys. 35, 12-35.

Carter, G.S., Merrifield, M.A., 2007. Open boundary conditions for regional tidal simulations. Ocean Modelling 18. 194-209.

Castro, C.L., Pielke Sr, R.A., Leoncini, G., 2005. Dynamical downscaling: Assessment of value retained and added using the regional atmospheric modeling system (RAMS). J. Geophys. Res. 110, D05108.

Caya, D., Laprise, R., 1999. A semi-implicit semi-Lagrangian regional climate model: the Canadian RCM. Mon Weather Rev 127: 314-362.

Chapman, D.C., 1985. Numerical treatment of cross-shelf boundaries in a barotropic coastal ocean model. Journal of Physical Oceanography, 15, 1060 - 1075.

Chang, K.I., Teague, W.J., Lyu, S.J., Perkins, H.T., Lee, D.K., Watts, D.R., Kim, Y.B., Mitchell, D.A., Lee, C.M., Kim, K., 2004. Circulation and currents in the southwestern East/Japan Sea: Overview and review. Prog. Oceanogr., 61, 105-156.

Chen, C., Huang, H., Beardsley, R.C., Liu, H., Xu, Q., Cowles, G., 2007. A finite-volume numerical approach for coastal ocean circulation studies: Comparisons with finite difference models, J. Geophys. Res., 112, C03018, doi:10.1029/2006JC003485.

Chu, P.C., Land, J., fan, C.W., 2001a. Japan Sea thermohaline structure and circulation. Part I: Climatology. J. Phys. Oceanogr. 31, 244-271.

Costa, P., Gomez, B., Venancio, A., Perez, E., Perez-Munuzuri, 5., 2012. Using the regional ocean modelling system (ROMS) to improve the sea surface temperature predictions of the MERCATOR ocean system. Sci. Mar. 76(S1): 165-175.

COAPS– Center for Ocean Atmospheric Prediction Studies (COAPS).http://hycom.coaps.fsu.edu/thredds/catalog.html.

Danilow, S.D., Gurarie, D., 2000. Quasi two dimensional turbulence. Uspekhi Fizicheskikh Nauk 170, 921-968

Denis, B., Laprise, R., Caya, D., Côté, J., 2002a. Downscaling ability of one-way nested regional climate model: the Big-Brother Experiment. Climate Dynamics 18: 627-646. DOI 10.1007/s00382-001-0201-0.

Denis, B., Côté, J., Laprise, R., 2002b. Spectral decomposition of two-dimensional atmospheric fields on limited-area domains using the discrete cosine transform (DCT). Mon. Wea. Re5., 130, 1812-1829.

Denis, B., Laprise, R., Caya, D., 2003. Sensitivity of a regional climate model to the spatial resolution and temporal updating frequency of lateral boundary conditions. Clim Dyn 20: 107-126.

Dickinson, R.E., Errico, R.M., Giorgi, F., Bates, G.T., 1989. A regional climate model for the western United States. Clim. Change, 15, 383-422.

Durran, D., 2001. Open boundary conditions: fact and fiction, in IUTAM Symposium on Advances in mathematical modeling of Atmosphere and Ocean dynamics, pp. 1-18. edited by P.F. Hodnett, Kluwer academic publisher.

Elía, R.D., Laprise, R., Denis, B., 2002. Forecasting skill limits of nested, limited area models: a perfect model approach. Mon. Wea. Re5. 130, 2006-2023.

Fang. W., Qiu. F., Guo. P., 2014. Summer circulation variability in the south china sea during 2006-2010. Journal of Marine Systems 137. 47-54.

Feser., F., Rockel, B., Storch, H.5., Winterfeldt, J., Zahn, M., 2011. Regional climate models add value to global model data. American Meteorology Society. DOI:10.1175/2011BAMS3061.1.

Flather, R.A., 1976. A tidal model of the northwest European continental shelf. Memoires Soc R Sci Liege Ser 6(10):141-146.

Flather, R.A., 1988. A numerical investigation of tides and diurnal-period continental shelf waves along Vancouver Island. J. Phys. Oceanogr., 18, 115-139.

Franklin, C.N., Vaillancourt, P.A., Yau, M.K., Bartello, P. Collision rates of cloud droplets in turbulent flow. J. Atmos. Sci., 62, 2451-2465.

Giorgi, F and Marinucci, M.R., 1996. An investigation of the sensitivity of simulated precipitation to model resolution and its implications for climate studies. Mon. Wea. R5., 124, 148-166.

Giorgi, F., Mearns, L.O., 1999. Introduction to special section: Regional climate modeling revisited. Journal of Geophysical Research, Vol. 104, No.D6, page 6335-6352.

Hedström, K.S., 2009. Draft technical manual for a coupled sea-ice/ocean circulation model (version 3). U.S. Department of the Interior Minerals Management Service Anchorage, Alaska. Contract No. M07PC13368.

Hellweger, F.L., Sebille, E.V., 2016. The role of ocean currents in the temperature selection of plankton: insights from an individual – based model. PloS ONE 11(12).

Herbert, G., Garreau, P., Garnier 5., Dumas, F., 2014. Downscaling from oceanic global circulation model towards regional and coastal model using spectral nudging techniques: application to the Mediterranean Sea and IBI area model. Mercator Ocean Quarterly Newsletter, 49, 44-59.

Hogan, P.J., Hurlburt, H.E., 2006. Why do intra thermocline eddies form in the Japan/East Sea. Oceanography. 19, 134-143.

Holloway, P.E., 1996. Internal tide generation by seamounts, ridges, and islands. J. Geophys. Res., 104, 25937-25951

Hu. J., Kawamura. H., Hong. H., Qi. Y., 2000. A review on the current in the south china sea: seasonal circulation, south china sea warm current and kuroshio intrusion. Journal of Oceanography, Vol. 56. 607-624.

Huang, H., Chen, C., Cowles, G.W., Winant, C.D., Beardsley, R.C., Hedström, K.S., Haidvogel, D.B., 2008. FVCOM validation experiments: comparisons with ROMS for three idealized barotropic test problems. J. Geophys. Res., 113, C07042,

doi:10.1029/2007JC004557.

Hurlburt, H.E., Metzger, E.J., Hogan, P.J., Tilburg, C.E., Shriver, J.F., 2008. Steering of upper ocean currents and fronts by the topographically constrained abyssal circulation. Dynatmoce. Dynam. Atmos. Oceans. 45. 102-134.

Katsumata, K., 2005. Two- and three-dimensional numerical models of internal tide generation at a continental slope. Ocean Modelling 12 (1-2), 32-45.

Kourafalou, V and Tsiaras, K., 2007. A nested circulation model for the North Aegean Sea. Ocean Sci., 3, 1-16.

Large, W.G., McWilliams, J.C., Doney, S.C., 1994. Ocean vertical mixing: A review and a model with a nonlocal boundary layer parameterization. Reviews of Geophysics, 32, 363-403.

Laprise, R., 2008. Regional climate modeling. J. Comput. Phys. 227, 3641-3666.

Laugier, M., Angot, P., Mortier, L., 1996. Nested grid methods for an ocean model: A comparative study. Int. J. Numer. Meth. Fluids. Vol 23, 1163-1195.

Leduc, M., Laprise, R., 2008. Regional climate model sensitivity to domain size.Clim.Dyn. 32:833-854.

Leduc, M., Laprise, R., Moretti-Poission, M., Morin, J.P., 2011. Sensitivity to domain size of Regional Climate Model Simulations in Middle latitudes for summer.Clim. Dyn. 37(1-2). 343-356, doi:10.1007/s00382-011-1008-2.

Ledwell, J.R., Wilson, A.J., Low, C.S., 1993. Evidence for slow mixing across the pycnocline from an open trcer-release experiment. Nature, 364: 701-703.

Li, H., Kanamitsu, M., Hong, S.Y., 2012. California reanalysis downscaling at 10 km using an ocean-atmosphere coupled regional model system. J. Geophys. Res., 117, D12118, doi:10.1029/2011JD017372.

Lim, H.S., Kim,C.S., Park, K.S., Shim, J.S., 2013. Down-scaled regional ocean modeling system (ROMS) for high-resolution coastal hydrodynamics in Korea. Acta Oceanol. Sin., Vol. 32, No. 9, P. 50-61.

Liu, F., Chai, F., 2009. Seasonal and inter-annual variation of physical and biological progresses during 1994-2001 in the Sea of Japan/East Sea: A three-

dimensional physical –biogeochemical modeling study. J. Mar. Sys., 79, 265-277.

Marchesiello, P., McWilliams, J.M., Shchepetkin, A., 2001. Open boundary conditions for long-term integration of regional oceanic models. Ocean Modelling 3, 1-20.

McDonald, A., 1999. A review of lateral boundary conditions for limited area forecast models. PINSA, 65, A, No.1, pp. 91-105.

Metzger, E.J., Hurlburt, H.E., Wallcraft, A.J., Chassignet, E.P., Cummings, J.A., Smedstad, O.M., 2008. Global Ocean Prediction Using HYCOM, HPCMP Users Group Conference, pp. 271–274.

Miller, M.J., Thorpe, A.J., 1981. Radiation conditions for the lateral boundaries of limited area numerical models. Quart. J. R. Meteorol. Soc. 107, 615-628.Nash, S and Hartnett, M., 2014. Development of a nested coastal circulation model: Boundary error reduction. Environmental Modelling & Software.53, 65-80.

Nash, S., Hartnett, M., 2014. Development of a nested coastal circulation model: Boundary error reduction. Environmental Modelling & Software. 53, 65.

NCEP – National Centers for Environmental Prediction. http://rda.ucar.edu/datasets/.

Oddo, B., Pinardi, N., 2008. Lateral open boundary conditions for nested limited area models: A scale selective approach. Ocean Modelling 20, 134-156.

Orlanski, I., 1976. A simple boundary condition for unbounded hyperbolic flows. J. Comput. Phys. 21, 251-269.

Palma, E.D., Matano, R.P., 1998. On the implementation of passive open boundary conditions for a general circulation model: The barotropic mode. J. Geophys. Res., 103(C1), 1319 - 1341.

Palma, E.D., Matano, R.P., 2001. Dynamical impacts associated with radiation boundary conditions. J. Sea Res., 46, 117-132.

Penven, P., Cambon, G., Tan, T.A., Marchesiello, P., Debreu, L., 2010. ROMS_AGRIF/ROMSTOOLS user's guide.Institut de Recherche pour le Développement (IRD).

Pham,V.S., Hwang, J.H., Ku, H., 2016. Optimizing dynamic downscaling in one-way nesting using a regional ocean model. Ocean Modelling 106. 104-120.

Pope and Stepphen. B., 2000. Turbulent flows. Cambridge University Press.

Raymond, W.H., Kuo, H.L., 1984. A radiation boundary condition for multidimensional flows.Quarterly Journal of the Royal Meterological Society 110, 535-551.

Richardon, L.F., 1992. Weather prediction by numerical process. Cambridge University Press.

Rao, K.L., De Bruyn Kops, S.M., 2011. A mathematical framework for forcing turbulence applied to horizontally homogeneous stratified flow. Phys, Fluids., 23, 065110.

Roed, L.P., Cooper, C., 1986. Open boundary conditions in numerical ocean models. In: Obrien, J.J. (Ed.), Advanced Physical Oceanographic Numerical Modeling, NATO ASI Series C. 186, 411-436.

Rowley, C and Mask, A., 2014. Regional and coastal prediction with the relocatable Ocean Nowcast/Forecast System. Oceanography 27(3): 44-55, http://dx.doi.org/10.5670/oceanog.2014.67.

Samelson, R.M., Allen, J.S., Maccready, P., 2008. Progress in coastal ocean modeling during CoOp. Special issue on coastal ocean processes observing technologies and models. Oceanography, Vol.21, No.4.

Spall, M.A., Robinson, A.R., 1989. A new open ocean, hybrid coordinate primitive equations model. Math. Comput. Simulate. 31, 241-269.

Spall, M., Holland, W., 1991. A nested primitive equation model for oceanic applications. Journal of Physical Oceanography, 21, 205-220.

Sullivan, N.P., Mahalingam, S., 1994. Deterministic forcing of homogeneous, isotropic turbulence. Phys, Fluids., 6, 1612-1614.

Takikawa, T, Yoon, J.H., Hase, H., Cho, K.D., 1999. Monitoring of the Tsushima Current at the Tsushima/Korea Straits. In Proceedings 3rd CREAMS International Symposium, Fukuoka, Japan, 15-18.

Tang, Y., Grimshaw, R., 1996. Radiation boundary conditions in barotropic coastal ocean numerical models. Journal of Computational physics 123, 96-110.

Taylor, K.E., 2001. Summarizing multiple aspects of model performance in a single diagram. Geophys. Res., 106, 7183-7192.

Teague, W.J., Ko, D.S., Jacobs, G.A., Perkin, H.T., Book, J.W., Smith, S.R., Chang, K.I., Suk, M.S., Kim, K., Luy, S.L., Tang, T.Y., 2006. The current thought Korea/Tsushima Strait. Oceanography. Vol. 19, No. 3.

Tennekes, H., Lumley, J.L., 1997. A first course in turbulence. The MIT Press. Cambridge, Massachusetts, and London, England.

Tréguier, A.M., Barnier, B., de Miranda, A.P., Molines, J.M., Grima, N., Imbard, M., Madec, G., Messager, C., 2001. An eddy permitting model of the Atlantic circulation: evaluating open boundary conditions. J. Geophys. Res. 106 (C10), 22115-22130.

Trzaska, S., Schnarr, E., 2014. A review of downscaling methods for climate change projections. African and Latin American Resilience to Chimate Change (ARCC).

Tsynkov, S.5., 1998. Numerical solutions of problems on unbounded domains. A review. Appl. Numer. Math., 27, 456-532.

Vannitsem, S., Chomé, F., 2005. One-way nested regional climate simulations and domain size. J. Clim., 18, 229-233

Warner, T.T., Peterson, R.A., Treadon, R.E., 1997. A tutorial on lateral boundary conditions as a basic and potentially serious limitation to regional numerical weather prediction.Bull.Am.Meteorol.Soc., 78, 2599-2617.

Winterfeldt, L., Geyer, B., Weisse., 2010. Using QuikSCAT in the added value assessment of dynamically downscaled wind speed. Int. J. Climatol., 31, 1028-1039.

ABSTRACT IN KOREAN

지역해양 모델의 일방향 둥지화 예측력 개선

By Pham Van Sy

Department of Civil and Environmental Engineering

College of Engineering

Graduation School of Seoul National University

Advisor: Professor Hwang, Jin Hwan

둥지화된 지역해 모델을 이용한 동적 다운스케일링은 국지적인 해양 날씨 예측과 미래의 기후 변화 및 해양에 미치는 영향을 예측하는데 효과적인 접근법으로 알려져 있다. 그러나, 전역 모델에서 지역 모델로 다운스케일링을 수행할 때, 크게 두 가지의 문제가 발생할 수 있다. 첫 번째는 격자크기 및 모델간의 정보 업데이트 간격의 차이로 발생하는 수치 오류 문제이다. 본 연구에서는 지역해양순환모델(ORCMs)로부터 다운스케일링된 결과를 활용하여 둥지화 과정에서 생기는 오류의 영향을 평가하였다. 오류는 Big-Brother Experiment (BBE)를 이용하여 ORCMs 의 소스와 특성에 따라 평가되었다. 본 논문에서는 격자 크기의 차이, 모의 시간 및 도메인 크기로 인한 오류를 논의하는데 초점을 두었다. 다양한 시나리오에 대해 독립적으로 BBE 를 모의한 후, 테일러 다이어그램을 사용하여 결과를 분석하고 격자 크기, 업데이트 기간 및 도메인 크기에 대한 최적의 조합을 제안하였다. 다운스케일링을 위해 제안된 모델의 설정은 변수들의 공간적인 상관관계 및 둥지화 된 모델과 원본간의 상대적인 분산 크기로 평가하였다.

두 번째는 둥지화된 지역해 모델의 동적 다운스케일링에서 소규모 거동 특성의 과소 평가 문제이다. 일방향으로 둥지화된 지역 순환 모델이 국지적으로 발생하는 에너지에 통합되고 측면 경계에서 전지구 모델의 결과로부터 입력되는 많은 양의 정보에 의해 모의 될 때 소규모 거동 특성이 성공적으로 재현됨을 많은 선행 연구자들에 의해 증명되었다. 하지만, 일부 다른 연구자들은 소규모 거동 특성이 과소 추정됨을 확인하였고, 이에 따른 모델의 재현성이 비합리적임을 의심하였다. 그들은 심지어 대규모의 에너지 손실이 발생함에 따른 둥지화 모델의 성능 저하를 의심하기도 하였다. 본 연구에서는 소규모 거동 특성의 재현율을 높이기 위해 선행연구에서 확인된 “모의 소스”와 관련된 두 번째 문제를 해결하기 위해 노력하였다. 이를 위해, 더 높은 해상도로 일방향 둥지화를 수행하여도 소규모 거동 특성을 유지시킬 수 있도록 “소규모 추가 경계기법”이라는 효율적인 기법을 제안하였다.

주요어 : 다운스케일링; 수치 오류; 지역해양순환모델; Big-Brother Experiment; 소규모 추가 경계기법

학 번 : 2014-30863

ACKNOWLEDGEMENT

Foremost, I would like to express my sincere gratitude and respect to my researcher advisor, Professor Jin Hwan Hwang for the support of my Ph.D study, for his motivation, patience and immense knowledge. Without his enthusiastic guidance and persistent help, this thesis would not have been possible. The professional knowledge that I learned from him have been useful in order to pursue my goal in life. Besides my advisor, I wish to thank the rest of my dissertation committee: Professor Il-won Seo, professor Young-Oh Kim, Professor Young-Gyu Park, Professor Sang-Young Son, and Professor, Van Thinh Nguyen, for their encouragement, and incisive and thoughtful comments.

Special thanks are given to the Seoul National University for supporting my tuition and living expenses through the Graduate Scholarship for Excellent Foreign Students (GSFS). The GSFS gives me an opportunity to continuously purse my dream. Also, it is really wonderful to study in the prestigious University, modern facility, friendly atmosphere and high standards in both education and research.

My sincere thanks also go to my lab members at Coastal Environmental System Laboratory: Nam-Hoon Kim, Houyng-Chul Park, Donghyeon Kim, Jaeyoung Jung, Jisu Kim, Seogeun Choi, Chang Hee Lee, and Nguyen Ngoc Minh for the kind and enthusiastic support, especially in work relating to Korean language, and giving me a nice atmosphere of collaboration and fellowship. I have had unforgettable memories with all of them

Last but not least, I would like to convey my heartfelt gratitude and sincere appreciation to my family members, especially, my wife. Without their support and encouragement, it is impossible for me to finish my graduate education.